ON THE IMPROVEMENT OF THE

ON THE IMPROVEMENT OF THE ACHIEVABLE BIT RATE IN MULTI-CARRIER COMMUNICATION SYSTEMS USING SIGNAL PROCESSING TECHNIQUES

By

BAHRAM BORNA, B.Sc., M.Sc.

NOVEMBER 2007

A Thesis

Submitted to the Department of Electrical & Computer Engineering

and the School of Graduate Studies

in Partial Fulfilment of the Requirements

for the Degree of

Doctor of Philosophy

McMaster University

DOCTOR OF PHILOSOPHY (2007) McMaster University
(Electrical & Computer Engineering) Hamilton, Ontario

TITLE:	On the improvement of the achievable bit rate in multi-carrier communication systems using signal processing techniques
AUTHOR:	Bahram Borna B.Sc. (Electronics Engineering) Isfahan University of Technology, Isfahan, Iran M.Sc. (Telecommunications Engineering) University of Tehran, Tehran, Iran
SUPERVISOR:	Timothy N. Davidson, Associate Professor
NUMBER OF PAGES:	xiii, 161

To my loving wife Roya

Abstract

With the growing demand for high data rate communication services, multi-carrier communication schemes have started to become the method of choice in many applications. In this thesis, multi-carrier communication systems are studied and various methods for improving their achievable bit rate are proposed.

Filtered multitone (FMT) is a multi-carrier communication scheme which is implemented using a modulated filter bank structure. In this thesis, an efficient design method for the prototype filter of the FMT system is proposed. This design method allows improvement of the achievable bit rate by efficient evaluation of the inherent trade-off between the subchannel spectral containment provided by the prototype filter and the intersymbol interference (ISI) that the filter generates. Numerical results further demonstrate the effectiveness of the proposed design method. The insight gained from this design is also used to determine the optimal number of subchannels in FMT systems. Moreover, since the presence of ISI in FMT subchannels outputs renders the conventional water-filling power loading algorithm suboptimal, we propose an efficient power loading algorithm for FMT that enables higher achievable bit rates.

Discrete multitone (DMT) is a popular multi-carrier communication scheme, mainly due to its rather low complexity. However. DMT suffers from poor subchannel spectral characteristics. In this thesis, a family of bi-windowed DMT transceivers is proposed that provide both improved subchannel spectral containment at the transmitter and improved spectral selectivity at the receiver, without requiring the cyclic prefix to be longer than the order of the channel impulse response. The windows are designed in a channel independent manner and are constrained to produce subchannel outputs that are free from ISI. Furthermore, the design allows the intersubchannel interference (ICI) to be controlled in such a way that it can be mitigated using a relatively simple minimum mean square error (MMSE) successive interference cancellation scheme. Numerical results demonstrate the significant gain in the achievable bit rate obtained by the proposed scheme.

Acknowledgements

In completion of this PhD thesis, I have been fortunate to receive valuable assistance, comments, suggestions, and support from many people, all of whom I would like to thank. My deepest gratitude is to my wife, Roya, for her great help and support during all these years. Many thanks to my parents and my parents in-law for all their support.

Special thanks to my supervisor, Dr. Tim Davidson, for his guidance on this research topic, his help, support, and inspiring advice and comments. I would like to thank Dr. Jim Reilly for his valuable comments as one of my PhD comittee members, also for all he taught me. I would also like to thank Dr. Max Wong for all his support and inspiring advice, and for his comments as one of my PhD committee members. Thank-you to my other examining comittee members, Dr. Robert Pelton, Dr. Bill Farmer, Dr. Doug Down, and Dr. Andrea Tonello, for reading my thesis and for their valuable feedback.

I would like to thank all my friends who have assisted me during the time this research work was done. Especially, thank-you to Dr. Ramy Gohary, Dr. Amin Zia, and Dr. Shahram Shahbazpanahi for all their help. Many thanks to the graduate secretary of the department, Cheryl Gies, for all her kindness and support throughout these years.

Contents

List of Figures

Glossary of acronyms

ADSL	Asymmetric digital subscriber line
AM	Amplitude modulation
AWGN	Additive white Gaussian noise
CO	Central office
CP	Cyclic prefix
CPE	Customer premises end
CPM	Continuous phase modulation
CS	Cyclic suffix
DFE	Decision feedback equalizer
DMT	Discrete multitone
DSL	Digital subsciber line
DWMT	Discrete wavelet multitone
FEQ	Frequency-domain equalizer
FEXT	Far-end crosstalk
FFT	Fast Fourier transform
FMT	Filtered multitone
FSK	Frequency shift keying
HAM	Amateur radio
ICI	Intersubchannel interference

IFFT	Inverse fast Fourier transform
ISI	Intersymbol interference
LPF	Lowpass filter
ML	Maximum likelihood
MMSE	Minimum mean square error
NEXT	Near-end crosstalk
OFDM	Orthogonal frequency division multiplexing
OFDMA	Orthogonal frequency division multiple access
PAM	Pulse amplitude modulation
PSD	Power spectral density
PSK	Phase shift keying
QAM	Quadrature amplitude modulation
RFI	Radio-Frequency Interference
SINR	Signal to interference plus noise ratio
SNR	Signal to noise ratio
TEQ	Time-domain equalizer
TIR	Target impulse response
VDSL	Very high-speed digital subscriber line

Chapter 1

Introduction

In recent years the demand for reliable high data rate communication services has been rapidly increasing. On the other hand, in a communication system with a given transmission power, as the data rate increases, the frequency bandwidth required by that system increases [1, 2]. Therefore, high data rate communication implies transmission through wideband communication channels. However, wideband communication channels are typically frequency-selective, meaning that their frequency response changes significantly over the frequency band. Consequently, when a signal is transmitted through such channels, the received signal will include a considerable amount of intersymbol interference (ISI), which can significantly degrade the performance of the system. The search for effective techniques for mitigating the ISI produced by frequency-selective channels has been the subject of research and study for many years. Traditionally, communication systems use a single-carrier transmission with a variety of choices for the modulation method, including pulse amplitude modulation (PAM), quadrature amplitude modulation (QAM), phase shift keying (PSK), frequency shift keying (FSK), and continuous phase modulation (CPM). In single-carrier transceivers, the optimal receiver is the maximum likelihood (ML) sequence detector in the sense that it minimizes the probability of error in detection of the transmitted data sequence from the received signal. However, ML receivers have a very large computational complexity, especially in highly frequency-selective channels [2]. In practice, single-carrier communication systems often use equalization techniques to compensate for the ISI produced by the frequency-selective channels. The design of efficient equalization techniques has been a subject of interest for researchers, and many equalization techniques have been proposed, several of which have been used in communication transceivers. Some of the most widely used equalizers are the zero-forcing and minimum mean square error (MMSE) linear equalizers, and the zero-forcing and MMSE decision feedback equalizers (DFEs) [2, 3]. While these equalizers are quite effective for communication systems with low to moderate bandwidths, as the frequency-selectivity of the channel increases, the complexity of the required equalization scheme increases rather quickly. In fact, the complexity of equalizers required in single-carrier transceivers for highly frequency-selective channels limits the achievable data rates in such transceivers.

Multi-carrier communication schemes have been proposed as effective solutions to this problem. The fundamental idea behind multi-carrier schemes is to divide the frequency-selective wideband channel into several narrowband subchannels, and to separately transmit and receive data on each subchannel. Indeed, if the subchannels are orthogonal, communication of data through each subchannel will be independent of other subchannels. Since each of the subchannels has a much narrower bandwidth than that of the whole channel, compensation of the distortion caused by each subchannel can be performed with a much lower complexity than that required for equalization of the whole wideband channel.

The basic principle of multi-carrier communication has a long history. For instance, it was used in Collin's Kineplex system [4] in 1957. A multi-carrier communication scheme called orthogonally multiplexed QAM (O-QAM) was proposed by Saltzberg [5] in 1967. The application of the discrete Fourier transform (DFT) for frequency-division multiplexing (FDM) systems was proposed by Darlington [6] in 1970, and was used in practice [7] in 1978. Hirosaki [8] proposed a DFT-based structure for the O-QAM system in 1981 and demonstrated that a reduction in complexity could be achieved by employing digital signal processing techniques in the implementation of the O-QAM system. Kalet [9] showed that for frequency-selective channels, when the available transmit power is appropriately divided among the subchannels, multi-carrier communications offers a considerable gain in the achievable bit rate compared to the equivalent single carrier linearly equalized system [9].

While the most desirable characteristic of multi-carrier communication systems is that they can efficiently overcome the ISI caused by frequency-selective wideband channels, they also have other desirable characteristics. One attractive characteristic of multi-carrier schemes is their immunity to impulse noise and fast fades [10–12]. Indeed, since the symbol period in multi-carrier modulation is much longer than that in single-carrier modulation schemes, the impact of impulse noise on a multi-carrier system is substantially less than that in a single-carrier system. Flexibility of duplexing is also an attractive property of multi-carrier schemes. Duplexing in multi-carrier systems is usually done by devoting a number of subchannels to one direction of communication, and devoting the rest to the opposite direction. This way, echo cancellation is a significantly easier task than in single-carrier systems.

Due to their desirable features, multi-carrier communication schemes have found extensive applications in the emerging technologies of the recent years. Discrete multitone (DMT) [13,14] has been one of the most widely-used multi-carrier modulation schemes. DMT is the modulation method in digital subscriber line (DSL) transceivers which communicate over twisted pair phone lines [15,16]. Several standards for different types of DSL transceivers have been established by the standardization section of international telecommunication union (ITU-T), and they use DMT as the modulation method [15,16]. This includes asymmetric DSL (ADSL) which is the most widely used broadband service in the world at the time this thesis is being written [17]. The ITU-T has recently approved the very high-speed DSL (VDSL) standard as well, in which DMT has been considered as the modulation method. DMT modulation has also been adopted by the power line communications (PLC) [18] standard bodies, such as the Home plug standard [19].

Multi-carrier transmission is implemented in DMT transceivers using the inverse fast Fourier transform (IFFT) at the transmitter and fast Fourier transform (FFT) at the receiver. In DMT modulation, a cyclic prefix is added to the data sequence at the transmitter. This redundant sequence is chosen to be at least as long as the order of the impulse response of the discrete-time equivalent model of the communication channel, and it is removed at the receiver. The use of cyclic prefix in DMT system prevents ISI at the subchannel outputs. In DMT modulation, different numbers of bits are loaded onto different subchannels based on the signal to noise ratio (SNR) of each of the subchannels at the receiver. Moreover, the available transmit power is efficiently divided among the subchannels, e.g., using the water-filling power loading algorithm [9, 15]. Because efficient bit loading and power loading algorithms are based on the subchannel SNR values at the receiver, in DMT transceivers there is a feedback from receiver to the transmitter by which the receiver provides the information regarding the number of bits and the amount of power to be allocated to each subchannel.

Orthogonal frequency division multiplexing (OFDM) is an other widely used multi-carrier modulation scheme. It is similar to DMT, except that in the OFDM scheme, a constant power and a constant number of bits is assigned to each of the subchannels, and this removes the need for feedback from the receiver to the transmitter regarding the information on bit and power allocation. OFDM has been adopted by several standards for the existing and emerging wireless technologies, including the digital video broadcasting-terrestrial (DVB-T), which is the European terrestrial digital television standard [20], the IEEE 802.11e standard for wireless local area networks (WLAN) [21], and the IEEE 802.16 standard for fixed and mobile broadband wireless access systems [22].

DMT and OFDM are particularly attractive multi-carrier schemes due to their relatively low complexity. They have an FFT-based implementation which makes their implementation cost-efficient. even when the number of subchannels is large. Moreover, if they use a cyclic prefix with a length larger than or equal to the order of the channel impulse response, the subchannel outputs are free from ISI and free from intersubchannel interference (ICI), and thereby, DMT and OFDM schemes practically transform the frequency-selective channel into a number of orthogonal frequency-flat subchannels. The equalization of each subchannel is then simply done by multiplying the subchannel output by a complex number.

Multi-carrier communication can also be used as a multiple access method. This is usually referred to as orthogonal frequency division multiple access (OFDMA) [22], in which, each user is assigned one or more subchannels for transmitting data. Multi-carrier schemes can also be combined with other multiple access methods, including time division multiple access (TDMA) and code division multiple access (CDMA). A combination of multi-carrier modulation and CDMA, known as multi-carrier CDMA (MC-CDMA) [23, 24] has been proposed for the fourth generation (4G) mobile communication systems.

While DMT and OFDM are the most widely-used types of multi-carrier modulation schemes, they do have some shortcomings. In practice, some communication channels have very long impulse responses, or even infinite impulse responses (IIR), e.g., the DSL channel. In order to achieve the zero ISI and zero ICI conditions, a DMT system uses a cyclic prefix which is at least as long as the order of the channel. When the order of the channel is very large, a very large cyclic prefix has to be used, which in turn, reduces the bandwidth efficiency. To avoid this problem, DMT and OFDM systems use a so-called time-domain equalizer (TEQ) at the receiver to shorten the equivalent channel impulse response. But, the implementation of TEQ can significantly increase the complexity of the overall system. Other shortcomings of DMT and OFDM systems include their poor subchannel spectral characteristics. In these systems, the subchannel pulse shaping filters and also the subchannel receiver filters have a rectangular time-domain shape and thus they have a sinc shape in the frequency domain. Consequently, the spectra of adjacent subchannels overlap in the frequency domain, the subchannel sidelobes are large and they decay slowly. As a result, these systems have poor subchannel spectral containment at the transmitter and poor subchannel spectral selectivity at the receiver. The poor spectral containment of the subchannels at the transmitter makes it quite awkward to design schemes that have to satisfy the egress standards. For example, the ITU-T specifies that the power spectral density (PSD) of DSL transmitters has to be below a certain level in the amateur (HAM) radio bands [15, 25]. The HAM radio bands are rather narrow, but, since the subchannel sidelobes in DMT transmitters are large and decay slowly, in order to satisfy the egress standards a large number of subchannels have to be turned off. The poor spectral containment at the transmitter also generates a significant amount of near-end crosstalk (NEXT), which is one of the harmful sources of interference in DSL channels. At the receiver side, the large sidelobes of the subchannel spectra make DMT and OFDM systems susceptible to both NEXT and narrowband interference, such as the radio frequency interference (RFI) emerging from amplitude modulation (AM) broadcast and HAM radio signals. Indeed, since the sidelobes of the subchannels spectra are large and roll off slowly, a narrowband interference can impact a large number of subchannels. Moreover, because of the poor subchannel spectral characteristics of OFDM transceivers, imperfections such as a frequency offset between the local oscillators at the transmitter and receiver, phase noise, and Doppler spread (in mobile transceivers) can result in large amounts of intersubchannel interference (ICI) among the subchannels.

The shortcomings of DMT and OFDM schemes mentioned above reduce the achievable bit rate of these systems. Finding methods to mitigate these problems has been the subject of research and study by a number of researchers in the recent years, and several approaches have been considered to improve the performance of these systems. Those approaches can be categorized into two main groups. In one category, multi-carrier schemes that have better spectral characteristics at the transmitter and receiver than DMT and OFDM have been proposed. One of such schemes is the filtered multitone (FMT) modulation [26], which offers a high level of subchannel spectral containment at the transmitter and a high level of spectral selectivity at the receiver. In the second category, DMT and OFDM systems have been considered, but different techniques have been applied to improve their performance. These include techniques for improving the subchannel spectra at the transmitter or receiver, and also methods for combatting near-end crosstalk and echo.

In the research reported in this thesis, different methods for improving the performance of multi-carrier transceivers were investigated using the achievable bit rate as the performance measure. The thesis is outlined as follows. In Chapter 2, an overview of multi-carrier communication systems is presented. First, several multi-carrier schemes, including DMT, OFDM, FMT, and discrete wavelet multitone (DWMT) [27] are described and their points of strength and shortcomings are compared. Then, we review different time domain equalizer (TEQ) methods that are used for impulse response shortening in multi-carrier communication systems. Among different TEQ methods, the minimum mean square error TEQ, which is the most widely used TEQ, is analyzed. Bit loading and power loading methods for DMT transceivers are studied next, and the water-filling algorithm, which is the optimal loading method in the absence of ISI and ICI, is presented. The established windowing techniques for DMT and OFDM systems are also studied in Chapter 2. Windowing techniques can be considered as some of the most efficient methods for improving the performance of DMT and OFDM transceivers, and several transmitter and receiver windowing methods are described. While our results obtained in Chapters 3 and 4 are valid for all communication environments, including wireless and wireline channels, in the numerical examples that will be presented in those chapters, we will consider a realistic model for the digital subscriber line (DSL) environment. Therefore, in Chapter 2 an introduction to the fundamentals of DSL communication is provided. The DSL fundamentals section is followed by a brief outline of a cyclic suffix scheme for elimination of near-end crosstalk in DSL systems.

While most of the material presented in Chapter 2 is based on the results obtained by other researchers, Chapters 3 and 4 consist of the major contributions of this thesis.

In Chapter 3, filtered multitone (FMT) systems are considered. We quantify the inherent trade-off between the channel-independent measures of ICI and ISI in FMT systems and propose an efficient channel-independent design method for the prototype filter of the FMT transceivers. We demonstrate the significant improvement that is offered by this method. Moreover, using the insight gained from this design, we explain the trade-off that has to be considered when choosing the appropriate number of subchannels in the FMT systems. As was mentioned earlier, the achievable bit rate of multi-carrier systems depends on the distribution of the available power among the subchannels. While the water-filling algorithm provides the optimal power loading method for DMT and OFDM systems, the presence of non-negligible ISI in the outputs of the FMT subchannels renders water-filling suboptimal for FMT applications. We propose an iterative power loading algorithm for FMT systems that incorporates the effects of ISI. We demonstrate performance achievements of the proposed prototype filter design and the proposed power loading algorithm using our numerical results which are obtained for a realistic model for the DSL environment.

In Chapter 4, we consider a general filter bank structure that can model DMT and OFDM systems, as well as FMT and DWMT systems. We derive the channel-independent necessary and sufficient conditions for this filter bank transceiver to be free from ISI, and we propose a family of bi-windowed discrete multitone transceivers that provide improved subchannel spectral characteristics at both ends of the transceiver, without requiring the cyclic prefix to be longer than the order of the channel impulse response. The windows are designed in a channel-independent manner and they satisfy the ISI-free conditions. Moreover, we explain how the design allows the ICI to be controlled in such a way that it can be mitigated using a relatively simple minimum mean square error successive ICI canceller. We demonstrate the performance of the proposed bi-windowed DMT system through numerical analysis using a realistic model for the DSL environment, and we show that the achievable bit rate of the proposed system is significantly higher than that of the conventional DMT system and the established windowed DMT systems with receiver-only windowing.

Finally, concluding remarks and suggestions for future work are presented in Chapter 5.

Chapter 2

Overview of multi-carrier communication systems

In this chapter, an overview of multi-carrier communication systems is presented, in which the established multi-carrier modulation schemes are described and compared to each other. In addition, several algorithms and techniques specific to multi-carrier communication systems are studied. These include the time domain equalizers (TEQ) that are used for channel impulse response shortening; loading algorithms that are used for assigning the appropriate number of bits and appropriate amount of power to different subchannels; windowing techniques that are used to improve the spectral characteristics of transmitter or receiver subchannel spectra; and other techniques associated with multi-carrier communication systems.

2.1 Major multi-carrier modulation schemes

The most prominent members of the class of multi-carrier modulation schemes are discrete multitone (DMT), orthogonal frequency division multiplexing (OFDM), filtered multitone (FMT), and discrete wavelet multitone (DWMT) [28–34]. In this section, these schemes are described and analyzed. We start the section by describing a general filter bank transceiver which, as will be seen later in this section, can model each of these schemes. In addition, in Chapter 4 a new windowed DMT system is proposed which has the same general structure as in the filter bank transceiver described in this section.

2.1.1 General filter bank transceiver

Figure 2.1 shows a filter bank transceiver with M subchannels, where $x_i[n]$ and $y_i[n]$, $i = 0, 1, \cdots, M-1$, denote the input and output symbols of the ith subchannel at instant n, respectively. In this system, sequences of complex-valued symbols chosen from not necessarily identical constellations are input into the system at a symbol rate $1/T$.[1] The inputs to the subchannels are first upsampled by a factor of N, and then filtered by the corresponding subchannel transmitter (pulse shaping) filters. In Figure 2.1, the impulse responses of the subchannel transmit filters are denoted by $h_i[n]$, $0 \leq i \leq M-1$. The outputs of the subchannel transmit filters are then added together. converted to an analog signal using a digital to analog converter at a sampling rate of $1/T_s = N/T$, and transmitted through the communication channel. At the receiver, after analog to digital conversion of the received signal, it is sent to M branches corresponding to the M subchannels. In each branch, the received signal is first filtered by the corresponding subchannel receiver filter, denoted

[1] Although the size of constellation used for different subchannels is generally different, the constellation family of choice is usually the quadrature amplitude modulation (QAM).

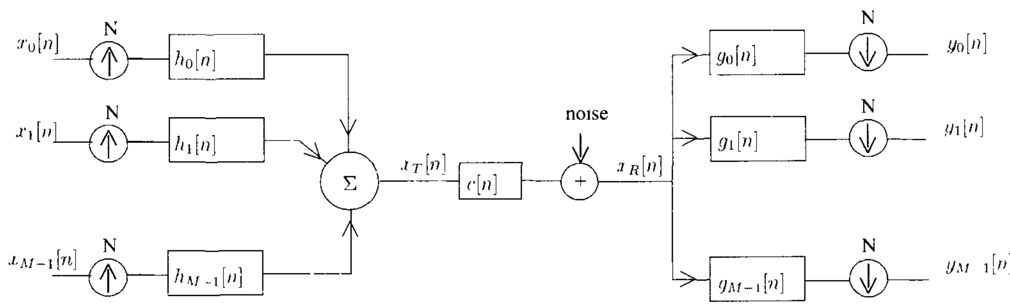

Figure 2.1: M-subchannel filter bank transceiver.

in Figure 2.1 by $g_i[n]$, $0 \leq i \leq M-1$, and then it is downsampled by a factor of N. In Figure 2.1, $c[n]$ denotes the impulse response of the equivalent discrete-time channel impulse response corresponding to the combination of the digital to analog converter, the analog channel, and the analog to digital converter. The additive noise in Figure 2.1 models all external additive noise and interferences. The filter bank transceiver of Figure 2.1 is called a critically sampled filter bank if $N = M$, and is called an oversampled filter bank if $N > M$.

In the following, the relation between the subchannel inputs and outputs of the filter bank transceiver of Figure 2.1 is derived. By applying the time-domain equation for upsampling [35] and convolution of the transmitter filters, the digital signal to be transmitted, i.e., $x_T[n]$ in Figure 2.1, can be written as

$$x_T[n] = \sum_{i=0}^{M-1} \sum_{k=-\infty}^{\infty} x_i[k] h_i[n-kN]. \tag{2.1}$$

Therefore, assuming that the channel is of order L, i.e.,

$$c[n] = 0, \quad n \notin [0, L], \tag{2.2}$$

the received signal, $x_R[n]$ of Figure 2.1, is given by

$$x_R[n] = \sum_{p=0}^{L} c[p] \sum_{i=0}^{M-1} \sum_{k=-\infty}^{\infty} x_i[k] h_i[n-p-kN] + \zeta[n]. \tag{2.3}$$

where $\zeta[n]$ represents the external additive noise and interference signals. The mth subchannel output, $y_m[n]$, is obtained by filtering $x_R[n]$ by $g_m[n]$ and downsampling by N. Therefore, $y_m[n]$ is given by

$$y_m[n] = \sum_{\ell=-\infty}^{\infty} g_m[\ell] \sum_{p=0}^{L} c[p] \sum_{i=0}^{M-1} \sum_{k=-\infty}^{\infty} x_i[k] h_i[Nn - \ell - p - kN] + v_m[n] \tag{2.4}$$

where $v_m[n]$ represents the additive noise after being filtered by $g_m[n]$ and downsampled by factor N, that is,

$$v_m[n] = \sum_{k=-\infty}^{\infty} g_m[k]\zeta[Nn - k] \tag{2.5}$$

The result in (2.4) can be equivalently written as

$$y_m[n] = \sum_{i=0}^{M-1} x_i[n] \star q_{mi}[n] + v_m[n] \tag{2.6}$$

$$= \sum_{i=0}^{M-1} \sum_{k=-\infty}^{\infty} x_i[n-k] q_{mi}[k] + v_m[n], \tag{2.7}$$

where $\star$ denotes the convolution operator, and

$$q_{mi}[n] = c_{mi}[Nn] \tag{2.8}$$

where

$$c_{mi}[n] = h_i[n] \star c[n] \star g_m[n]. \tag{2.9}$$

Notice that (2.4)-(2.9) represent the input-output formulas for the general filter bank transceiver of Figure 2.1. From (2.4), it can be seen that, in general, the output of each subchannel at an instant n can depend on all subchannel inputs at all time instants. Thus, in general, at each subchannel output, both intersubchannel interference (ICI) and intrasubchannel intersymbol interference (ISI) are present. More specifically, if k_0 denotes the synchronization delay of the system, then, for subchannel m, the term $\sum_{k\neq k_0} x_m[n-k]q_{mm}[k]$ in (2.7) is the ISI, and $\sum_{i\neq m}\sum_k x_i[n-k]q_{mi}[k]$ is the ICI.

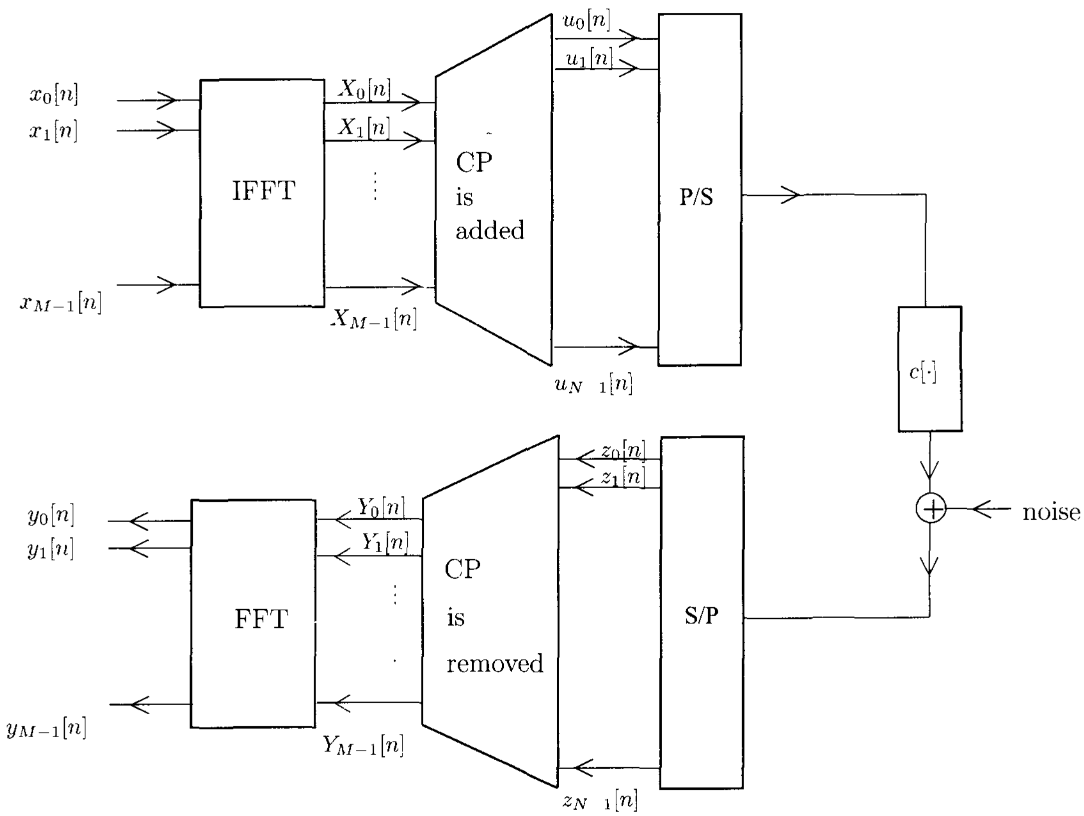

Figure 2.2: The basic DMT system with M subchannels and a cyclic prefix of length $P = N - M$.

2.1.2 DMT and OFDM transceivers

Fig. 2.2 shows the basic DMT communication system. Recall from Chapter 1 that DMT and OFDM systems are similar except that in OFDM systems a fixed number of bits and power is assigned to the subchannels while in DMT system different number of bits are assigned to different subchannels based on the signal to noise ratio (SNR) of the subchannel outputs at the receiver. Therefore, Fig. 2.2 models both DMT and OFDM systems. In the rest of this section we will use the term DMT for the system of Fig 2.2. In this system, sequences of complex-valued symbols chosen from not necessarily identical constellations are input into the system at a symbol rate $1/T$. The symbol $x_i[n]$ denotes the input to the ith subchannel at instant n. In other words, at each instant n, a symbol block of size M is input to the system. Therefore, we can refer to n as the block index. At the transmitter, an M-point inverse Fourier transform (IFFT) is applied to the inputs, $x_i[n]$, $i = 0, 1, \cdots, M-1$, which results in $X_k[n]$, $k = 0, 1, \cdots, M-1$. A cyclic prefix[2] (CP) of length P is then added which produces $u_k[n]$, $k = 0, 1, \cdots, N-1$, where $N = M + P$. The result is transformed to a serial sequence using a parallel to serial converter (P/S), then it is converted to an analog signal using a digital to analog converter (D/A) at a sampling rate of $1/T_s = N/T$, and the analog signal is transmitted over the communication channel. The received signal is transformed to a discrete-time sequence using an analog to digital converter (A/D), then using a serial to parallel converter (S/P) it is transformed to the parallel form, the cyclic prefix is removed, and an M-point fast Fourier transform (FFT) is applied. The relationship between inputs and outputs of this system is analyzed below. Notice that the equivalent of the cascade of the D/A, the analog channel impulse response, and the A/D is denoted by the discrete-time channel impulse response $c[\cdot]$. We assume that the discrete-time channel impulse response is of order L, specifically, we assume that

$$c[k] = 0, \quad k \notin [0, L] \tag{2.10}$$

The most convenient way to analyze the DMT system of Fig. 2.2 is to use the matrix form [29]. Denoting the input block at instant n by the $M \times 1$ vector $\mathbf{x}_n$ we have

$$\mathbf{x}_n = (x_0[n], x_1[n], \cdots, x_{M-1}[n])^T \tag{2.11}$$

where the superscript T denotes the matrix transpose. After applying the M-point

[2]The structure of this cyclic prefix will be defined later in this section; see (2.17) and (2.18).

IFFT, the $M \times 1$ vector $\mathbf{X}_n$ is obtained where

$$\mathbf{X}_n = (X_0[n], X_1[n], \cdots, X_{M-1}[n])^T \tag{2.12}$$

and

$$X_i[n] = \frac{1}{\sqrt{M}} \sum_{k=0}^{M-1} x_k[n] e^{j\frac{2\pi}{M}ki} \tag{2.13}$$

Equivalently, in matrix form, $\mathbf{X}_n$ can be computed from $\mathbf{x_n}$ as

$$\mathbf{X}_n = \mathbf{F}^H \mathbf{x}_n \tag{2.14}$$

where the superscript H denotes the matrix Hermitian (conjugate transpose) and $\mathbf{F}$ is the M-point FFT matrix ($M \times M$) in which the (k, n)th entry is given by

$$[\mathbf{F}]_{k,n} = \frac{1}{\sqrt{M}} e^{-j\frac{2\pi}{M}kn}. \tag{2.15}$$

(Since the FFT is an orthogonal transform, $\mathbf{F}\mathbf{F}^H = \mathbf{F}^H\mathbf{F} = \mathbf{I}_M$, where $\mathbf{I}_M$ is the $M \times M$ identity matrix.) After applying the IFFT, a cyclic prefix of length P is added to the signal which results in the $N \times 1$ vector $\mathbf{u}_n$, where $N = M + P$,

$$\mathbf{u}_n = (u_0[n], u_1[n], \cdots, u_{N-1}[n]) \tag{2.16}$$

and

$$\mathbf{u}_n = \mathbf{T}\mathbf{X}_n \tag{2.17}$$

where $\mathbf{T}$ is the $N \times M$ matrix defined as

$$\mathbf{T} = \begin{pmatrix} \mathbf{I}_{\mathrm{CP}} \\ \mathbf{I}_M \end{pmatrix} \tag{2.18}$$

which is a concatenation of the $M \times M$ identity matrix $\mathbf{I}_M$ and $\mathbf{I}_{\mathrm{CP}}$ which consists of the last P rows of $\mathbf{I}_M$. In other words, the CP adder module adds the last P samples of the IFFT output to the beginning of the block. Specifically,

$$\mathbf{u}_n = (X_{M-P}[n], X_{M-P+1}[n], \cdots, X_{M-1}[n], X_0[n], X_1[n], \cdots, X_{M-1}[n])^T \tag{2.19}$$

Denoting the outputs of the serial to parallel converter at the receiver by the $N \times 1$ vector $\mathbf{z}_n$, the combination of the parallel to serial conversion at the transmitter, the convolution performed by the channel impulse response $c[\cdot]$, and the serial to parallel conversion at the receiver can be represented in the matrix form as [29]

$$\mathbf{z}_n = \mathbf{C}_0\mathbf{u}_n + \mathbf{C}_1\mathbf{u}_{n-1} + \boldsymbol{\eta}_n \tag{2.20}$$

where $\mathbf{C}_0$ and $\mathbf{C}_1$ are the $N \times N$ channel matrices defined as

$$[\mathbf{C}_0]_{i,k} = c[i-k] \tag{2.21}$$

and

$$[\mathbf{C}_1]_{i,k} = c[N+i-k] \tag{2.22}$$

and $\boldsymbol{\eta}_n$ represents the $N \times 1$ vector of the additive noise, that is,

$$\boldsymbol{\eta}_n = (\eta_0[n], \eta_1[n], \cdots, \eta_{N-1}[n])^T \tag{2.23}$$

The removal of cyclic prefix at the receiver can be written in the matrix form as

$$\mathbf{Y}_n = \mathbf{R}\mathbf{z}_n \tag{2.24}$$

where $\mathbf{Y}_n$ is the $M \times 1$ vector representing the output of the CP removal module and is given by

$$\mathbf{Y}_n = (Y_0[n], Y_1[n], \cdots, Y_{M-1}[n])^T \tag{2.25}$$

and $\mathbf{R}$ is the $M \times N$ CP removal matrix given by

$$\mathbf{R} = (\mathbf{0}_{M\times P}\,\mathbf{I}_M) \tag{2.26}$$

where $\mathbf{0}_{M\times P}$ is the $M \times P$ matrix with all entries equal to zero. Finally, the FFT transform at the receiver can be represented in the matrix form as

$$\mathbf{y}_n = \mathbf{F}\mathbf{Y}_n \tag{2.27}$$

where $\mathbf{F}$ is the FFT matrix defined in (2.15) and $\mathbf{y}_n$ is the $M \times 1$ output vector given by

$$\mathbf{y}_n = (y_0[n], y_1[n], \cdots, y_{M-1}[n]) \tag{2.28}$$

Substituting (2.20) into (2.24) and the result into (2.27), it can be seen that

$$\mathbf{y}_n = \mathbf{FR}(\mathbf{C}_0\mathbf{u}_n + \mathbf{C}_1\mathbf{u}_{n-1} + \boldsymbol{\eta}_n) \tag{2.29}$$

Referring to the structure of $\mathbf{R}$ defined in (2.26) and that of $\mathbf{C}_1$ defined in (2.22), and recalling the non-zero interval of the channel impulse response given by (2.10), one can verify that if $P \geq L$, i.e., if the cyclic prefix length is at least equal to the order of the channel impulse response, we have $\mathbf{RC}_1 = \mathbf{0}_{M\times N}$. In that case, (2.29) can be simplified to

$$\mathbf{y}_n = \mathbf{FRC}_0\mathbf{u}_n + \mathbf{FR}\boldsymbol{\eta}_n \tag{2.30}$$

Substituting (2.14) into (2.17) and the result into (2.30), the following is obtained

$$\mathbf{y}_n = \mathbf{FRC}_0\mathbf{TF}^H\mathbf{x}_n + \mathbf{FR}\boldsymbol{\eta}_n \tag{2.31}$$

It can be shown [29] that $\mathbf{RC}_0\mathbf{T}$ is a circulant matrix. Moreover, it is well known that a circulant matrix can be diagonalized by pre- and post-multiplication with FFT and IFFT matrices. Specifically, it can be shown that [29]

$$\mathbf{FRC}_0\mathbf{TF}^H = \mathbf{D} = \mathrm{diag}\left(C(e^{j0}), C(e^{j\frac{2\pi}{M}}), \cdots, C(e^{j\frac{2\pi}{M}(M-1)})\right) \tag{2.32}$$

where $C(e^{j\omega})$ is the Fourier transform of $c[k]$, i.e., $C(e^{j\omega}) = \sum_{k=0}^{L} c[k]e^{-j\omega k}$. Substituting (2.32) into (2.31), we get

$$\mathbf{y}_n = \mathbf{D}\mathbf{x}_n + \tilde{\boldsymbol{\eta}}_n \tag{2.33}$$

where $\tilde{\boldsymbol{\eta}}_n = \mathbf{FR}\boldsymbol{\eta}_n$. Since $\mathbf{D}$ is a diagonal matrix (defined in (2.32)), (2.33) can be equivalently written as

$$y_i[n] = C(e^{j\frac{2\pi}{M}i})x_i[n] + \tilde{\eta}_i[n], \quad i = 0, 1, \cdots, M-1 \tag{2.34}$$

where $\tilde{\eta}_i[n]$ is the ith entry of $\tilde{\boldsymbol{\eta}}_n$, and therefore

$$\tilde{\eta}_i[n] = \frac{1}{\sqrt{M}} \sum_{\ell=0}^{M-1} e^{-j\frac{2\pi}{M}i\ell} \eta_{P+\ell}[n] \tag{2.35}$$

The formula in (2.34) defines the input-output relation for the ith subchannel in the DMT system of Fig. 2.2. From (2.34) it can be seen that in the DMT system, the whole frequency-selective channel is divided into M frequency-flat subchannels, where $x_i[n]$, $i = 0, 1, \cdots, M-1$, are the subchannel input sequences and $y_i[n]$, $i = 0, 1, \cdots, M-1$, are the subchannel output sequences, and $C(e^{j\frac{2\pi}{M}i})$ is the (complex) gain of the ith consequent frequency-flat subchannel. From (2.34) one can see that the output of the ith subchannel consists of two terms, a signal term and a noise term, where the signal term is equal to the transmitted symbol through that subchannel, i.e., $x_i[n]$, multiplied by the ith entry of the discrete Fourier transform (DFT) of the channel impulse response. Notice from (2.34) that the output of each subchannel at a specific time instant, depends on the input signal of that subchannel at the same time instant, but there is no interference from other subchannels, i.e., no ICI, and that there is no interference from the input sequence of that subchannel corresponding to other time instants, i.e., there is no ISI. Recall that this zero ISI and zero ICI property of the DMT system was obtained under the assumption that the length of the cyclic prefix is larger than or equal to the order of the channel impulse response., i.e., $P \geq L$.

Since the subchannel outputs of the DMT system (when $P \geq L$) are free from ISI and ICI, one-tap per subchannel equalization is sufficient for channel equalization. Specifically, from (2.34), it can be seen that for the ith subchannel, if $C(e^{j\frac{2\pi}{M}i}) \neq 0$, the channel effect can be equalized by multiplying $y_i[n]$ by $1/C(e^{j\frac{2\pi}{M}i})$. This one-tap per subchannel equalization in DMT systems is referred to as frequency-domain equalization (FEQ).[3] If $C(e^{j\frac{2\pi}{M}i}) = 0$, no data should be transmitted on the ith

[3]Since this equalization takes place after the FFT module, it is known as the frequency-domain equalizer (FEQ). This is in contrast to the time-domain equalization which takes place before FFT module. Time-domain equalizers are studied in Section 2.2.

subchannel, as the receiver will not be able to recover it.

The architecture that was presented for the DMT system in Figure 2.2 represents an efficiently implementable structure for DMT system. In addition, in the literature this is the structure that is usually used to describe the DMT system. On the other hand, in the following it is shown that the DMT system of Figure 2.2 can be equivalently represented using the general filter bank transceiver of Figure 2.1.

Consider the filter bank structure of Figure 2.1 with the parameters M, N, and L being the same defined in the above discussion; that is, M is the number of subchannels and $N = M + P$, where P is the cyclic prefix length, and L is the order of the channel, where it is assumed that $L \leq P$. Moreover, assume the following DFT modulated structure for the transmit and receive filters

$$h_i[n] = h[n]e^{j\frac{2\pi}{M}in}, \tag{2.36}$$

$$g_m[n] = g[n]e^{j\frac{2\pi}{M}mn}, \tag{2.37}$$

where[4]

$$h[n] = \begin{cases} 1/\sqrt{M}, & n \in [-N, -1] \\ 0, & n \notin [-N, -1] \end{cases} \tag{2.38}$$

and

$$g[n] = \begin{cases} 1/\sqrt{M}, & n \in [1, M] \\ 0, & n \notin [1, M] \end{cases} \tag{2.39}$$

Substituting (2.36)-(2.39) into (2.4), one can verify that

$$y_m[n] = \sum_{i=0}^{M-1} x_i[n] \sum_{p=0}^{L} c[p]e^{-j\frac{2\pi}{M}ip} \sum_{\ell=1}^{M} \frac{1}{M}e^{j\frac{2\pi}{M}\ell(m-i)} + v_m[n] \tag{2.40}$$

On the other hand,

$$\sum_{\ell=1}^{M} \frac{1}{M}e^{j\frac{2\pi}{M}\ell(m-i)} = \begin{cases} 1, & m = i \\ 0, & m \neq i \end{cases} \tag{2.41}$$

[4]Here, $h[n]$ and $g[n]$ are chosen so that the filter bank transceiver of Figure 2.1 models the DMT system. Consequently, $h[n]$ is chosen to be a non-causal filter in order to achieve an input-output equation for the filter bank model identical to that for the DMT system.

Therefore,

$$y_m[n] = x_m[n]\sum_{p=0}^{L} c[p]e^{-j\frac{2\pi}{M}mp} + v_m[n] \tag{2.42}$$

which can be further simplified to

$$y_m[n] = x_m[n]C(e^{j\frac{2\pi}{M}m}) + v_m[n] \tag{2.43}$$

where $C(e^{j\omega}) = \sum_{p=0}^{L} c[p]e^{-j\omega p}$ is the Fourier transform of $c[n]$. Comparing (2.43) with (2.34) it can seen that if $v_m[n] = \tilde{\eta}_m[n]$, the DMT system of Figure 2.2 is equivalent to the filter bank transceiver of Figure 2.1 when (2.36)-(2.39) hold. In the following it is shown that $v_m[n] = \tilde{\eta}_m[n]$. Recall that $v_m[n]$ is given by (2.5). After substitution of (2.37) and (2.39), (2.5) simplifies to

$$v_m[n] = \frac{1}{\sqrt{M}}\sum_{k=1}^{M} e^{j\frac{2\pi}{M}mk}\zeta[Nn-k] \tag{2.44}$$

On the other hand, from (2.35) $\tilde{\eta}_m[n]$ is given by

$$\tilde{\eta}_m[n] = \frac{1}{\sqrt{M}}\sum_{\ell=0}^{M-1} e^{-j\frac{2\pi}{M}m\ell}\eta_{P+\ell}[n] \tag{2.45}$$

Since n in $\eta_k[n]$ denotes the nth block transmission of size N, $\eta_k[n]$ in Figure 2.2 is related to $\zeta[\cdot]$ in Figure 2.1 as

$$\eta_i[n] = \zeta[N(n-1)+i], \quad i = 0, 1, \cdots, N-1 \tag{2.46}$$

Substituting (2.46) into (2.45) and defining $k = -\ell + M$ will result in

$$\tilde{\eta}_m[n] = \frac{1}{\sqrt{M}}\sum_{k=1}^{M} e^{j\frac{2\pi}{M}mk}\zeta[Nn-k] \tag{2.47}$$

comparing (2.47) with (2.44) it can be seen that $v_m[n] = \tilde{\eta}_m[n]$.

2.1.3 FMT transceivers

DMT and OFDM are the most widely-used multi-carrier systems due to their relatively low complexity. They have an efficient FFT-based structure (see Figure 2.2) which allows a cost-effective silicon implementation as a system on chip (SOC). even for large number of subchannels. Moreover, they enjoy very simple per subchannel equalization, as was explained in the previous section. Finally, the most attractive feature of DMT and OFDM is that these systems provide ISI-free and ICI-free outputs for any FIR channel with an order less than or equal to the length of the cyclic prefix used in those systems.

That said, DMT (and OFDM) systems have some shortcomings. First, DMT requires a cyclic prefix which is not smaller than the order of the channel. This reduces the bandwidth efficiency [5], especially when the channel impulse response is long. In such cases, insertion of the cyclic prefix would either impose a significant reduction of bandwidth efficiency or it would require the use of a very large number of subchannels. which in turn increases the complexity of the system. Another shortcoming of the DMT system is its poor spectral characteristics at the transmitter and receiver. It was mentioned in Section 2.1.2 that the DMT system can be equivalently modelled with a filter bank transceiver in which the transmitter pulse shaping filters and receiver filters of the subchannels have rectangular time-domain impulse responses. Therefore, the frequency response of the transmit and receive filters of the subchannels are sinc functions.[6] It is well-known that the sinc function has large sidelobes which decay slowly. Consequently, the DMT system suffers from poor subchannel spectral containment at the transmitter and poor subchannel spectral selectivity at the receiver. The poor spectral characteristics of DMT and OFDM systems at the transmitter

[5]The bandwidth efficiency is defined as the communication binary data rate divided by the used bandwidth. Denoting the binary data rate in units of bit per second (bps) by r, and the transmission bandwidth in units of Hz by B, the bandwidth efficiency is defined as r/B (bps/Hz).

[6]The sinc function is defined as $\mathrm{sinc}(x) = \frac{\sin(\pi x)}{\pi x}$.

makes it quite awkward for these systems to meet some of the egress requirements set in the communication standards. Moreover, the poor spectral characteristics of DMT and OFDM systems at the receiver makes these systems susceptible to narrowband noise, near-end crosstalk, and imperfections, such as frequency offset between the local oscillators at the transmitter and receiver, phase noise and Doppler spread.

Filtered multitone (FMT) [26] is an alternative multi-carrier communication scheme with somewhat different characteristics and trade-offs than those of the DMT scheme. FMT is a filter bank transceiver in which the pulse shaping filter for each of the subchannels at the transmitter is a frequency-shifted version of a prototype filter and the receiver filter of each subchannel is the matched filter of the corresponding transmitter filter.[7] In an FMT system, the prototype filter is designed so that a high level of subchannel spectral containment is achieved, and hence the ICI is negligible compared to other noise and interference signals [26].

Recall the filter bank transceiver model in Figure 2.1. For that transceiver to model an FMT system, the impulse response of the subchannel filters at the transmitter, $h_i[n]$, $0 \leq i \leq M-1$, and that of the subchannel filters at the receiver, $g_i[n]$, $0 \leq i \leq M-1$, are given as

$$h_i[n] = h[n]e^{j\frac{2\pi}{M}in} \tag{2.48}$$

and

$$g_i[n] = h_i^*[-n] \tag{2.49}$$

where $h[n]$ is the impulse response of the prototype filter of the FMT system, and the superscript $*$ denotes the complex conjugate operator. Denoting the Fourier transforms of $h_i[n]$, $h[n]$, and $g_i[n]$ by $H_i(e^{j\omega})$, $H(e^{j\omega})$, and $G_i(e^{j\omega})$, respectively, (2.48) and (2.49) are translated into the frequency domain as

$$H_i(e^{j\omega}) = H(e^{j(\omega-\omega_i)}) \tag{2.50}$$

[7] A filter bank in which the branch filters are frequency-shifted versions of a prototype filter is often called a DFT modulated filter bank [35].

and

$$G_i(e^{j\omega}) = H^*(e^{j(\omega-\omega_i)}) \tag{2.51}$$

where

$$\omega_i = \frac{2\pi}{M}i \tag{2.52}$$

As mentioned earlier, in an FMT transceiver, the prototype filter has to be designed in a way that a high level of subchannel spectral containment is achieved so that at the subchannel outputs, ICI is negligible compared to other noise and interference signals [26].

Recall the filter bank structure of the FMT system in Figure 2.1. By upsampling each subchannel input by a factor of N in the time domain, the Fourier transform of the corresponding signal is shrunk by a factor of N. Let us denote the Fourier transform of $x_i[n]$ by $X_i(e^{j\omega})$. Since $X_i(e^{j\omega})$ is periodic in frequency with period 2π, after upsampling by N, the consequent signal is periodic in frequency with period $2\pi/N$. In an ideal FMT system, $H(e^{j\omega})$ is an ideal lowpass filter with the passband $\omega \in [-\pi/M, \pi/M]$. This is shown in Figure 2.3. With such a prototype filter, if we choose $N = M$, since $H_i(e^{j\omega})$ is the frequency shifted version of $H(e^{j\omega})$ by the amount of $\omega_i = \frac{2\pi}{M}i$, the whole 2π bandwidth is divided into M orthogonal subchannels. With this ideal prototype filter, the receiver filter of the ith subchannel, $G_i(e^{j\omega})$, would filter out all other subchannel signals and the signal corresponding to the ith subchannel would be passed through. In that case, because of the orthogonality of the subchannels, there will be no intersubchannel interference (ICI). Therefore, the equalization of each subchannel can be done independently, i.e., at the receiver, only per subchannel equalization will be required. Notice that since the ideal prototype filter has a frequency-flat transfer function in the passband, no ISI will be imposed by the filter bank. The only ISI incurred on each subchannel will be the ISI created by the portion of the channel that resides in the subchannel bandwidth.

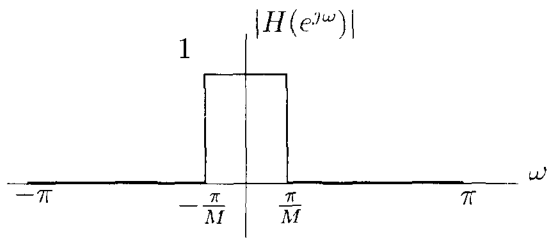

Figure 2.3: Ideal lowpass filter with a bandwidth $2\pi/M$.

However, the ideal prototype filter of Figure 2.3 has an infinitely long impulse response and it is not realizable in practice. A practical FMT system has an FIR prototype filter, which inevitably, has a non-rectangular frequency response. Such a frequency response has two shortcomings. Firstly, it is not flat in the passband, and as a result some ISI is imposed to the subchannel outputs by the transmit and receive filters, in addition to the ISI created by the communication channel. Secondly, the energy of an FIR prototype filter in the stopband is not equal to zero, and this causes ICI.

In order to allow per subchannel detection while using a prototype filter with a limited complexity, in the FMT systems over-sampled filter banks are usually employed. In an over-sampled filter bank, the up- and down-sampling factor is chosen to be larger than the number of subchannels, i.e., $N > M$. This creates an excess bandwidth equal to

$$\text{Excess bandwidth} = \frac{N}{M} - 1 \tag{2.53}$$

which provides a guard band for the subchannel spectrum. While the excess bandwidth reduces the bandwidth efficiency, it allows the possibility of suppressing the ICI when the prototype filter is appropriately designed. Notice from (2.50)-(2.52) that since there are M subchannels in the system, the bandwidth allocated to each subchannel is equal to $2\pi/M$. On the other hand, after upsampling the subchannel inputs by a factor of N, the subchannel signals will have a bandwidth of $2\pi/N$, which is smaller than the available bandwidth of $2\pi/M$. This excess bandwidth makes it possible for the frequency response of the prototype filter to have a smoother transition from the passband to the stopband. Recall that a sharper transition in the frequency response requires a longer impulse response in the time domain [36]. Thus, by allowing a non-zero excess bandwidth, it becomes possible to implement the filter bank with lower complexity. On the other hand, by introducing a nonzero excess bandwidth, a redundancy is introduced which reduces the bandwidth efficiency. The larger the excess bandwidth, the smaller the bandwidth efficiency. Thus an appropriate value should be chosen for the excess bandwidth to keep a balance in the trade-off between the cost of implementation and the reduction in the bandwidth efficiency. Some typical values for the excess bandwidth in FMT systems are 6.25%, and 12.5%.

In an FMT system, the design of the prototype filter is a key design challenge. One of the contributions of this thesis is a new design method for the prototype filter of the FMT system that is based on the trade-off between the ISI and ICI caused by the filter bank. This is presented in Chapter 3; see also [37, 38].

Recall the input-output equation for the filter bank transceiver of Figure 2.1 given by (2.4). From that equation, it can be seen that for the mth subchannel the output at an instant n depends on all subchannel inputs at all time instants. Thus, in general, at each subchannel output, both ICI and ISI are present. As was mentioned earlier, in an FMT system, the subchannel transmit and receive filters are designed so that ICI is negligible. In order to get a better understanding about the mechanism of ICI removal in FMT, we point out that the equivalent of (2.9) in the frequency domain is given by

$$C_{mi}(e^{j\omega}) = H_i(e^{j\omega})C(e^{j\omega})G_m(e^{j\omega}) \tag{2.54}$$

where $C_{mi}(e^{j\omega})$ is the Fourier transform of $c_{mi}[n]$. Recall from (2.50)-(2.52) that $H_i(e^{j\omega})$ is shifted version of $H(e^{j\omega})$ by $w_i = i\frac{2\pi}{M}$ and $G_m(e^{j\omega})$ is the shifted version of $H^*(e^{j\omega})$ by $w_m = m\frac{2\pi}{M}$, and recall that the passband of $H(e^{j\omega})$ is defined as

$-\pi/M < \omega < \pi/M$. Therefore, if the energy of the prototype filter in its stopband is small enough, the product of $H_i(e^{j\omega})G_m(e^{j\omega})$ is negligible unless $i = m$. In that case, from (2.54) it can be seen that $C_{mi}(e^{j\omega})$ will be negligible for $m \neq i$, and thus, in (2.6), among all the terms in the summation, only the term corresponding to $i = m$ will be non-negligible. In that case, (2.6) simplifies to

$$y_m[n] \approx x_m[n] \star q_{mm}[n] + v_m[n] \tag{2.55}$$

which implies that ICI will be negligible. That said, the convolution of $x_m[n]$ and $q_{mm}[n]$ in (2.55) implies the existence of ISI terms in the subchannel outputs. However, because of the subchannel transmit and receive filtering, only a bandwidth equal to $2\pi/M$ of the channel is seen by each subchannel. Thus, if the number of subchannels is large enough, the frequency selectivity of the portion of the channel seen by each subchannel will be much less than that of the whole channel, and the amount of ISI at the output of each subchannel can be small. In Chapter 3, we will see that in order to maximize the achievable bit rate in FMT systems, the prototype filter has to be designed so that at the same time that ICI is forced to be small, a balance is obtained between the ISI and ICI imposed by the prototype filter.

As an example, Figure 2.4 shows the frequency response of a prototype filter for an FMT system with $M = 32$ subchannels, up- and down-sampling factor $N = 36$ (excess bandwidth 12.5%), and a length of 320 for the impulse response of the prototype filter. This prototype filter has been designed by the design method which will be presented in Chapter 3 and, as shown in that chapter, it provides an appropriate balance between the ISI and ICI created by the prototype filter. For comparison, the frequency response of an ideal prototype filter is also plotted in that figure. Moreover, a sinc function, corresponding to a rectangular impulse response of length $N = 36$ is also shown in Figure 2.4. This corresponds to the transmitter prototype filter of a DMT system with $M = 32$ subchannels and a cyclic prefix of length $P = 4$, i.e.,

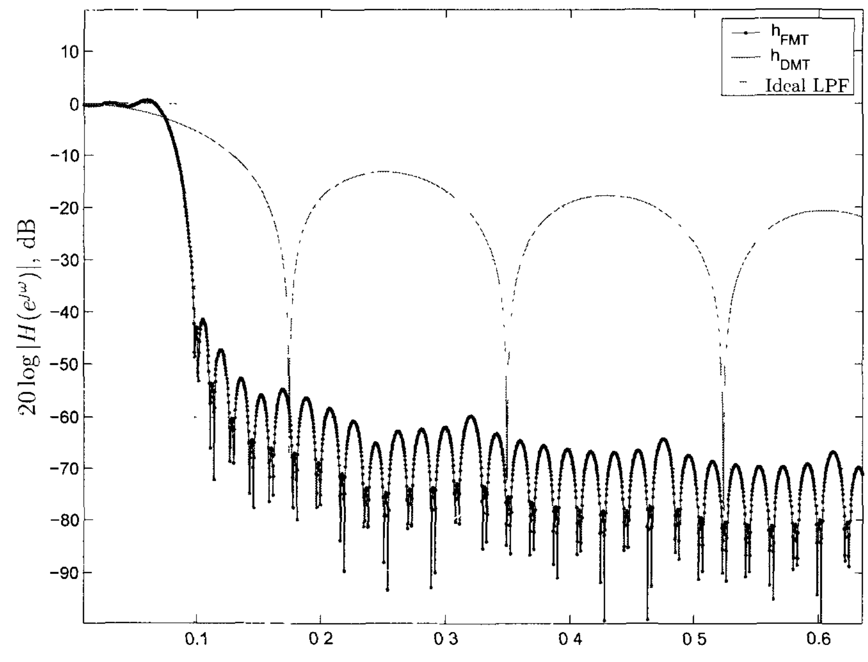

Figure 2.4: Frequency response of a typical prototype filter for an FMT system with $M = 32$ subchannels and an excess bandwidth of 12.5%, i.e. $N = 36$ (h_{FMT}). For comparison, the frequency response of the transmitter prototype filter in a DMT system with the same number of subchannels and excess bandwidth is also shown (h_{DMT}), as is the frequency response of an ideal prototype filter.

transmission block size of $N = M + P = 36$.[8]

In Figure 2.4 the frequency response of the ideal prototype filter can be used as a reference to distinguish the passband and the stopband (see Figure 2.3). From Figure 2.4 looking at the frequency response of the FMT prototype filter it can be seen that the level of sidelobes in the stopband are more than 40 dB below the maximum level in the passband. In comparison, it can be seen that the transmitter prototype filter of a DMT system has very large sidelobes which decay slowly, and even its main lobe is not confined within the passband.

[8]Recall from Section 2.1.2 that the DMT transceiver can be modelled by the filter bank transceiver of Figure 2.1 in which the transmitter filters have rectangular impulse responses of length $N = M+P$, and receiver filters have rectangular impulse responses of length M.

The improved spectral characteristics of FMT compared to DMT provide a number of advantages for FMT systems. Specifically, the small stopband energy of the prototype filter in the FMT transceivers, makes these systems robust to narrowband noise and interferences, such as the radio frequency interference (RFI) emerging from the amplitude modulation (AM) broadcast and amateur radio (HAM) signals in digital subscriber lines. Moreover, small stopband energy of the prototype filter of FMT systems, reduces the impact of near-end crosstalk (NEXT) in these systems. In some applications, such as in digital subscriber lines, NEXT is one of the very harmful types of noise and interference affecting the transmitted signal. In addition, the high level of subchannel spectral containment in the FMT systems makes FMT systems robust against other imperfections such as frequency offset between the local oscillators at the transmitter and receiver, phase noise, and Doppler spread.

That said. FMT has a few shortcomings compared to DMT. First of all, as can be seen from (2.55), some ISI is present at the subchannel outputs of an FMT system. Consequently, per-subchannel equalization is required. Typically, decision feedback equalizers (DFEs) are used for per-subchannel equalization in FMT systems [26, 37–39]. Some other equalization approaches for the FMT system have been developed and studied in [40, 41]. A second shortcoming of the FMT system is that in order to obtain a negligible level of ICI, the length of the prototype filter has to be quite large, typically about ten times the number of subchannels [26, 37]. In the example of Figure 2.4, $M = 32$ and the impulse response of the prototype filter is of length 320. Finally, although the FMT system can be realized using an efficient FFT-based polyphase implementation [26, 35, 42, 43], its implementation remains more complicated than that of DMT [26, 28].

2.1.4 DWMT transceivers

Discrete wavelet multitone (DWMT) represents another family of multi-carrier communication systems [27]. The DWMT transceiver has the general filter bank structure of Figure 2.1, and to allow an efficient polyphase-based implementation, its filter bank is usually a DFT modulated filter bank [27, 35, 43], a cosine-modulated filter bank [27, 44, 45], or a binary tree structured filter bank [46, 47]. In DWMT systems, in order to allow a large bandwidth efficiency and efficient implementation, critically-sampled filter banks are used, i.e., $M = N$ [35, 48].

The criterion for the design of the prototype filters in DWMT systems is to achieve the perfect reconstruction condition [35, 48] in the absence of channel distortion.[9] Consider the filter bank transceiver of Figure 2.1 and recall that the relation between the subchannel outputs and subchannel inputs is given by (2.4)-(2.9). To obtain a perfect reconstruction filter bank, it is assumed that the channel is ideal, i.e.,

$$c[n] = \delta[n] \tag{2.56}$$

where $\delta[\cdot]$ is the Kronecker delta function. The filter bank of Figure 2.1 is called a perfect reconstruction filter bank if, assuming the ideal channel of (2.56), the subchannel outputs are free from ICI and free from ISI. From (2.6), the perfect reconstruction condition can be written as

$$q_{mi}[n] = \beta\delta[m-i]\delta[n] \tag{2.57}$$

where β is a non-zero constant. Using (2.7), (2.9), and (2.56), the perfect reconstruction condition in (2.57) can be equivalently written as

$$\sum_{k=-\infty}^{\infty} h_i[k]g_m[Nn-k] = \beta\delta[m-i]\delta[n] \tag{2.58}$$

[9]The perfect reconstruction condition is a well-known condition in the design of filter bank transceivers [48, 49].

In [27], matched filtering is used at the receiver. In that case, we have

$$g_k[n] = h_k^*[-n] \tag{2.59}$$

Even with the assumption of matched filtering at the receiver, the answer to (2.58) is not unique. This degree of freedom allows to design filters with different spectral characteristics. The prototype filter in DWMT system is usually designed so that the perfect reconstruction condition in (2.58) is satisfied and the stopband energy of the prototype filter is minimized [27].

Compared to DMT, DWMT system can provide improved subchannel spectral characteristics and ISI-free and ICI-free outputs for an ideal channel. However, when the channel is frequency-selective, the subchannels will no longer be orthogonal, and both ISI and ICI will appear in the subchannel outputs. It has been proposed [27,50] that a time-domain equalizer be used at the receiver, right before the receiver filter bank, to shorten the impulse response of the channel, so that smaller values of ISI and ICI appear at the subchannel outputs. Yet, even with the use of TEQs, in practical broadband scenarios, e.g., in very high-speed digital subscriber line (VDSL) systems, a considerable amount of ISI and ICI can appear in the subchannel outputs of the DWMT systems. Therefore, in a DWMT system, ISI and ICI terms have to be mitigated at the subchannel outputs.

Unfortunately, there is no simple method for simultaneous mitigation of ISI and ICI in DWMT systems. In [27], in order to detect the transmitted symbol on the mth subchannel at instant n, i.e., to detect $x_m[n]$, a linear combination of the received signals from several subchannels at a number of time instants is considered, i.e.,

$$\hat{x}_m[n] = \sum_{j \in S} \sum_{k \in \Omega(m)} \lambda_m(j,k) y_k[j] \tag{2.60}$$

where $\Omega(m)$ denotes a set that contains the indices of the subchannels that interfere with the mth subchannel, and S is a set of time instants. Assuming that S includes

ℓ_S indices and $\Omega(m)$ includes ℓ_Ω indices, to detect $x_m[n]$ using (2.60), the outputs from ℓ_Ω subchannels are used, and for each of these subchannels, the outputs at ℓ_S instants are employed. The coefficients $\lambda_m(j,k)$ are chosen based on the minimum mean square error (MMSE) criterion [27]. Obviously, it can be seen that the detection process in DWMT system (e.g., using (2.60)) is a complex task.

The DWMT scheme has a number of attractive features which are summarized below. Firstly, DWMT scheme does not employ redundancy; recall than in DWMT, critically-sampled filter banks are used. In contrast, DMT needs redundancy in the form of cyclic extension and FMT needs redundancy in the form of redundant filter banks. Secondly, DWMT provides improved spectral characteristics at both the transmitter and receiver compared to DMT systems. The improved spectral characteristics of DWMT make it more robust against narrow band noise, near-end crosstalk, and imperfections such as frequency offset between the local oscillators at the transmitter and receiver, phase noise and Doppler spread.

On the other hand, DWMT has a much higher complexity than DMT. The high complexity of DWMT arises because it requires a complex detector module that has to suppress both ISI and ICI at the subchannel outputs. Moreover, in order to have desirable spectral characteristics, the prototype filter in DWMT system has to be much longer than the prototype filters in the filter bank equivalent of a DMT system, typically about ten times the number of subchannels [27].

To compare DWMT with FMT, we note that the spectral containment obtained by FMT is stronger than that obtained by DWMT. On the other hand, FMT systems use oversampled filter banks which reduces their bandwidth efficiency in comparison with DWMT systems. From the complexity point of view, for a given number of subchannels, the typical length of the prototype filter used in FMT is similar to that used in DWMT system. However, in FMT systems, the ICI at the subchannel outputs is negligible and per-subchannel equalization is used to remove the ISI. In contrast, in DWMT system, a considerable amount of both ICI and ISI is present at the subchannel outputs and in order to suppress these interferences, a complex post-detection combining scheme which includes both intra-subchannel and cross-subchannel equalization has to be used, c.f.,(2.60).

2.2 Time-domain equalizer (TEQ) schemes

In Section 2.1.2 we observed that in a DMT (or OFDM) system if the cyclic prefix length is at least as long as the order of the channel impulse response the subchannel outputs will be ISI-free and ICI-free. In some practical scenarios, e.g., in digital subscriber lines, the channel length can be very large. In such situations, a long cyclic prefix would be required to avoid ISI and ICI. However, a large cyclic extension would either require the employment of a large number of subchannels, which would in turn result in high complexity, or it would impose a large redundancy ratio, which would result in a low bandwidth efficiency.

To avoid this problem, in the applications where the channel impulse response is too long, an equalizer is used right after the analog to digital converter at the receiver, to shorten the impulse response of the equivalent channel. This type of equalizer is called a time-domain equalizer (TEQ) [51–54]. If the cyclic prefix of the DMT system is of length P, the role of the TEQ is to equalize the channel so that the impulse response of the combination of the channel and the TEQ is of length $P + 1$ or less (i.e., of order P or less).

As was described in Section 2.1.3, in FMT transceivers there is no constraint on the length of the channel impulse response. Therefore, FMT systems do not require a channel impulse response shortening mechanism. On the other hand, we recall from Section 2.1.4 that in DWMT systems, when the channel is not ideal, regardless of the length of the channel impulse response, both ISI and ICI will be present at the subchannel outputs, and a very high complexity post-detection scheme (c.f., (2.60)) is required to mitigate ISI and ICI. Therefore, DWMT systems, in general, do not require channel impulse response shortening techniques.[10] However, if the channel is shortened using a TEQ, the complexity of the post-detection scheme in DWMT system can be reduced. In [27], the same type of TEQ used for DMT is used for DWMT to shorten the channel impulse response. In the rest of this section, TEQ schemes for DMT systems are reviewed.

Several methods have been proposed for the design of time-domain equalizers in DMT systems [51–60]. The most widely used TEQ is the minimum mean square error (MMSE) TEQ [54,56,60], due to its good performance, comparatively low complexity, and straightforward design procedure. In [53] and [59] impulse response shortening methods based on bit rate maximization criterion have been proposed. However, those methods result in non-convex optimization problems for which complicated numerical methods are required, e.g., using iterative numerical techniques [53, 59]. Unfortunately, these methods do not guarantee a globally optimum solution. In [52], impulse response shortening for the DMT transceiver is performed by an equalizer that ignores the additive noise and minimizes the ISI energy, where the ISI components are defined as the coefficients of the impulse response of the combination of the channel and the TEQ that do not lie in the interval $[0, P]$, where P is the cyclic prefix length. Indeed, the TEQ of [52] can be considered as a zero-forcing TEQ [56]. Since the additive noise is not taken into consideration in the impulse response shortening of [52], the consequent TEQ is suboptimal compared to the MMSE-TEQ. However, if the signal to noise ratio (SNR) at the receiver is large enough, the performance of the TEQ of [52] and the MMSE-TEQ will be similar [56].

In the following subsection, the details of the MMSE-TEQ design method are

[10] In the DWMT system, if the TEQ reduces the length of the equivalent channel to one, ISI and ICI will be eliminated, but in that case, the TEQ will be very complicated.

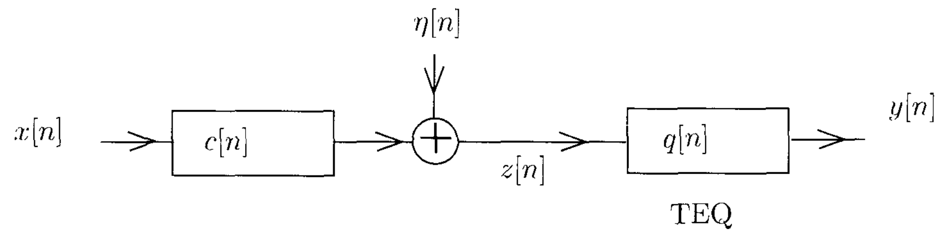

Figure 2.5: The discrete-time channel followed by the time-domain equalizer (TEQ).

presented [54–56].

2.2.1 MMSE-TEQ

Figure 2.5 shows a discrete-time channel with impulse response $c[n]$ and additive noise $\eta[n]$, cascaded with a TEQ with impulse response $q[n]$. It is assumed that

$$c[n] = 0, \quad n \notin [0, L] \tag{2.61}$$

and

$$q[n] = 0. \quad n \notin [0, L_q - 1] \tag{2.62}$$

The objective in the MMSE-TEQ design is to find a target impulse response (TIR), $t[n]$ of length L_t, i.e.,

$$t[n] = 0, n \notin [0, L_t - 1], \tag{2.63}$$

so that the mean-squared value of the difference between $y[n]$ in Figure 2.5 and $\hat{y}[n]$ in Figure 2.6 is minimized. In other words, the objective is to find $t[n]$ of length L_t so that the mean-squared error, J, defined as

$$\begin{aligned} J &= E|e[n]|^2 = E|y[n] - \hat{y}[n]|^2 \\ &= E\left|\sum_{k=0}^{L_q-1} q[k]z[n-k] - \sum_{k=0}^{L_t-1} t[k]x[n-\Delta-k]\right|^2 \end{aligned} \tag{2.64}$$

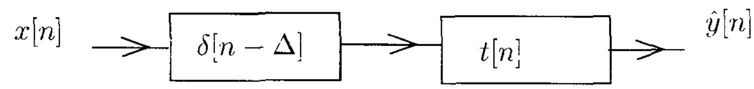

Figure 2.6: Target equivalent channel.

is minimized, where Δ denotes the equalizer delay [54,61] and E denotes the expected value operator.

Assuming the joint wide sense stationary condition [62] for the input signal $x[n]$ and the additive noise $\eta[n]$ in Figure 2.5, the MSE value in (2.64) can be written in the matrix form as

$$J = \mathbf{q}^H \mathbf{R}_z \mathbf{q} + \mathbf{t}^H \mathbf{R}_x \mathbf{t} - \mathbf{t}^H \mathbf{R}_{zx}^{\Delta} \mathbf{q} - \mathbf{q}^H \mathbf{R}_{xz}^{\Delta} \mathbf{t} \tag{2.65}$$

where the superscript H denotes the matrix Hermitian (conjugate transpose), and $\mathbf{q}$ and $\mathbf{t}$ are the $L_q \times 1$ and $L_t \times 1$ vectors that consist of the impulse response coefficients of the TEQ and TIR as

$$\mathbf{q} = (q[0], q[1], \cdots, q[L_q - 1])^T \tag{2.66}$$

and

$$\mathbf{t} = (t[0], t[1], \cdots, t[L_t - 1])^T \tag{2.67}$$

respectively, and $\mathbf{R}_z$, $\mathbf{R}_x$, $\mathbf{R}_{zx}^{\Delta}$, and $\mathbf{R}_{xz}^{\Delta}$ are correlation matrices of size $L_q \times L_q$, $L_t \times L_t$, $L_t \times L_q$, and $L_q \times L_t$, respectively, which are defined as

$$[\mathbf{R}_z]_{m,k} = r_{zz}[m-k], \tag{2.68}$$

$$[\mathbf{R}_x]_{m,k} = r_{xx}[m-k], \tag{2.69}$$

$$[\mathbf{R}_{zx}^{\Delta}]_{m,k} = r_{zx}[m-k+\Delta], \tag{2.70}$$

$$[\mathbf{R}_{xz}^{\Delta}]_{m,k} = r_{xz}[m-k-\Delta], \tag{2.71}$$

respectively, where $r_{ab}[\cdot]$ denotes the correlation function defined as

$$r_{ab}[k] = E\{a[n+k]b^*[n]\} \tag{2.72}$$

where the superscript $*$ denotes the complex conjugation. The MMSE-TEQ is obtained when J in (2.65) is minimized. In order to find the MMSE solution, the orthogonality principle [62] can be used, i.e., the following must hold

$$E\{e[n]z^*[n-\ell]\} = 0, \quad \forall \ell = 0, 1, \cdots, L_q - 1 \tag{2.73}$$

Substituting $e[n]$ from (2.64) into (2.73), the MMSE condition in (2.73) is simplified to

$$\sum_{k=0}^{L_q-1} q[k] r_{zz}[\ell - k] = \sum_{k=0}^{L_t-1} t[k] r_{xz}[\ell - k - \Delta], \quad \forall \ell = 0, 1, \cdots, L_q - 1 \tag{2.74}$$

which, can be written in the matrix form as

$$\mathbf{R}_z \mathbf{q} = \mathbf{R}_{xz}^{\Delta} \mathbf{t} \tag{2.75}$$

and thus

$$\mathbf{q} = \mathbf{R}_z^{-1} \mathbf{R}_{xz}^{\Delta} \mathbf{t}. \tag{2.76}$$

The result in (2.76) provides the MMSE-TEQ coefficients as a function of TIR coefficients. By substituting (2.76) into (2.65), the MSE value is obtained as

$$J = \mathbf{t}^H \left(\mathbf{R}_x - \mathbf{R}_{zx}^{\Delta} \mathbf{R}_z^{-1} \mathbf{R}_{xz}^{\Delta} \right) \mathbf{t} \tag{2.77}$$

By defining $\mathbf{R}^{\Delta}$ as

$$\mathbf{R}^{\Delta} = \mathbf{R}_x - \mathbf{R}_{zx}^{\Delta} \mathbf{R}_z^{-1} \mathbf{R}_{xz}^{\Delta}. \tag{2.78}$$

the MSE value in (2.77) can be written as $J = \mathbf{t}^H \mathbf{R}^{\Delta} \mathbf{t}$. The MMSE TIR function is thus the solution of the following optimization problem

$$\text{minimize} \quad \mathbf{t}^H \mathbf{R}^{\Delta} \mathbf{t} \tag{2.79a}$$

$$\text{subject to} \quad \mathbf{t}^H \mathbf{t} = 1 \tag{2.79b}$$

where the constraint $\mathbf{t}^H \mathbf{t} = 1$ has been added to avoid the trivial solution of $\mathbf{t} = \mathbf{0}$. The solution for this optimization problem is well-known [54, 63, 64], and is the unit-norm eigenvector corresponding to the minimum eigenvalue of $\mathbf{R}^{\Delta}$. After the optimum

TIR is found ($\mathbf{t}$ in (2.79)), the optimum TEQ is found by substituting the optimum $\mathbf{t}$ in (2.76).

We have used the MMSE-TEQ of this section to shorten the impulse response of the DSL channels in the numerical examples of Chapter 4.

2.3 Bit and power loading in multi-carrier transceivers

In a multi-carrier transceiver, the symbols that are transmitted through different subchannels can be chosen from different constellations. Therefore, the number of bits assigned to different subchannels are, in general, different. Moreover, the power assigned to each subchannel can vary for different subchannels. The process of assigning power and the number of bits to each subchannel is called loading. In a communication system with a given total transmission power, it is desirable to maximize the data rate at which a reliable communication can be achieved. Therefore, in a multi-carrier transceiver, an appropriate loading method is one that would maximize the achievable bit rate.

Consider a multi-carrier transceiver with M subchannels in which the noise on each subchannel is Gaussian and is uncorrelated in time and across subchannels. Based on Shannon's capacity formula [65], for the ith subchannel, the maximum information transfer per dimension per channel use, or capacity, is equal to

$$c_i = \frac{1}{2}\log_2(1 + \mathrm{SNR}_i) \quad \text{bits/dimension/channel use} \tag{2.80}$$

where SNR_i is the signal to noise ratio at the ith subchannel output. While (2.80) provides an upper bound on the data rate in bits per dimension, in practice, for a given signaling, i.e., a given modulation and channel coding scheme, the number of bits per dimension that can be communicated with a given reliability through the ith subchannel is [15]

$$b_i = \frac{1}{2}\log_2\left(1+\frac{\mathrm{SNR}_i}{\Gamma}\right) \quad \text{bits/dimension/channel use} \tag{2.81}$$

where Γ is the SNR gap which depends on the signaling scheme used for communication over the ith subchannel and on the desired bit error probability. The smaller the gap, the closer the data rate to the capacity. For example, the SNR gap for QAM constellations (with no channel coding) at a bit error probability of 10^{-7} is equal to 9.8 dB [15].

Since (2.81) provides the number of bits per dimension that can be communicated with a given reliability, for two-dimensional constellations, such as QAM, the number of bits per channel use that can be loaded on the ith subchannel is given by [15,26,66]

$$\beta_i = \log_2\left(1+\frac{\mathrm{SNR}_i}{\Gamma}\right) \quad \text{bits/channel use} \tag{2.82}$$

Digital communication systems usually employ channel coding techniques to combat the additive noise and interference signals [2, 15, 67], and thereby, improve the achievable bit rate.[11] In that case, the coding gain should be considered in the bit loading formula in (2.82). Moreover, most communication standards mandate the consideration of an SNR margin [15]. An SNR margin is defined as the amount of the increase in the power of noise that should be tolerated by the system, while maintaining the desired reliability. While the effect of the coding gain and the SNR margin can be included in Γ in (2.82) as $\Gamma = \Gamma_{\mathrm{constellation}}/\gamma_{\mathrm{code}} \times \gamma_{\mathrm{margin}}$, where γ_{code} denotes the coding gain and γ_{margin} denotes the SNR margin, some authors prefer to

[11] At the time this thesis is being written, most of the multi-carrier systems adopted by global standards use a combination of linear block codes, e.g., Reed Solomon codes, and trellis codes to provide a coding gain and thus improve the achievable bit rate [15, 22]. On the other hand, more advanced coding methods, such as turbo codes and low density parity check (LDPC) codes have been accepted as optional coding methods in some globally standardized systems [22], or they are candidate coding schemes for future generations of multi-carrier transceivers [68 70]. At a given bit error probability, turbo codes and LDPC codes provide larger coding gains compared to conventional linear block codes and convolutional codes. However, the increased coding gain in these schemes is achieved at the price of increased complexity and delay in the encoder and decoder.

emphasize on them by rewriting (2.82) as

$$\beta_i = \log_2\left(1 + \frac{\mathrm{SNR}_i \gamma_{\mathrm{code}}}{\Gamma \gamma_{\mathrm{margin}}}\right) \tag{2.83}$$

In this section, for simplicity, we use (2.82) and we assume any coding gain or SNR margin is included in the SNR gap Γ. In Chapters 3 and 4, we will use the form in (2.83) to emphasise on the values assumed for the coding gain, γ_{code}, and SNR margin, γ_{margin}.

In duplex multi-carrier communication systems, in order to reduce the impact of echo and near-end crosstalk (NEXT), duplexing is usually done by assigning a number of subchannels only for downstream communications and assigning the rest of the subchannels only for upstream communications [15, 21, 26]. The achievable bit rate for downstream or upstream communication is obtained by adding the number of bits per symbol interval, given by (2.82), over the subchannels corresponding to the downstream or upstream communications and multiplying the result by the symbol rate. Thus, the achievable bit rate for downstream or upstream communications is given by

$$R = \frac{1}{T}\sum_{i\in\mathcal{A}} \log_2\left(1 + \frac{\mathrm{SNR}_i}{\Gamma}\right) \quad \text{bits/second} \tag{2.84}$$

where $1/T$ is the symbol rate, and $\mathcal{A}$ denotes the set of subchannel indices used for the corresponding direction of transmission, i.e., downstream or upstream.

2.3.1 Optimal power loading

In multi-carrier transceivers, the total transmit power is normally constrained to a maximum value. An optimal power loading is one that maximizes the achievable bit rate for a given transmit power. Denoting the total transmit power for downstream (or upstream) communication by P_{total}, and assuming that $\mathcal{A}$ denotes the set of subchannel indices used in that communication direction, and denoting the power assigned to the ith subchannel by P_i, using (2.84), the optimal power loading can be formulated as

$$\text{maximize} \quad \sum_{i\in\mathcal{A}} \log_2\left(1+\frac{\mathrm{SNR}_i}{\Gamma}\right) \tag{2.85a}$$

$$\text{subject to} \quad \sum_{i\in\mathcal{A}} P_i = P_{\text{total}} \tag{2.85b}$$

$$P_i \geq 0\,, \quad \forall i \in \mathcal{A} \tag{2.85c}$$

When the subchannel outputs are ISI-free and ICI-free, as in a DMT system with a cyclic prefix at least as long as the order of the channel, the water-filling power loading algorithm provides the solution for the optimal power loading problem in (2.85) [9,15, 66]. While that algorithm will be discussed in more detail below, it is worth noting that the optimal power loading formulation in (2.85) is with the assumption that the bit distribution given by (2.82) can be realized. However, generally, (2.82) results in a real number that may not be an integer. In practice, realization of bit distributions with arbitrary non-integer values can be complicated. A sub-optimal approach is to use the power distribution obtained from (2.82) and for each subchannel, round β_i given by (2.82) to the closest integer value. On the other hand, there have been a number of other solutions for discrete bit loading, e.g., see [15, 66, 71, 72].

Water-filling power loading

When there is no ICI and no ISI at the subchannel outputs, the SNR at the ith subchannel output is equal to

$$\mathrm{SNR}_i = \frac{P_i}{\sigma_i^2 \ell_i} \tag{2.86}$$

where σ_i^2 denotes the noise power at the ith subchannel output and ℓ_i denotes the power loss over the ith subchannel. The water-filling algorithm is an iterative algorithm for solving the optimal power loading problem in (2.85). The algorithm begins by solving (2.85) in the absence of (2.85c), i.e., by solving the following optimization problem

$$\text{maximize} \quad \sum_{i\in\mathcal{A}} \log_2\left(1+\frac{P_i}{\sigma_i^2\ell_i\Gamma}\right) \tag{2.87a}$$

$$\text{subject to} \quad \sum_{i\in\mathcal{A}} P_i = P_{\text{total}} \tag{2.87b}$$

The optimization problem in (2.87) is a convex optimization problem with a single equality constraint. Therefore, a closed-form solution can be found for it using the classical Lagrange multiplier method [73]. By applying that method, it can be shown that the optimal solution for (2.87) is the solution to the following set of linear equations

$$P_k + \sigma_k^2\ell_k\Gamma = \nu, \quad \forall k \in \mathcal{A}, \ \exists\, \nu \tag{2.88a}$$

$$\sum_{i\in\mathcal{A}} P_i = P_{\text{total}} \tag{2.88b}$$

where ν is the Lagrange multiplier. From (2.88) one can see that for the subchannels that $\sigma_k^2\ell_k$ is larger, the assigned power, P_k, should be smaller. If we add the terms in (2.88a) for all $k \in \mathcal{A}$ and substitute $\sum_{i\in\mathcal{A}} P_i$ with P_{total} from (2.88b), ν can be computed as

$$\nu = \frac{1}{M_1}\left(P_{\text{total}} + \Gamma\sum_{k\in\mathcal{A}}\sigma_k^2\ell_k\right) \tag{2.89}$$

where it has been assumed that the number of elements in $\mathcal{A}$ is equal to M_1. After computing ν using (2.89), from (2.88a) it can be seen that the power assigned to each of the subchannels is

$$P_k = \nu - \sigma_k^2\ell_k\Gamma, \quad \forall\, k \in \mathcal{A} \tag{2.90}$$

The power values obtained by (2.90) can be negative. This is because in (2.87) there is no constraint that $P_k \geq 0$. If one or more of the values computed for P_k, $k \in \mathcal{A}$ are negative, the equation with the largest $\sigma_k^2\ell_k$ has to be eliminated from the set of linear equations in (2.88a) and the corresponding P_k should be set to zero, and the equations in (2.89) and (2.90) have to be modified accordingly, and solved for the new set of power values. This iteration continues until no negative power occurs.

2.4 Windowing for DMT transceivers

As discussed in Section 2.1.2, the transmitter and receiver filters of the DMT filter bank have a rectangular shape in the time domain and their corresponding frequency responses are sinc functions. These filters have large sidelobes in the stopband and their stopband energy is relatively large. As a result, DMT systems suffer from poor spectral characteristics both at the transmitter and at the receiver. The poor subchannel spectral containment at the transmitter makes it difficult to design schemes that have to satisfy the egress standards, and the high level of subchannel spectral sidelobes at the transmitter makes DMT system susceptible to near-end crosstalk (NEXT). On the other hand, the poor subchannel spectral selectivity of DMT system at the receiver, makes DMT system vulnerable to NEXT and narrowband interference signals.

Windowing methods [25, 74–80] can be considered as one of the most practical solutions for improving the spectral characteristics of the DMT system. Windowing schemes have the attractive feature that they allow for efficient FFT-based implementation similar to that in conventional DMT scheme. Moreover, they can be designed in a channel-independent manner. In this section, a number of receiver and transmitter windowing schemes for DMT systems are studied. One of the contributions of this thesis is a new windowing technique for DMT systems that will be presented in Chapter 4; see also [81].

2.4.1 Nyquist windowing at the receiver

In the DMT system, if the cyclic prefix length is greater than or equal to the order of the equivalent discrete-time channel, the subchannel outputs will be ISI-free and ICI-free. If the length of the cyclic prefix is larger than the order of the channel, the excess cyclic prefix can be employed to improve the subchannel spectral characteristics at the receiver, using the Nyquist windowing method [74–76]. In this section, the Nyquist windowing scheme is studied and it is shown how the extra cyclic prefix can be used to improve the subchannel spectral selectivity at the receiver while maintaining the ISI-free and ICI-free characteristics of the DMT system.

Figure 2.7 shows the DMT transceiver with Nyquist windowing at the receiver. Notice that this system is similar to the conventional DMT system of Figure 2.2 except that the cyclic prefix (CP) removal block is replaced by the windowing block in Figure 2.7. Recall from Section 2.1.2 that in the DMT system, for the nth received block, i.e., $z_k[n]$, $k = 0, 1, \cdots, N-1$, the DMT receiver discards the first P samples and applies an M-point FFT on the result. Therefore, the subchannel outputs of the DMT system (with no windowing) can be written as

$$y_k[n] = \frac{1}{\sqrt{M}} \sum_{\ell=0}^{M-1} z_{\ell+P}[n] e^{-\jmath \frac{2\pi}{M} k\ell}, \quad k = 0, 1, \cdots, M-1 \tag{2.91}$$

It was observed in Section 2.1.2 that if the order of the channel impulse response, L, is less than or equal to the cyclic prefix length, i.e., if $L \leq P$, the combination of the cyclic prefix removal matrix at the receiver, the channel, and the cyclic prefix adder matrix at the transmitter, makes a circulant matrix which is diagonalized by the FFT and IFFT matrices, and therefore, (2.91) simplifies to[12]

$$y_k[n] = C(e^{\jmath \frac{2\pi}{M} k}) x_k[n] + \tilde{\eta}_k[n], \quad k = 0, 1, \cdots, M-1 \tag{2.92}$$

where $C(e^{\jmath\omega})$ is the frequency response of the channel and $\tilde{\eta}$ represents the effect of

[12]A detailed mathematical derivation of (2.91) was presented in Section 2.1.2.

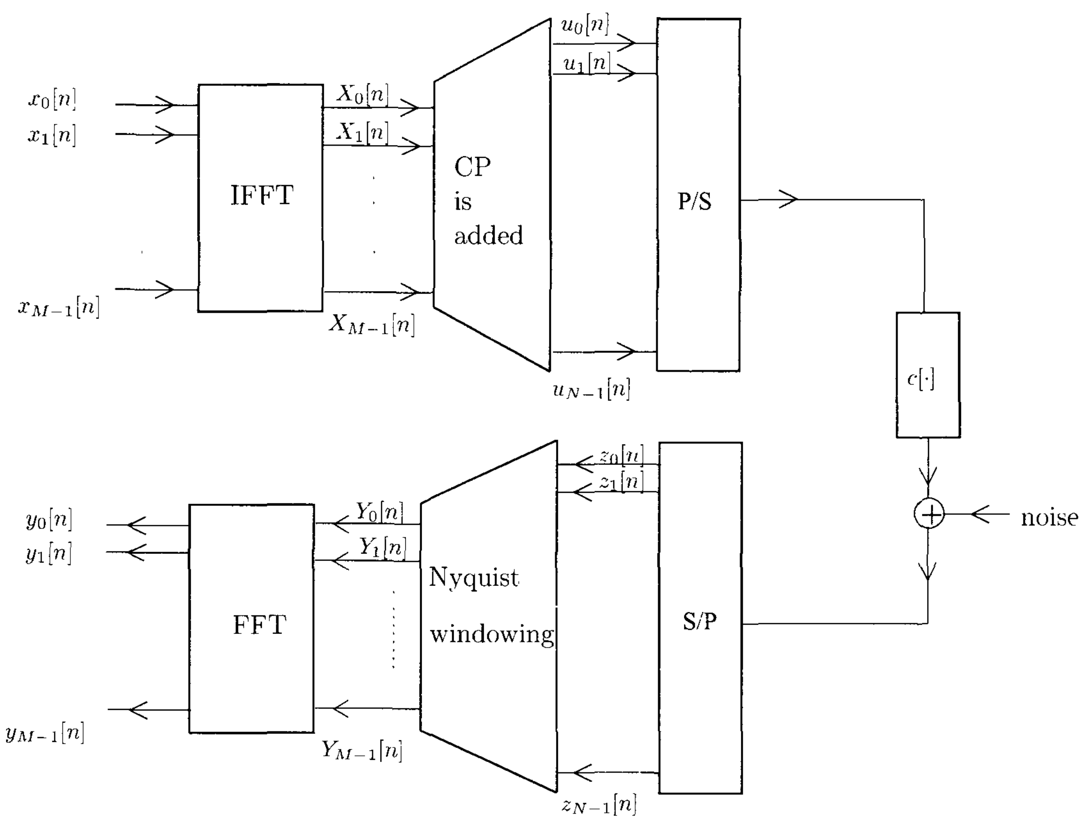

Figure 2.7: DMT system with Nyquist windowing at the receiver.

the additive noise and interference signals of the channel at the subchannels outputs. Comparing (2.91) and (2.92), we have that

$$\frac{1}{\sqrt{M}}\sum_{\ell=0}^{M-1} z_{\ell+P}[n]e^{-j\frac{2\pi}{M}k\ell} = C(e^{j\frac{2\pi}{M}k})x_k[n] + \tilde{\eta}_k[n] \tag{2.93}$$

Now consider the DMT system with Nyquist windowing at the receiver shown in Figure 2.7, where the cyclic prefix removal module of the conventional DMT system is replaced with the windowing module. In Nyquist receiver windowing, a windowing parameter W is considered which satisfies the following constraint

$$0 < W \leq P - L \tag{2.94}$$

From (2.94) it is implied that the Nyquist windowing can be applied only if $P > L$, i.e., the cyclic prefix length is larger than the order of the equivalent discrete-time channel. In this section we assume that this is true.

In the system of Figure 2.7, the windowing module at the receiver discards the first $P - W$ samples of the received sample block (of size N) and applies a window, w_k, to the other samples in the following manner

$$Y_k[n] = w_{k+W}\, z_{k+P}[n] + w_{k+W-M}\, z_{k+P-M}[n]\,, \quad k = 0, 1, \cdots, M-1 \tag{2.95}$$

where the Nyquist window, w_k, is defined as

$$w_k = \begin{cases} \gamma_k, & 0 \leq k \leq W-1 \\ 1, & W \leq k \leq M-1 \\ 1-\gamma_{k-M}, & M \leq k \leq M+W-1 \\ 0, & k < 0 \quad \text{or} \quad k > M+W-1 \end{cases} \tag{2.96}$$

where γ_k is an arbitrary function defined on the interval $k \in [0, W-1]$ and is chosen in accordance with the desired spectral characteristics.

After Nyquist windowing at the receiver, an M-point FFT is applied to $Y_k[n]$, $k = 0, 1, \cdots, M-1$, which results in the subchannel outputs

$$y_\ell[n] = \frac{1}{\sqrt{M}} \sum_{k=0}^{M-1} Y_k[n] e^{-\jmath \frac{2\pi}{M} \ell k}, \quad \ell = 0, 1, \cdots, M-1 \tag{2.97}$$

By substituting (2.95) into (2.97) we have that

$$y_\ell[n] = \frac{1}{\sqrt{M}} \sum_{k=0}^{M-1} w_{k+W}\, z_{k+P}[n] e^{-\jmath \frac{2\pi}{M} \ell k} + \frac{1}{\sqrt{M}} \sum_{k=0}^{M-1} w_{k+W-M}\, z_{k+P-M}[n] e^{-\jmath \frac{2\pi}{M} \ell k} \tag{2.98}$$

Substituting (2.96) into (2.98) results in

$$\begin{aligned} y_\ell[n] =& \frac{1}{\sqrt{M}} \left(\sum_{k=0}^{M-W-1} z_{k+P}[n] e^{-\jmath \frac{2\pi}{M} \ell k} + \sum_{k=M-W}^{M-1} (1 - \gamma_{k+W-M}) z_{k+P}[n] e^{-\jmath \frac{2\pi}{M} \ell k} \right) \\ &+ \frac{1}{\sqrt{M}} \sum_{k=M-W}^{M-1} \gamma_{k+W-M}\, z_{k+P-M}[n] e^{-\jmath \frac{2\pi}{M} \ell k} \end{aligned} \tag{2.99}$$

Furthermore, (2.99) can be simplified to

$$\begin{aligned} y_\ell[n] =& \frac{1}{\sqrt{M}} \sum_{k=M-W}^{M-1} \gamma_{k+W-M} e^{-\jmath \frac{2\pi}{M} k\ell} \left(z_{k+P-M}[n] - z_{k+P}[n] \right) \\ &+ \frac{1}{\sqrt{M}} \sum_{k=0}^{M-1} z_{k+P}[n] e^{-\jmath \frac{2\pi}{M} \ell k} \end{aligned} \tag{2.100}$$

By substituting (2.93) into (2.100), we have that

$$\begin{aligned} y_\ell[n] =& \frac{1}{\sqrt{M}} \sum_{k=M-W}^{M-1} \gamma_{k+W-M} e^{-\jmath \frac{2\pi}{M} k\ell} \left(z_{k+P-M}[n] - z_{k+P}[n] \right) \\ &+ C(e^{\jmath \frac{2\pi}{M} \ell}) x_\ell[n] + \tilde{\eta}_\ell[n] \end{aligned} \tag{2.101}$$

On the other hand, with the assumption that (2.94) holds, we have

$$z_k[n] = \sum_{\imath=0}^{L} c[i] u_{k-\imath}[n] + \eta_k[n], \quad P - W \leq k \leq N - 1 \tag{2.102}$$

By substituting (2.102) into (2.101) the following is obtained

$$y_\ell[n] = C(e^{j\frac{2\pi}{M}\ell})x_\ell[n] + \tilde{\eta}_\ell[n] + \frac{1}{\sqrt{M}}\sum_{k=M-W}^{M-1} \gamma_{k+W-M} e^{-j\frac{2\pi}{M}k\ell} \left(\sum_{i=0}^{L} c[i](u_{k+P-M-i}[n] - u_{k+P-i}[n]) + \eta_{k+P-M}[n] - \eta_{k+P}[n]\right) \quad (2.103)$$

Because of the cyclic property of the transmitted signal (c.f. (2.17)), the term $(u_{k+P-M-i}[n] - u_{k+P-i}[n])$ in (2.103) is equal to zero. Thus, (2.103) simplifies to

$$y_\ell[n] = \frac{1}{\sqrt{M}}\sum_{k=M-W}^{M-1} \gamma_{k+W-M}\, e^{-j\frac{2\pi}{M}k\ell}\, (\eta_{k+P-M}[n] - \eta_{k+P}[n]) + C(e^{j\frac{2\pi}{M}\ell})x_\ell[n] + \tilde{\eta}_\ell[n] \quad (2.104)$$

Notice that in (2.104), the term $C(e^{j\frac{2\pi}{M}\ell})x_\ell[n]$ represents the desired signal and other terms represent the impact of the additive noise. From (2.104) it can be seen that by applying a Nyquist window at the receiver, as defined by (2.96) and (2.95), the ISI-free and ICI-free properties of the transceiver are maintained, as long as the condition in (2.94) is satisfied. Therefore, similar to the DMT system with no windowing, $x_\ell[n]$ can be recovered from $y_\ell[n]$ in (2.104), using a one-tap per-subchannel equalizer.

Notice that in order to satisfy (2.94), the cyclic prefix length needs to be longer than the order of the discrete-time channel. In this case, the excess cyclic prefix can be used for improving the spectral characteristics of the subchannels at the receiver, using the window defined in (2.96). Recall that γ_k in (2.96) is an arbitrary function defined on the interval $k \in [0, W-1]$ which is chosen so that the desired spectral improvements are obtained for the subchannels spectra at the receiver. A typical application of Nyquist receiver windowing in DSL transceivers is described in the following example from [76].

Consider a DMT system with $M = 512$ subchannels and a cyclic prefix of length $P = 32$ used in a communication channel of order $L = 24$. Since $P > L$, the receiver

Nyquist windowing can be applied (see (2.94)). In order to extract the greatest advantage of the difference between the cyclic prefix length and the order of the channel, the maximum value for W is chosen, i.e., $W = P - L = 8$. Recall from the structure of the window given in (2.96) that γ_n is an arbitrary function. Some typical choices for the window, w_k, are raised cosine[13] , trapezoidal, and piecewise constant window. Notice that when w_k is a raised cosine window, γ_k is part of a Hann window, when w_k is a trapezoidal window, γ_k is a linear function, and when w_k is a piecewise constant window, γ_k is a constant function. The γ_k functions corresponding to the raised cosine, trapezoidal, and piecewise constant windows are plotted in Figure 2.8 and are given by

$$\gamma_k = .5\left(1 - \cos\frac{\pi(k+1)}{W+1}\right), \quad 0 \leq k \leq W-1.$$

$$\gamma_k = \frac{k+1}{W+1}, \quad 0 \leq k \leq W-1.$$

and

$$\gamma_k = .5, \quad 0 \leq k \leq W-1$$

respectively [74–76]. Figure 2.9 shows the (magnitude) frequency response of the window w_k when it is a rectangular woindow corresponding to conventional DMT, a raised cosine window, a trapezoidal window, or a piecewise constant window.

In order to demonstrate a typical application of the Nyquist receiver windowing, in the following, we report some of the numerical results obtained by Redfern in [76]. Consider the DMT system of the above example, i.e., with $M = 512$ subchannels and a cyclic prefix of length $P = 32$. Redfern [76] used a time-domain equalizer to shorten the DSL channel to length 25, i.e., order $L = 24$, and considered QAM constellations, a sampling rate of 2.208 MHz, 26-gauge twisted pair model for the channel, AWGN noise with power spectral density of -140 dBm/Hz, and an RFI model including

[13]While in some publications this may be referred to as a "cosine roll-off" window, in this thesis we refer to this window as a "raised cosine" window to comply with the terminology in [74].

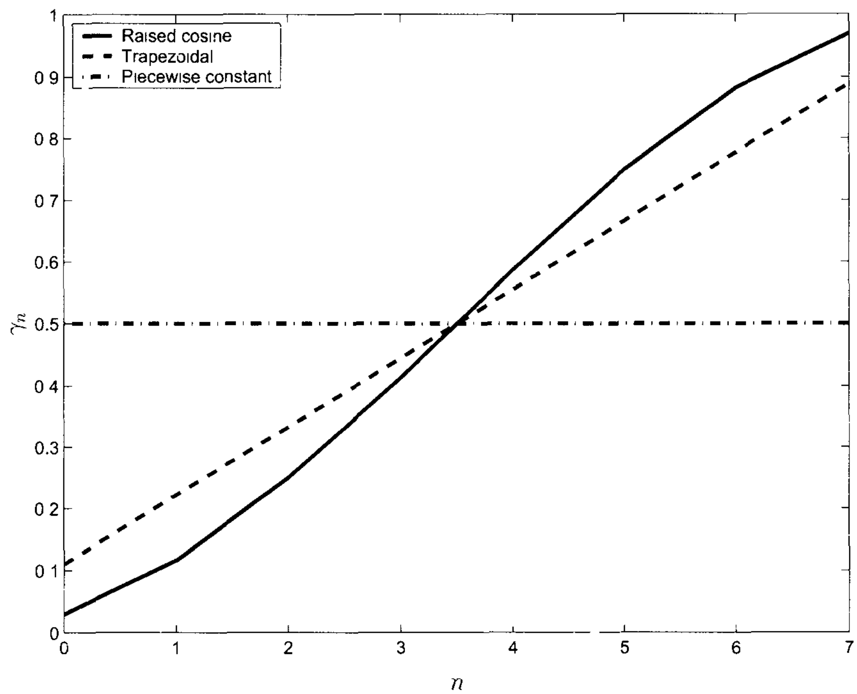

Figure 2.8: Receiver window shapes.

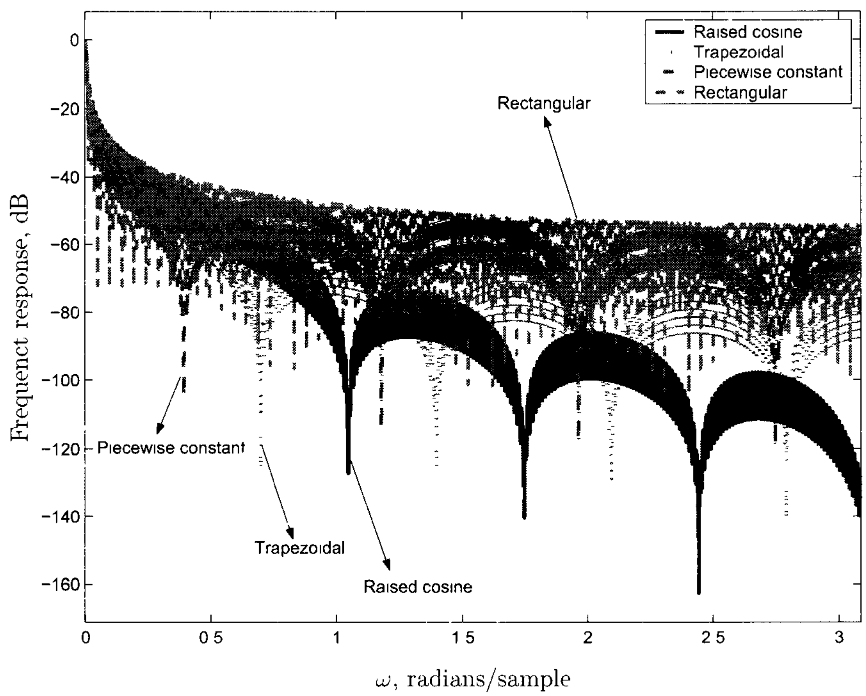

Figure 2.9: Frequency response of the receiver window, w_k.

Window	Achievable bit rate (Mbit/sec) 6-kft cable length	Achievable bit rate (Mbit/sec) 12-kft cable length
None	9.947	1.469
Piecewise constant	10.734	1.749
Raised cosine	11.763	2.156

Table 2.1: Achievable bit rates for the DMT system with no window, piecewise constant window, and raised cosine window for cable lengths of 6 kft and 12 kft 2.1.

seven AM interference signals [76]. He considered a coding gain of 5 dB and an SNR margin of 6 dB. Table 2.1 shows the achievable bit rates obtained in [76] for the conventional DMT system (no windowing), and the windowed DMT system with the raised cosine window and the piecewise constant window of Figure 2.8. The results shown in Table 2.1 correspond to the achievable bit rates for a cable length of 6 kft and 12 kft. In both cases it can be seen that the achievable bit rates can be improved by windowing. The improvement in the achievable bit rates is due to the improved robustness against narrowband noise (RFI) offered by the windowing [76].

2.4.2 Transmitter windowing

For DMT systems with applications in ISI channels, two windowing methods have been proposed for the improvement of the subchannel spectral containment at the transmitter. A transmitter windowing method that requires extra cyclic prefix was proposed in [78]. In other words, this method requires the cyclic prefix length to be larger than the order of the channel. When there is no extra cyclic prefix, windowing will require extra post-processing at the receiver. In [25,79,80], a windowing method that improves the subchannel spectral characteristics at the transmitter and does not require extra cyclic prefix has been proposed, but requires extra processing at the receiver.

In the first part of this section, we describe the transmitter windowing method with excess cyclic prefix [78]. In the second part of this section, we study the transmitter windowing method for DMT systems without excess cyclic prefix [25, 79, 80].

Transmitter windowing using the extra cyclic prefix

Consider the DMT transceiver in Figure 2.2 of Section 2.1.2. A transmitter window for this system is applied after the cyclic prefix is added. In this section we will use the same matrix formulation and notation as in Section 2.1.2. The transmitter windowing can be modelled by a diagonal matrix $\mathbf{W}$ defined as

$$\mathbf{W} = \operatorname{diag}(w_0, w_1, \cdots, w_{N-1}) \tag{2.105}$$

where w_k, $k = 0, 1, \cdots, N-1$ are the window coefficients. Figure 2.10 shows the DMT system with the transmitter windowing. The transmitter windowing method that is studied in this section requires the cyclic prefix length to be larger than the order of the channel. Therefore, in this section we assume that

$$P - L > 0 \tag{2.106}$$

In the following, we study how the extra cyclic prefix can be exploited to improve the spectral characteristics of the subchannels at the transmitter while maintaining the zero ISI and zero ICI properties of the DMT system.

Recall from Section 2.1.2 that for the nth transmitted block of symbols, the subchannel outputs of the DMT system with no windowing are given by (2.30). A similar equation holds for the windowed DMT system of Figure 2.10 with a minor modification to account for windowing. Considering the effect of the transmitter windowing, the transmitted block $\mathbf{u}_n$ is related to the subchannel input vector $\mathbf{x}_n$ by

$$\mathbf{u}_n = \mathbf{W}\mathbf{T}\mathbf{F}^H\mathbf{x}_n \tag{2.107}$$

Substituting (2.107) into (2.30), we obtain

$$\mathbf{y}_n = \mathbf{F}\mathbf{R}\mathbf{C}_0\mathbf{W}\mathbf{T}\mathbf{F}^H\mathbf{x}_n + \mathbf{F}\mathbf{R}\boldsymbol{\eta}_n \tag{2.108}$$

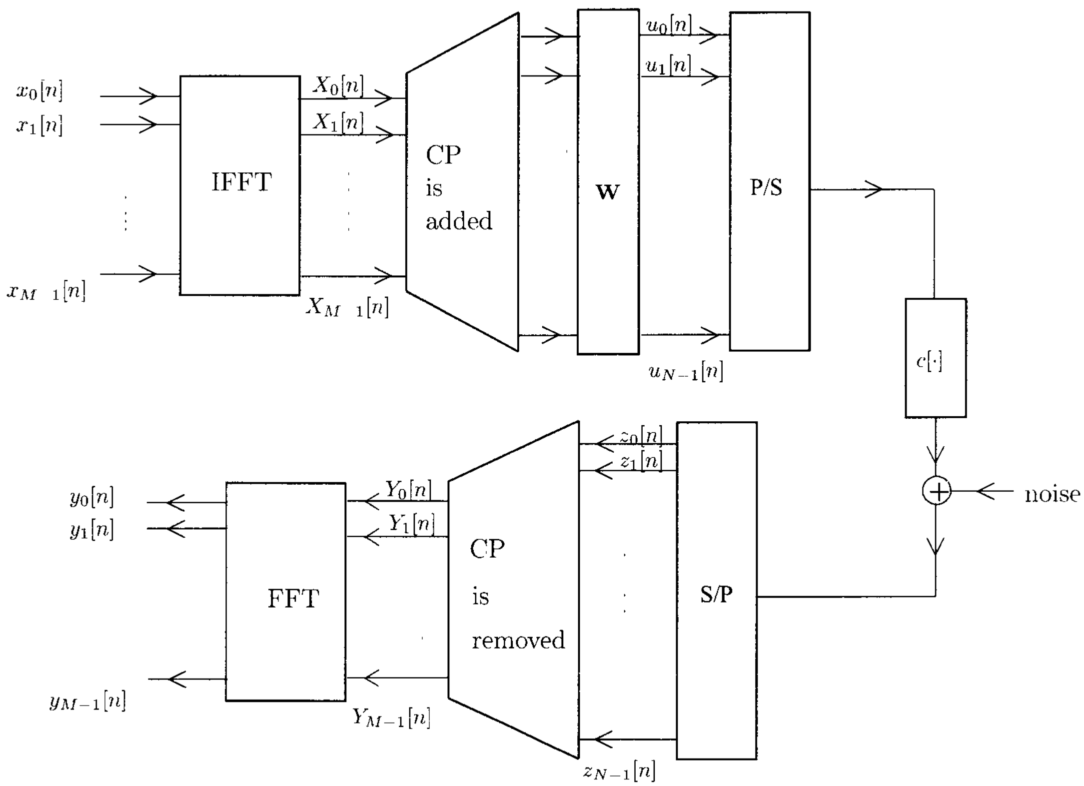

Figure 2.10: The DMT system with transmitter windowing using extra cyclic prefix. The windowing module is labelled as **W**.

Using the definition of the cyclic prefix adder matrix $\mathbf{T}$ defined by (2.18) in Section 2.1.2, it can be shown that the product of $\mathbf{W}$ and $\mathbf{T}$ is an $N \times M$ matrix given by

$$\mathbf{WT} = \begin{pmatrix} 0 & 0 & \cdots & 0 & w_0 & 0 & \cdots & 0 \\ 0 & 0 & \cdots & 0 & 0 & w_1 & \cdots & 0 \\ \vdots & & & & \vdots & & \ddots & \vdots \\ 0 & 0 & \cdots & 0 & 0 & 0 & \cdots & w_{P-1} \\ w_P & 0 & \cdots & 0 & 0 & 0 & \cdots & 0 \\ 0 & w_{P+1} & \cdots & 0 & 0 & 0 & \cdots & 0 \\ \vdots & & \ddots & & \vdots & & & \vdots \\ 0 & 0 & \cdots & 0 & 0 & 0 & \cdots & w_{N-1} \end{pmatrix} \tag{2.109}$$

In addition, using the definition of $\mathbf{R}$ given in (2.26) and that of $\mathbf{C}_0$ given in (2.21), one can verify that the product of these two matrices, $\mathbf{RC}_0$, is the $M \times N$ matrix

$$\mathbf{RC}_0 = \begin{pmatrix} c[P] & c[P-1] & \cdots & c[0] & 0 & \cdots & 0 \\ 0 & c[P] & \cdots & c[1] & c[0] & \cdots & 0 \\ \vdots & & & \vdots & & \ddots & \\ 0 & 0 & \cdots & 0 & 0 & \cdots & c[0] \end{pmatrix} \tag{2.110}$$

where, as in Section 2.1.2, $c[k]$ denotes the impulse response of the equivalent discrete-time channel. Recall from Section 2.1.2 that for the DMT system with no windowing (i.e., when $\mathbf{W} = \mathbf{I}_N$), when the cyclic prefix length is larger than or equal to the order of the channel ($P \geq L$), the matrix $\mathbf{RC}_0\mathbf{T}$ is a circulant matrix and therefore it is diagonalized using the FFT and IFFT matrices. Now, for the windowed DMT system under discussion, by looking at $\mathbf{WT}$ in (2.108) and $\mathbf{RC}_0$ in (2.110), one can see that if $c[P] = 0$, the matrix $\mathbf{RC}_0\mathbf{WT}$ will not depend on w_0. Moreover, if $c[P] = c[P-1] = 0$, the matrix $\mathbf{RC}_0\mathbf{WT}$ will neither depend on w_0 nor on w_1. Similarly, if

$$c[P] = c[P-1] = \cdots = c[L+1] = 0, \tag{2.111}$$

the matrix $\mathbf{RC}_0\mathbf{WT}$ will not include any of $w_0, w_1, \cdots, w_{P-L-1}$. Thus, when $P > L$, the window coefficients w_k, $k \in [0, P-L-1]$ can be chosen arbitrarily, without affecting the output values of the transceiver. On the other hand, if the rest of the window coefficients are chosen to be unity, i.e.,

$$w_k = 1, \quad \forall k \in [P-L, N-1], \tag{2.112}$$

we will have $\mathbf{RC}_0\mathbf{WT} = \mathbf{RC}_0\mathbf{T}$, and therefore, $\mathbf{RC}_0\mathbf{WT}$ will be diagonalized using the FFT and IFFT matrices and the relationship between the subchannel outputs and subchannel inputs of the system will be identical to that for the DMT system with no windowing, which was given by (2.34). As a result, the subchannel outputs will be ISI-free and ICI-free, and the subchannel equalization from the conventional DMT can be used to recover the transmitted symbols. Although the subchannel outputs do not depend on $w_0, w_1, \cdots, w_{P-L-1}$, these coefficients do appear in the transmitted signal, $\mathbf{u}_n$, and they can be appropriately chosen to improve the subchannel spectral characteristics at the transmitter. Notice, however, that the improvement in the spectral characteristics of the transmitter is obtained at the cost of a longer cyclic prefix.

In the windowing technique that was described above it was assumed that the channel impulse response, $c[k]$, can be non-zero only on the interval $[0, L]$, and it was observed that if the cyclic prefix length, P, is larger than L, the first $P-L$ coefficients of the window can be chosen arbitrarily which allows them to be chosen in a manner that the transmit subchannels spectra are improved. Now let's assume $c[k] = 0$, $k \notin [L_1, L_2]$, where $L_1 > 0$ and $L_2 - L_1 = L$.[14] Moreover, assume that $P > L_2$. As was described earlier, in this case, $w_0, w_1, \cdots, w_{P-L_2-1}$ can be chosen arbitrarily to improve the transmit subchannel spectra. Moreover, by looking at (2.109) and (2.110), it can be seen that since $c[0] = c[1] = \cdots = c[L_1-1] = 0$, the window

[14]For a given channel of order L, the condition of $c[k] = 0$, $k \notin [L_1, L_2]$, $L_2 - L_1 = L$, can be achieved by considering the appropriate amount of delay at the receiver.

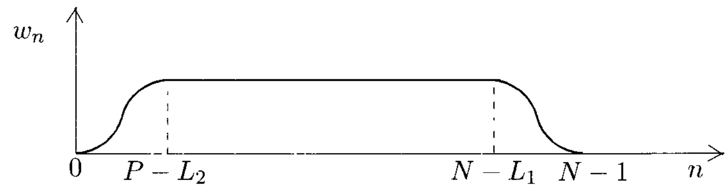

Figure 2.11: Transmitter window.

coefficients $w_{N-1}, w_{N-2}, \cdots, w_{N-L_1}$ will have no effect in the matrix $\mathbf{RC}_0\mathbf{WT}$, and thus, they too, can be chosen arbitrarily to improve the transmit subchannel spectra. As long as $w_k = 1, \forall k \in [P - L_2, N - L_1 - 1]$, we have $\mathbf{RC}_0\mathbf{WT} = \mathbf{RC}_0\mathbf{T}$, and therefore the zero ICI and zero ISI conditions of the conventional DMT system will be maintained. Indeed, while the midpoints of the window have a constant value, i.e., $w_k = 1, \forall k \in [P - L_2, N - L_1 - 1]$, if extra cyclic prefix is available, the extra cyclic prefix can be used to smoothen the transition of the window at both sides of the window. This is shown in Figure 2.11, where the first $P - L_2$ and the last L_1 coefficients of the window are chosen so that a smooth transition is obtained for the window (compared to the rectangular window in the conventional DMT system). Notice, again, this is possible only when $P > L_2$, i.e., when $P > L + L_1$, where $L + 1$ is the length of the channel.

As a numerical example, assume an equivalent discrete-time channel $c[k]$ where $c[k] = 0$, $k \notin [5, 35]$, and consider a DMT transceiver with $M = 512$ subchannels and a cyclic prefix of length $P = 40$. The raised cosine window given by

$$w_n = \begin{cases} 1, & 5 \le n \le 546 \\ .5\left(1 - \cos\frac{\pi(n+1)}{6}\right), & 0 \le n < 5 \\ .5\left(1 - \cos\frac{\pi(n-540)}{6}\right), & 546 < n \le 551 \\ 0, & \text{otherwise} \end{cases} \tag{2.113}$$

was used to improve the transmit subchannel spectra. Figure 2.12 shows the transmitter power spectral density of the system when subchannels $0, 1, \cdots, 49$ are used and the rest of subchannels are turned off. The results are obtained assuming uncorrelated subchannel inputs and uniform power distribution among the used subchannels. For comparison, the power spectral density of the DMT system with no windowing (rectangular windowing) is also shown in Figure 2.12. It can be seen that the out of band radiation is considerably decreased by windowing.

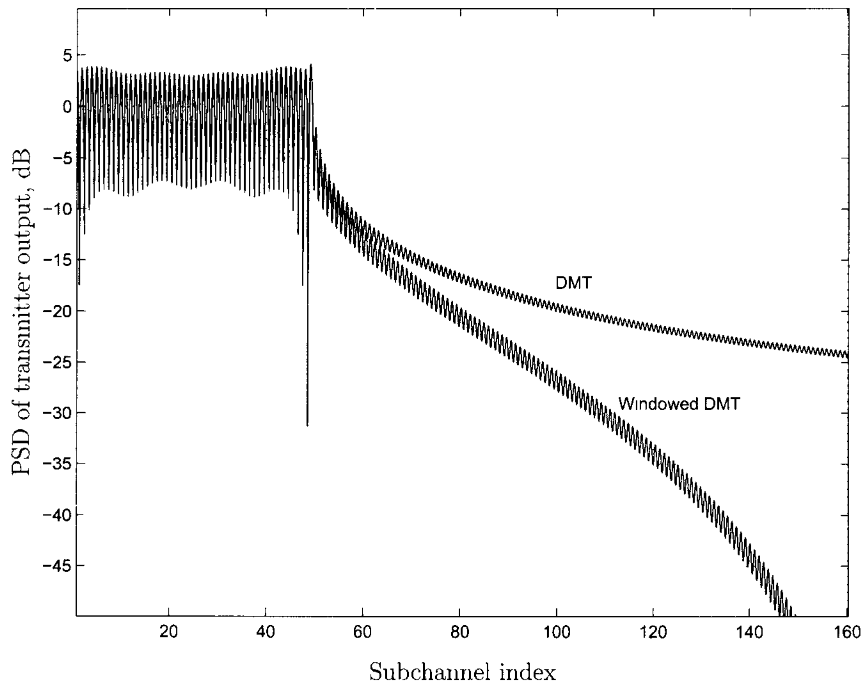

Figure 2.12: Power spectral density of transmitter output when the subchannels 0-49 are used and the rest of subchannels are turned off.

For reference, the (magnitide) frequency response of the raised cosine window of (2.113) along with that of the rectangular window of the conventional DMT are shown in Figure 2.13.

Transmitter windowing with post-processing at the receiver

If no extra cyclic prefix is available, windowing at the transmitter requires extra processing at the receiver in the form of ICI cancellation. In [25, 79, 80], a transmitter

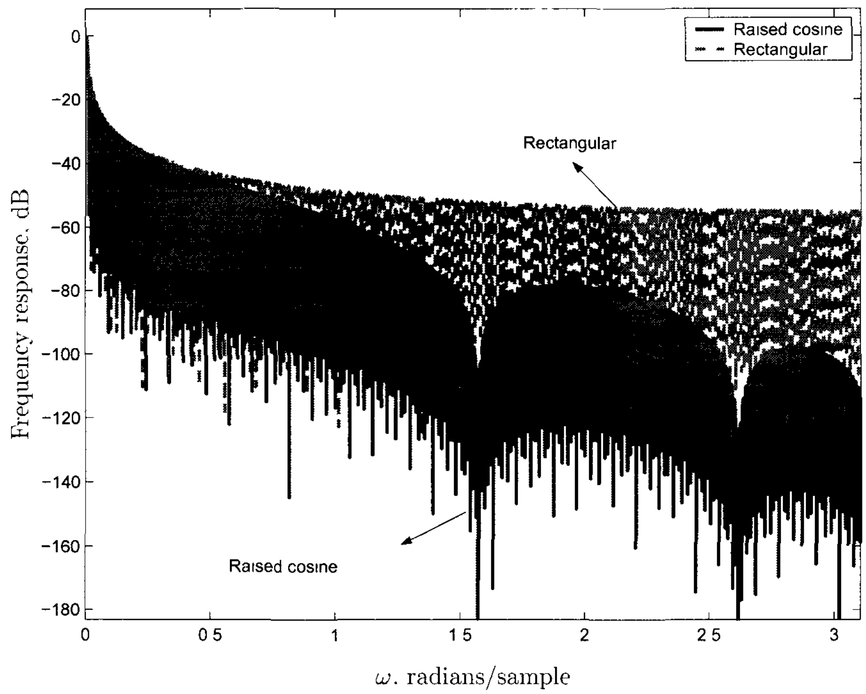

Figure 2.13: Frequency response of the transmitter window, w_k.

windowing method that improves the subchannel spectral containment at the transmitter without using extra cyclic prefix and requires relatively simple post-processing at the receiver has been proposed. It was first realized by Cuypers *et al.* [25] that the post-processing will be channel-independent if the window itself possesses cyclic-prefix property. In this section, the transmitter windowing method of [25, 79, 80] is studied.

Recall Figure 2.2 in Section 2.1.2. In this section we will use the same notations as in Section 2.1 2. Similar to the previous section, the transmitter windowing is applied after the cyclic prefix is added, and the window can be represented by the $N \times N$ diagonal matrix $\mathbf{W}$, where

$$\mathbf{W} = \mathrm{diag}\left(w_0, w_1, \cdots, w_{N-1}\right) \tag{2.114}$$

where w_k, $k = 0, 1, \cdots, N-1$, represent the transmitter window coefficients. In order to ensure a cyclic structure for the transmitted signal, which is required for a reduced complexity ICI cancellation at the receiver [25, 79, 80], the window is constrained to satisfy the following cyclic prefix property

$$w_k = w_{k+M}, \quad k = 0, 1, \cdots, P-1 \tag{2.115}$$

Due to the cyclic property in (2.115), applying the window $\mathbf{W}$ after the cyclic prefix adding module in Figure 2.2, is equivalent to applying the window $\widetilde{\mathbf{W}}$ before the module that adds the cyclic prefix, where the window $\widetilde{\mathbf{W}}$ is the $M \times M$ diagonal matrix

$$\widetilde{\mathbf{W}} = \operatorname{diag}(\psi_0, \psi_1, \cdots, \psi_{M-1}) \tag{2.116}$$

where

$$\psi_k = w_{k+P}, \quad k = 0, 1, \cdots, M-1 \tag{2.117}$$

Recall that for the DMT system with no windowing, the vector of subchannel outputs is given by (2.31). After applying the window of (2.116), the subchannel outputs are given by

$$\mathbf{y}_n = \mathbf{F}\mathbf{R}\mathbf{C}_0\mathbf{T}\widetilde{\mathbf{W}}\mathbf{F}^H\mathbf{x}_n + \mathbf{F}\mathbf{R}\boldsymbol{\eta}_n \tag{2.118}$$

It is known [82] that the product of a diagonal matrix and the IFFT matrix can be written as the product of the IFFT matrix and a circulant matrix. Specifically, it can be shown that

$$\widetilde{\mathbf{W}}\mathbf{F}^H = \mathbf{F}^H\boldsymbol{\Psi} \tag{2.119}$$

where $\boldsymbol{\Psi}$ is the $M \times M$ circulant matrix defined by

$$\boldsymbol{\Psi} = \begin{pmatrix} \Psi_0 & \Psi_1 & \cdots & \Psi_{M-1} \\ \Psi_{M-1} & \Psi_0 & \cdots & \Psi_{M-2} \\ \ddots & \ddots & \ddots & \ddots \\ \Psi_1 & \Psi_2 & \cdots & \Psi_0 \end{pmatrix} \tag{2.120}$$

and Ψ_i is the ith component of the IFFT of ψ_k, i.e.,

$$\Psi_i = \frac{1}{\sqrt{M}} \sum_{k=0}^{M-1} \psi_k e^{j\frac{2\pi}{M}ki} \tag{2.121}$$

Substituting (2.119) into (2.118), we get

$$\mathbf{y}_n = \mathbf{F}\mathbf{R}\mathbf{C}_0\mathbf{T}\mathbf{F}^H\mathbf{\Psi}\mathbf{x}_n + \mathbf{F}\mathbf{R}\boldsymbol{\eta}_n \tag{2.122}$$

Recall from (2.32) in Section 2.1.2 that $\mathbf{F}\mathbf{R}\mathbf{C}_0\mathbf{T}\mathbf{F}^H = \mathbf{D}$, where $\mathbf{D}$ is the diagonal matrix defined in (2.32). Therefore, (2.122) simplifies to

$$\mathbf{y}_n = \mathbf{D}\mathbf{\Psi}\mathbf{x}_n + \mathbf{F}\mathbf{R}\boldsymbol{\eta}_n \tag{2.123}$$

The first step in the recovery of $\mathbf{x}_n$ from $\mathbf{y}_n$ is to apply the per-subchannel one-tap equalization as in the DMT system with no windowing, i.e., by multiplying $\mathbf{y}_n$ by the matrix inverse of $\mathbf{D}$, which we denote by $\mathbf{D}^{-1}$, where $\mathbf{D}^{-1}$ is the $M \times M$ diagonal matrix defined as

$$\mathbf{D}^{-1} = \mathrm{diag}\left(\frac{1}{C(e^{j0})}, \frac{1}{C(e^{j\frac{2\pi}{M}})}, \cdots, \frac{1}{C(e^{j\frac{2\pi}{M}(M-1)})}\right) \tag{2.124}$$

Multiplying both sides of (2.123) by $\mathbf{D}^{-1}$, and denoting the result by $\tilde{\mathbf{y}}_n$, we get

$$\tilde{\mathbf{y}}_n = \mathbf{D}^{-1}\mathbf{y}_n = \mathbf{\Psi}\mathbf{x}_n + \mathbf{D}^{-1}\mathbf{F}\mathbf{R}\boldsymbol{\eta}_n \tag{2.125}$$

In order to recover $\mathbf{x}_n$ from $\mathbf{y}_n$ in (2.125), notice that from (2.119) we have $\mathbf{\Psi} = \mathbf{F}\widetilde{\mathbf{W}}\mathbf{F}^H$. Thus, the matrix inverse of $\mathbf{\Psi}$ is given by

$$\mathbf{\Psi}^{-1} = \mathbf{F}\mathbf{\Lambda}\mathbf{F}^H \tag{2.126}$$

where $\mathbf{\Lambda}$ is the $M \times M$ matrix given by

$$\mathbf{\Lambda} = \mathrm{diag}\left(\frac{1}{\psi_0}, \frac{1}{\psi_1}, \cdots, \frac{1}{\psi_{M-1}}\right) \tag{2.127}$$

multiplying both sides of (2.125) by $\mathbf{\Psi}^{-1}$ given in (2.126), we have

$$\mathbf{F}\mathbf{\Lambda}\mathbf{F}^H\tilde{\mathbf{y}}_n = \mathbf{x}_n + \bar{\boldsymbol{\eta}}_n \tag{2.128}$$

where $\bar{\boldsymbol{\eta}}$ is the noise vector given by

$$\bar{\boldsymbol{\eta}}_n = \mathbf{F}\mathbf{\Lambda}\mathbf{F}^H\mathbf{D}^{-1}\mathbf{F}\mathbf{R}\boldsymbol{\eta}_n \tag{2.129}$$

Figure 2.14 shows the DMT system with the transmitter windowing method of this section. It can be seen from (2.128) that $\mathbf{x}_n$ can be recovered with a relatively simple receiver. The simplicity of the receiver of this system can be seen both from (2.128) and Figure 2.14. Indeed, comparing this system with the DMT system with no windowing, the extra processing required at the receiver consists of an M-point IFFT, M scalar multiplications (captured by $\mathbf{\Lambda}$), and an M-point FFT, all of which can be done efficiently. Recall that since no extra cyclic prefix is used in this method, if this extra processing is not done, ICI will appear in the subchannel outputs. Notice that the relatively simple FFT-based ICI cancellation of the system in this section becomes possible because of the cyclic-prefixed structure of the window, as defined in (2.115). On the other hand, the coefficients ψ_k, $k \in [0, M-1]$, can be chosen in a manner such that the spectral characteristics of the subchannels at the transmitter are improved. In [79, 80], the transmitter window with minimum stopband energy has been used, where the stopband energy of the window is defined as

$$E_{sb} = \frac{1}{2\pi}\int_{\omega_s}^{2\pi-\omega_s} |W(e^{\jmath\omega})|^2\, d\omega \tag{2.130}$$

where $W(e^{\jmath\omega})$ is the Fourier transform of the window defined in (2.115) and ω_s is a parameter that has been considered for defining the stopband. From (2.130), it can be shown that

$$E_{sb} = \boldsymbol{\psi}^T\mathbf{Q}\boldsymbol{\psi} \tag{2.131}$$

where $\boldsymbol{\psi}$ is the $M \times 1$ vector

$$\boldsymbol{\psi} = (\psi_0, \psi_1, \cdots, \psi_{M-1})^T \tag{2.132}$$

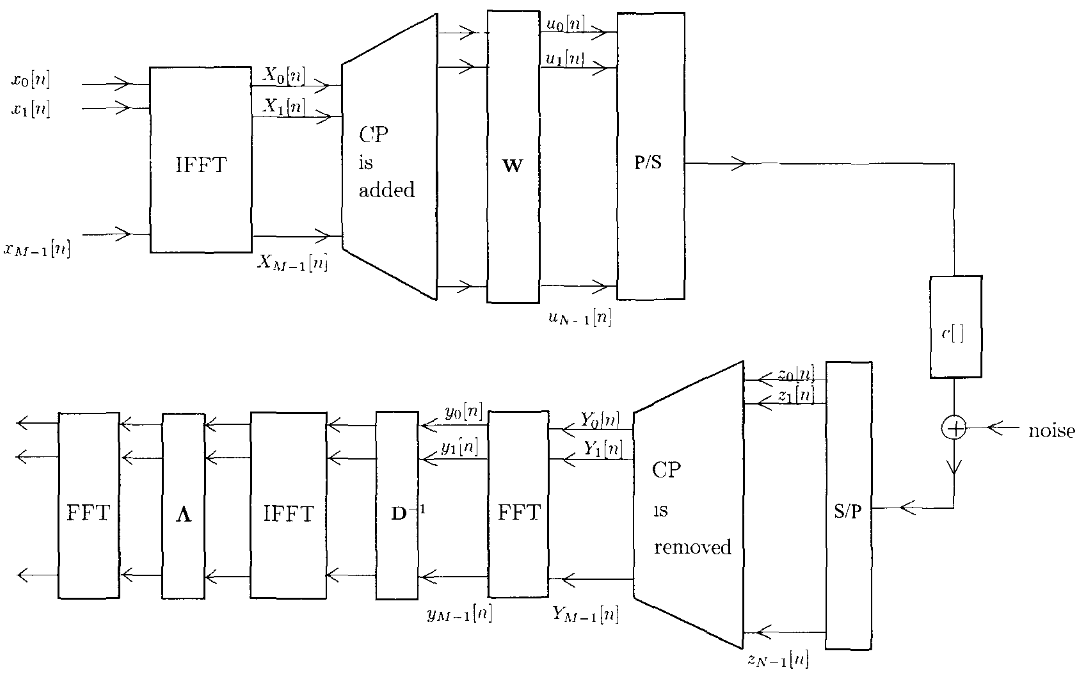

Figure 2.14: Transmitter windowing in the DMT system without using extra cyclic prefix. The efficient FFT-based ICI cancellation is possible at the receiver due to the cyclic-prefixed structure of the window (see (2.115)).

and $\mathbf{Q}$ is the $N \times N$ matrix defined as

$$[\mathbf{Q}]_{i,k} = \begin{cases} 1 - \frac{\omega_s}{\pi}, & i = k \\ -\frac{\sin((i-k)\omega_s)}{\pi(i-k)}, & i \neq k \end{cases} \tag{2.133}$$

The window coefficients in [79, 80] are designed using the following optimization problem

$$\text{minimize} \quad \boldsymbol{\psi}^H \mathbf{Q} \boldsymbol{\psi} \tag{2.134a}$$

$$\text{subject to} \quad \boldsymbol{\psi}^H \boldsymbol{\psi} = 1 \tag{2.134b}$$

Since $\mathbf{Q}$ is positive semi-definite, the solution for the optimization problem in (2.134) is the eigen vector corresponding to the smallest eigen value of $\mathbf{Q}$.

In order to evaluate the performance of the windowed DMT system of Figure 2.14, Lin *et al.* [79] have considered two parameters. One parameter is the spectral leakage, β, which is defined as the ratio of the stopband energy (defined in (2.130)) of the optimal transmitter window obtained by (2.134) to the stopband energy of the rectangular window of DMT system with no windowing. The other parameter considered for the evaluation of this system is the SNR loss, α. To define the SNR loss, Lin *et al.* [79] have considered the same transmission power in both the windowed and nonwindowed DMT systems, and have defined the SNR loss as the ratio of the total output noise power in the windowed system to the total output noise power in the non-windowed DMT system, where the total output noise power of the system of Figure 2.14 is defined as $E(\bar{\boldsymbol{\eta}}^H\bar{\boldsymbol{\eta}})$, where E denotes the expected value operator and $\bar{\boldsymbol{\eta}}$ is the output noise vector, as defined in (2.129).

Consider a DMT system with $M = 512$ subchannels and a cyclic prefix of length $P = 32$. For these parameters and a few different values for the stopband parameter, ω_s, the optimal windows, which are obtained through the optimization problem in (2.134) are plotted in Figure 2.15. Figure 2.16 shows the spectral leakage, β, and the SNR loss, α for the windowed system with $M = 512$ and $P = 32$. This figure is extracted from the numerical results in [79]. From this figure it can be seen that as ω_s increases, the spectral leakage decreases, but the SNR loss increases. It is also seen that for all the shown ω_s values, the SNR loss is larger than one and the spectral leakage is smaller than one. Therefore, it can be seen that although the windowed system has less spectral leakage than the DMT system with no window, this improvement is achieved at the price of an SNR loss. Moreover, in this windowing scheme, the smaller the spectral leakage, the larger the SNR loss.

In order to further illustrate the reduction in spectral leakage achieved by the

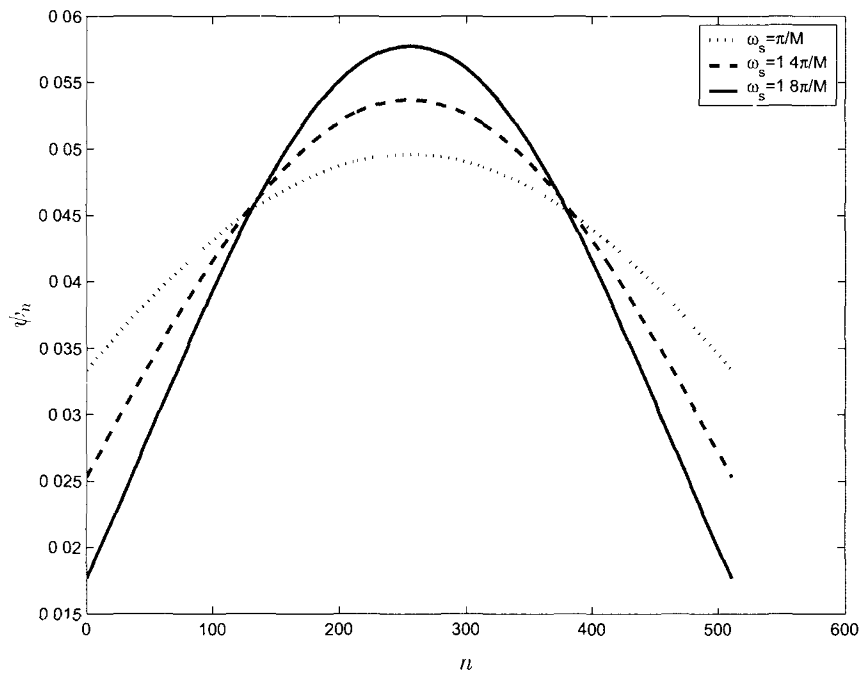

Figure 2.15: The optimal windows obtained by solving (2.134) for three different values of the parameter ω_s.

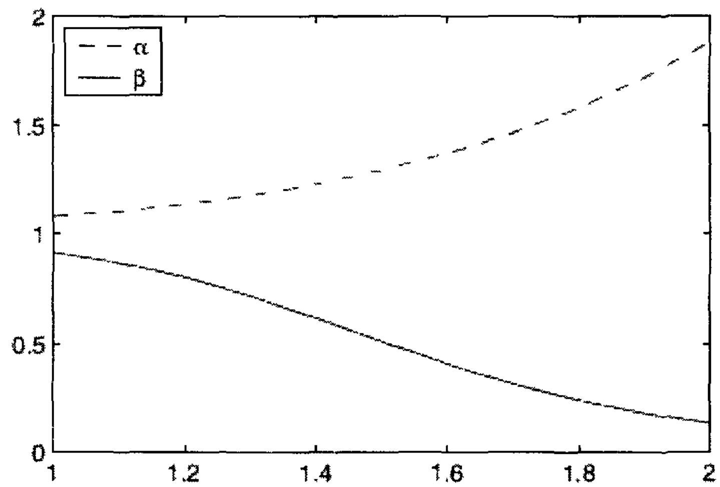

Figure 2.16: Spectral leakage, β, and SNR loss, α, as a function of ω_s, for the windowed system with $M = 512$ and $P = 32$ [79].

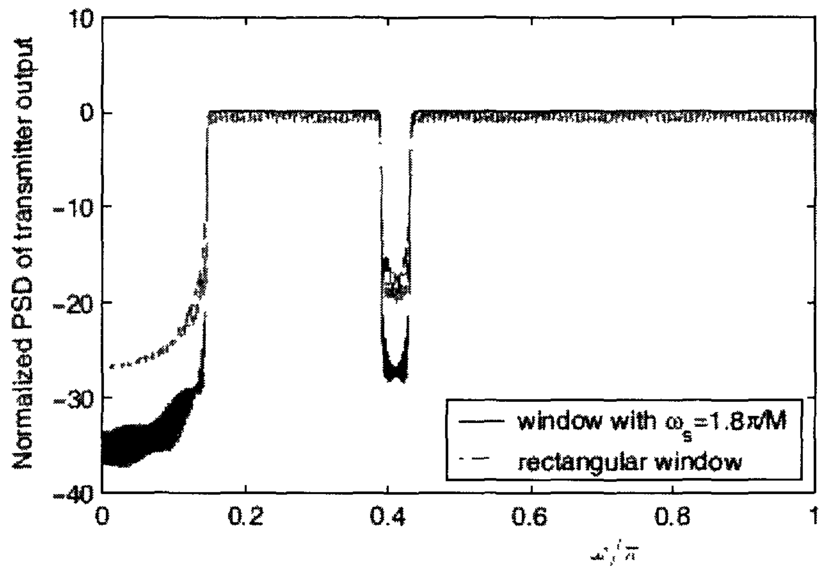

Figure 2.17: Transmitter output power spectral density (in dB) for the conventional DMT system and the windowed DMT system obtained by (2.134) when $\omega_s = 1.8\pi/M$ [79].

windowing scheme of this section, following numerical example is presented which is reported from the numerical results obtained in [79,80]. Figure 2 17 shows the power spectral density at the transmitter output for the conventional DMT system with no windowing and for the windowed DMT system with the window obtained by (2.134) with $\omega_s = 1.8\pi/M$. The subchannels 38 to 99 and 111 to 255 are used, while the subchannels 0 to 37 and 100 to 110 are left blank (not used). It can be seen that the spectral leakage in the frequency bands in which the corresponding subchannels are off is considerably reduced by the transmitter windowing. Recall that, however, this reduction in the spectral leakage is obtained at the price of a loss in SNR.

2.5 DSL fundamentals

In Chapters 3 and 4, the schemes proposed in this thesis for improving the achievable bit rate in multi-carrier communication systems will be presented. While those schemes are valid for applications in any communication environment, including wireless and wireline channels, the numerical examples that will be presented will consider realistic models for digital subscriber line (DSL) channels. In this section, the basic characteristics of DSL channels are studied and the practical challenges encountered in the design of transceivers for these channels are described. The background information presented in this section will allow a more efficient exposition of the numerical examples in Chapters 3 and 4.

DSL technology enables high data rate communications over telephone subscriber lines. Although telephone twisted wire pairs were originally deployed to carry voice signals with a bandwidth of less than 4 kHz, they are capable of carrying much broader bandwidths. In recent years, advances in silicon technology, digital communications engineering, and digital signal processing have made it possible to communicate over DSL lines outside the voiceband at data rates of several megabits per second. Several DSL standards have been established and are used by tens of millions of customers throughout the world [83]. These are generally referred to as xDSL, and include basic rate DSL (ISDN), high bit rate DSL (HDSL), asymmetric DSL (ADSL), and very high-speed DSL (VDSL) [84]. Among different DSL standards, ADSL is the one which is used most widely. In fact, according to the DSL Forum [17], ADSL is currently the most chosen broadband option in the world. ADSL is used for internet services and its newest standard version, ADSL2plus, is capable of providing services with maximum downstream and upstream rates of 24 Mbit/sec and 1 Mbit/sec, respectively [17]. On the other hand, in response to the increasing demand for services with even higher data rates, the VDSL standard has been established with the potential maximum

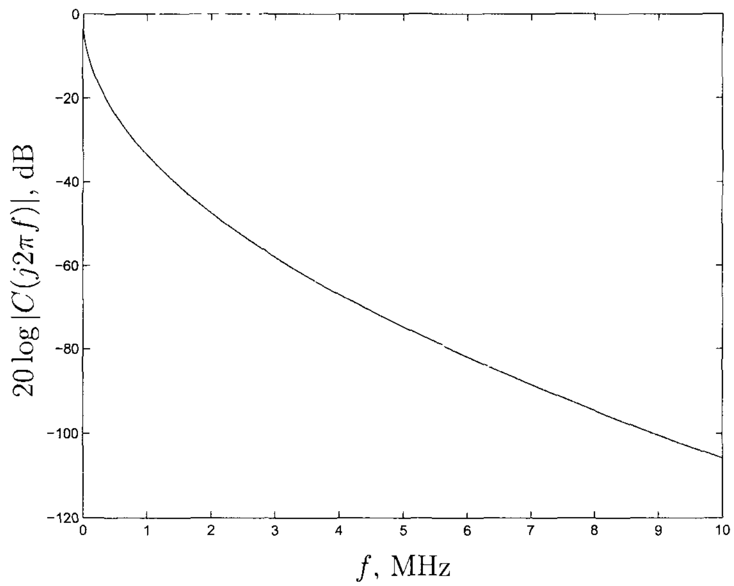

Figure 2.18: Frequency response of the DSL channel for a cable length of $\ell = 1$ km.

downstream and upstream data rates of 100 Mbit/sec. In the rest of this section, the major characteristics of DSL channels are studied.

The frequency response of a voice-grade unshielded twisted pair (UTP-3) is reasonably accurately modelled by [26]

$$C(j2\pi f) = e^{-3.85\times 10^{-6}(1+j)\sqrt{f}\ell} \tag{2.135}$$

where $j = \sqrt{-1}$, f is the frequency in Hz, ℓ is the length of the cable in meters, and the constant propagation delay has been ignored. Notice that the frequency response in (2.135) is a function of both frequency and the cable length. Figure 2.18 shows the magnitude response of a DSL channel for a cable length of $\ell = 1$ km. From this figure it can be seen that the DSL channel is highly frequency-selective. Figure 2.19 shows the magnitude response of the DSL channel versus different cable lengths. at a fixed frequency of $f = 1$ MHz. From Figure 2.19 it can be seen how increasing the length of the cable increases the attenuation over the DSL channel.

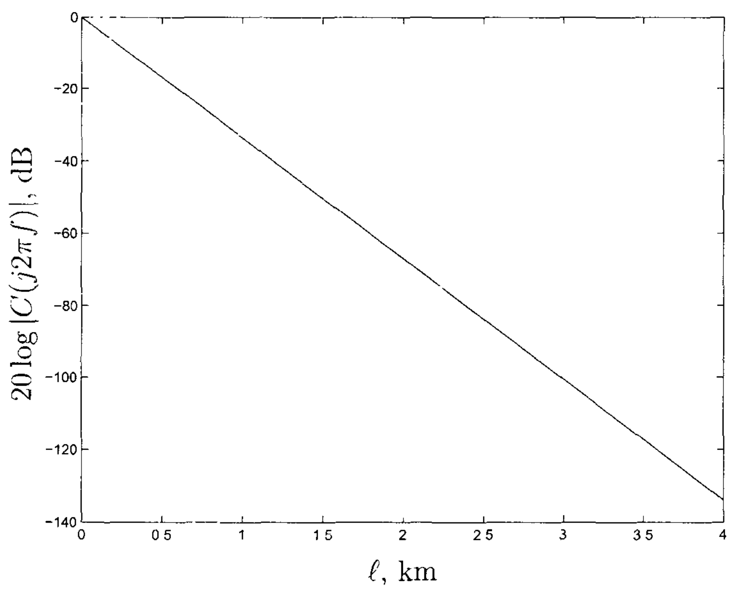

Figure 2.19: Variation of the magnitude response of the DSL channel as a function of the cable length at the frequency $f = 1$ MHz.

As can be seen from (2.135) and Figure 2.18, the DSL channel is highly frequency-selective. Indeed, a major challenge in transceiver design for DSL channels is to overcome the ISI caused by these channels. Multi-carrier modulation schemes have been considered as efficient methods to overcome the ISI caused by this frequency-selectivity. On the other hand, in addition to the ISI, which is one of the major challenges in DSL transceiver design, there are a number of other noise and interference signals that have to be considered in the design of DSL transceivers. These include additive white Gaussian noise (AWGN), near-end crosstalk (NEXT), far-end crosstalk (FEXT), echo, narrowband noise, and impulse noise.

Crosstalk noise in DSL channels is created among the wires in a cable binder because of the coupling of signals from the data-carrying wires to each other. Figure 2.20 shows the two types of crosstalk in a typical DSL channel. Transceiver 1 at the central office (CO) is connected to Transceiver 2 at the customer end, which in the DSL terminology is often referred to as the customer premises equipment (CPE).

Similarly, Transceiver 3 is connected to Transceiver 4 via a wire pair, and it is assumed that the two wire pairs are in the same cable bundle. Crosstalk, by definition, is the interference from one wire pair to another wire pair. If the signal transmitted by a transceiver at one end, interferes with the signal received by another transceiver at the same end, that interference is called near-end crosstalk (NEXT). If the signal transmitted by a transceiver at one end interferes with the signal received by another transceiver at the other end (other than the one targeted for the transmitted signal), it is called far-end crosstalk (FEXT). Crosstalk can be the most disturbing type of noise in twisted pair channels, and can considerably reduce the performance of the DSL transceivers if it is not suppressed or eliminated [15]. Based on the empirical studies in [15], the power spectral density (PSD) of NEXT and FEXT signals in a 50-pair binder caused by n disturbers, all having the same power spectral density $\mathrm{PSD}(f)$, can be modelled as

$$\mathrm{PSD}_{\mathrm{NEXT}}(f) = \mathrm{PSD}(f)\left(\frac{n}{49}\right)^{0.6} 10^{-13} f^{1.5}, \tag{2.136}$$

and

$$\mathrm{PSD}_{\mathrm{FEXT}}(f) = \mathrm{PSD}(f)\left(\frac{n}{49}\right)^{0.6} |C(j2\pi f)|^2 \left(3 \times 10^{-19}\right) \ell f^2, \tag{2.137}$$

respectively [15, 26]. In (2.136) and (2.137), f is the frequency in Hz, ℓ is the cable length in meter, and $C(j2\pi f)$ is the frequency response of the DSL channel given by (2.135). Figure 2.21 depicts the coupling functions of NEXT and FEXT when $n = 49$ and the cable length is $\ell = 1$ km.

Another type of interference that affects DSL transceivers is narrowband radio frequency interference (RFI), which is mainly caused by AM broadcast and amateur (HAM) radio signals. In DSL terminology, radio frequency interference is also referred to as radio frequency (RF) ingress, or narrowband noise. Twisted pair phone lines make relatively good antennas for AM and HAM signals [15], and thus, these signals appear at DSL receivers. AM radio signals typically have a bandwidth of 10 kHz and

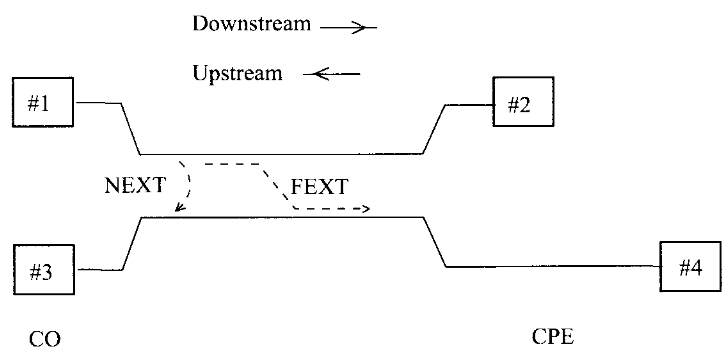

Figure 2.20: The two types of crosstalk, NEXT and FEXT, in a DSL system.

Frequency kHz	Differential mode power dBm
660	-60
710	-30
770	-70
1050	-55
1130	-30
1190	-60
1280	-55
1330	-60
1480	-70
1600	-60

Table 2.2: Model 1 radio noise of [85] for AM radio signals.

are broadcast in the frequency band 560 kHz to 1.6 MHz. While many AM radio signals are generally active in an urban area, ADSL and VDSL test specifications consider a 10-frequency model for AM radio noise [15,85]. Table 2.2 lists the frequency and power values for these AM signals [85]. Amateur radio signals, on the other hand, are transmitted in the frequency bands shown in Table 2.3 [15]. Amateur radio transmitters use a bandwidth of 2.5 kHz, and generally use frequency shift keying (FSK) modulation.

Impulse noise is another type of interference that has to be considered in the design of DSL transceivers. Impulse noise is a nonstationary interference signal which

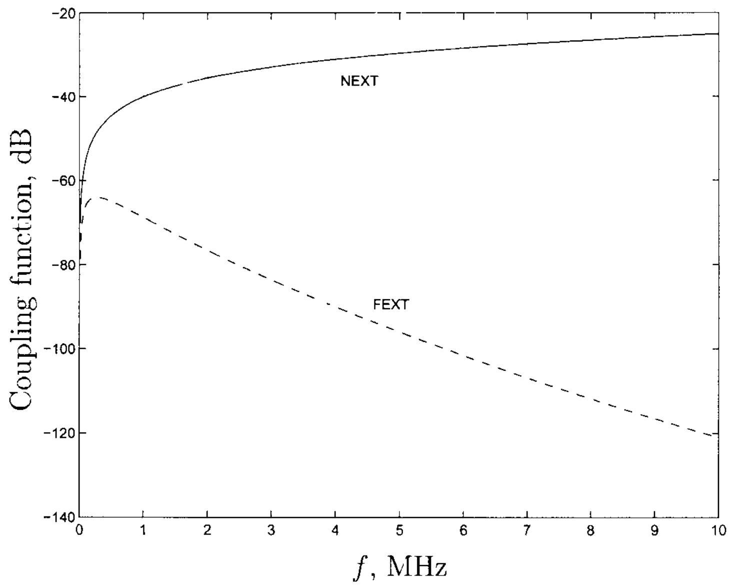

Figure 2.21: The coupling functions for NEXT and FEXT for a cable length $\ell = 1$ km when there are $n = 49$ disturbers.

is usually generated by electromagnetic-based systems in the vicinity of the phone lines [15]. For instance, in buildings, impulse noise could be created by the elevator electrical systems, turning on and off of the electric motors of refrigerators, washing and dryer machines, and also by the ringing of phones that share the same cable binder. Each of these noises is transient. Indeed, the impulse noise is considered to be a burst noise, and therefore, in ADSL and VDSL standards, a combination of error correction coding, such as Reed-Solomon codes, and interleaving is used to overcome the impact of impulse noise [16, 86].

Another disturbing interference in DSL transceivers is echo. Each DSL transceiver simultaneously transmits data in one direction, and receives data in the opposite direction. To avoid echo, DSL transceivers use hybrid circuits [15]. If the perfect impedance matching in the hybrid circuit is achieved, echo will be eliminated. In addition to hybrid circuits which are generally analog circuits [15], DSL transceivers often use digital echo cancellation schemes to suppress the residual echo which is

Band lowest frequency MHz	Band highest frequency MHz
1.81	2.0
3.5	4.0
7.0	7.1
10.1	10.15
14.0	14.35
18.068	18.168
21	21.45
24.89	24.99
28.0	29.7

Table 2.3: Amateur radio bands

caused because of the imperfect impedance matching in phone line analog circuits. For instance, in [87], the authors have proposed a high-speed echo cancellation technique for DMT transceivers.

2.6 Near-end crosstalk cancellation using cyclic suffix extension

It was mentioned earlier that in DMT systems, near-end crosstalk (NEXT) is one of the most significant types of interference degrading the achievable bit rate of these systems. This is especially the case in DSL channels, where several twisted pair wires are bound together in a single cable.

While windowing methods can be employed to mitigate NEXT in DMT transceivers, they do not completely eliminate NEXT. In this section, a NEXT cancellation method is studied which totally eliminates NEXT. In this method, proposed by Sjoberg *et al.* in [88], in order to eliminate NEXT, in addition to a cyclic prefix with a length larger than or equal to the order of the channel, a cyclic suffix of an appropriate length is applied to the transmitted DMT signal.

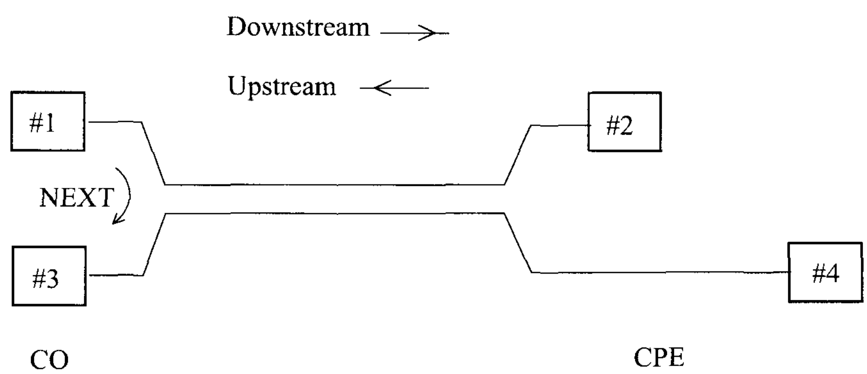

Figure 2.22: A schematic diagram of the DSL transceivers and their connection via twisted pairs. Transceivers 1 and 3 at the central office (CO) are connected to the Transceivers 2 and 4 at the customer premises end (CPE), respectively.

Figure 2.22 shows a schematic diagram of the transceivers of two users at the customer premises end (CPE) connected to their corresponding transceivers at the central office (CO), in a typical DSL application [15]. Each pair of transceivers are connected using a twisted wire pair, and it is assumed that the twister pairs of the two users are in the same cable. Consider Transceiver 3 at the CO side in Figure 2.22. The received signal at this transceiver will have three components. One component is the desired upstream signal transmitted by Transceiver 4 at the CPE side. Another component is the NEXT signal emerging from the downstream transmission by Transceiver 1 at the CO side, and the third component consists of other noise and interference signals. Notice that in multi-carrier systems, in general, in order to reduce the impact of NEXT and echo, distinct subchannels are used for downstream and upstream transmission. Yet, because of the high level of subchannel spectral sidelobes in DMT systems, NEXT can significantly degrade the performance of the system. In the rest of this section, it will be shown that if the transmitters are synchronized and a cyclic suffix of appropriate length is added to the transmitted signal of each transmitter (in addition to the cyclic prefix of length at least equal to the order of the channel), NEXT will be eliminated [88].

Recall the basic DMT system of Figure 2.2 in Section 2.1.2. In the following, we consider the same structure for the DMT transceiver, except the CP adder and CP removal modules will be different from those in the basic DMT system, as will be described later. Also, in this section, we will use the same notation as in Section 2.1.2 and the DMT system equations presented in Section 2.1.2 will be frequently used.

In Figure 2.22, the upstream signal arriving at the receiver of Transceiver 3 goes through a larger delay than the NEXT signal arriving at that receiver. We denote this difference in the delays by Δ. Denoting the nth upstream transmitted block of data transmitted by Transceiver 4 as $\mathbf{u}_n$ (see Figure 2.2), and the nth downstream transmitted block of data transmitted by Transceiver 1 as $\mathbf{v}_n$, because of the existence of a difference of Δ in the delays of the two paths, when $\mathbf{u}_n$ is received at Transceiver 3, the NEXT signal that is received at that transceiver will be $\mathbf{v}_n^{\Delta}$ which is an $N \times 1$ vector with kth entry

$$v_k^{\Delta}[n] = \begin{cases} v_{k+\Delta}[n], & 0 \leq k < N - \Delta \\ v_{k-N+\Delta}[n+1], & N - \Delta \leq k < N \end{cases} \tag{2.138}$$

where $v_k[n]$ is the kth entry of $\mathbf{v}_n$. Denoting the impulse response of the upstream channel by $c[k]$ and that of the NEXT channel by $\tilde{c}[k]$, using (2.20), the nth received symbol block can be written as

$$\mathbf{z}_n = (\mathbf{C}_0\mathbf{u}_n + \mathbf{C}_1\mathbf{u}_{n-1}) + \left(\widetilde{\mathbf{C}}_0\mathbf{v}_n^{\Delta} + \widetilde{\mathbf{C}}_1\mathbf{v}_{n-1}^{\Delta}\right) + \boldsymbol{\gamma}_n \tag{2.139}$$

where $\mathbf{C}_0$ and $\mathbf{C}_1$ are the $N \times N$ channel matrices defined in (2.21) and (2.22), respectively, corresponding to the upstream channel, $\widetilde{\mathbf{C}}_0$ and $\widetilde{\mathbf{C}}_1$ are the channel matrices corresponding to the NEXT channel which are defined as

$$[\widetilde{\mathbf{C}}_0]_{i,k} = \tilde{c}[i-k], \tag{2.140}$$

and

$$[\widetilde{\mathbf{C}}_1]_{i,k} = \tilde{c}[N+i-k], \tag{2.141}$$

and $\boldsymbol{\gamma}_n$ denotes the $N \times 1$ vector which represents other noise and interference signals. Recall from (2.10) that $c[k] = 0$, $k \notin [0, L]$, where L is the order of the upstream channel. Denoting the order of the NEXT channel by $\tilde{L}$, we assume $\tilde{c}[k] = 0$, $k \notin [0, \tilde{L}]$. Since the physical length of the NEXT channel is much shorter than that of the upstream channel, as a practical assumption, it is assumed that $\tilde{L} < L$. In order to eliminate NEXT, in addition to a cyclic prefix of length P (where $P \geq L$), a cyclic suffix of length S is added to the transmitted signal. Therefore, the system equations of Section 2.1.2 have to be modified accordingly. First of all, each transmitted block of data is of size N where $N = M + P + S$. For the nth transmitted block of symbols the cyclic prefix and suffix are created by multiplying the $M \times 1$ vector $\mathbf{X}_n$ in Figure 2.2 by $\widetilde{\mathbf{T}}$, where $\widetilde{\mathbf{T}}$ is an $N \times M$ matrix given by

$$\widetilde{\mathbf{T}} = \begin{pmatrix} \mathbf{I}_{\mathrm{CP}} \\ \mathbf{I}_M \\ \mathbf{I}_{\mathrm{CS}} \end{pmatrix} \tag{2.142}$$

where $\mathbf{I}_{\mathrm{CP}}$ and $\mathbf{I}_M$ remain as they are defined in Section 2.1.2 and $\mathbf{I}_{\mathrm{CS}}$ is the $S \times M$ matrix consisting of the first S rows of the identity matrix $\mathbf{I}_M$. The cyclic prefix and suffix are removed at the receiver by multiplying $\mathbf{z}_n$ (see Figure 2.2) by $\widetilde{\mathbf{R}}$, where $\widetilde{\mathbf{R}}$ is the $M \times N$ matrix given by

$$\widetilde{\mathbf{R}} = (\mathbf{0}_{M\times P}\, \mathbf{I}_M\, \mathbf{0}_{M\times S}) \tag{2.143}$$

Looking at $\widetilde{\mathbf{R}}$ in (2.143) and $\mathbf{C}_1$ in (2.22), it can be seen that if $P \geq L$, we have $\widetilde{\mathbf{R}}\mathbf{C}_1 = \mathbf{0}$. Moreover, by considering the definition of $\widetilde{\mathbf{C}}_1$ in (2.141), since $\tilde{L} < L$, if $P \geq L$, we also have $\widetilde{\mathbf{R}}\widetilde{\mathbf{C}}_1 = \mathbf{0}$. Recall from Figure 2.2 that at the receiver, after the removal of cyclic prefix (and suffix), the FFT is applied. Thus, the vector of the subchannel outputs is given by

$$\mathbf{y}_n = \mathbf{F}\widetilde{\mathbf{R}}\mathbf{z}_n \tag{2.144}$$

Substituting $\mathbf{z}_n$ from (2.139) and replacing $\widetilde{\mathbf{R}}\mathbf{C}_1 = \mathbf{0}$ and $\widetilde{\mathbf{R}}\widetilde{\mathbf{C}}_1 = \mathbf{0}$ in the result, we get

$$\mathbf{y}_n = \mathbf{F}\widetilde{\mathbf{R}}\mathbf{C}_0\mathbf{u}_n + \mathbf{F}\widetilde{\mathbf{R}}\widetilde{\mathbf{C}}_0\mathbf{v}_n^{\Delta} + \mathbf{F}\widetilde{\mathbf{R}}\gamma_n \tag{2.145}$$

Recall that

$$\mathbf{u}_n = \widetilde{\mathbf{T}}\mathbf{F}^H\mathbf{x}_n, \tag{2.146}$$

and

$$\mathbf{v}_n = \widetilde{\mathbf{T}}\mathbf{F}^H\tilde{\mathbf{x}}_n, \tag{2.147}$$

where $\mathbf{x}_n$ is the $M \times 1$ subchannel input vector corresponding to the upstream transmission, transmitted by Transceiver 4, and $\tilde{\mathbf{x}}_n$ is the $M \times 1$ subchannel input vector corresponding to the downstream transmission, transmitted by Transceiver 1. From (2.145) it can be seen that $\mathbf{y}_n$ consists of three components, the desired signal, the NEXT interference, and other noise and interference signals. The desired signal in (2.145) is equal to $\mathbf{F}\widetilde{\mathbf{R}}\mathbf{C}_0\mathbf{u}_n$ which, using (2.146), is equivalently given by $\mathbf{F}\widetilde{\mathbf{R}}\mathbf{C}_0\widetilde{\mathbf{T}}\mathbf{F}^H\mathbf{x}_n$. It can be shown that $\widetilde{\mathbf{R}}\mathbf{C}_0\widetilde{\mathbf{T}}$ is a circulant matrix and thus it is diagonalized by FFT and IFFT matrices. Specifically, it can be shown that[15]

$$\mathbf{F}\widetilde{\mathbf{R}}\mathbf{C}_0\mathbf{u}_n = \mathbf{F}\widetilde{\mathbf{R}}\mathbf{C}_0\widetilde{\mathbf{T}}\mathbf{F}^H\mathbf{x}_n = \mathbf{D}\mathbf{x}_n \tag{2.148}$$

where $\mathbf{D}$ is the diagonal matrix defined in (2.32). The NEXT term in (2.145) is equal to $\mathbf{F}\widetilde{\mathbf{R}}\widetilde{\mathbf{C}}_0\mathbf{v}_n^{\Delta}$. By looking at $\widetilde{\mathbf{R}}$ in (2.143) and $\widetilde{\mathbf{C}}_0$ in (2.140), it can be seen that the last S columns of $\widetilde{\mathbf{R}}\widetilde{\mathbf{C}}_0$ are all-zero columns. Therefore, recalling the structure of $\mathbf{v}_n^{\Delta}$ in (2.138), it can be seen that if $S \geq \Delta$. in $\mathbf{v}_n^{\Delta}$, the last Δ entries will not have any effect in the NEXT term, and consequently the orthogonality among the subchannels will be maintained. In order to further analyze the NEXT term, if we denote the nth subchannel input vector of the downstream transmission of Transceiver 1 by $\tilde{\mathbf{x}}_n$ and the resulting $M \times 1$ vector after IFFT module by $\widetilde{\mathbf{X}}_n$, the $N \times 1$ vector $\mathbf{v}_n$ will be

[15] The proof is similar to that for the conventional DMT system.

equal to $\mathbf{v}_n = \widetilde{\mathbf{T}}\widetilde{\mathbf{X}}_n$, which using (2.142) can be written as

$$\mathbf{v}_n = \left(\tilde{X}_{M-P}[n], \cdots, \tilde{X}_{M-1}[n], \tilde{X}_0[n], \cdots, \tilde{X}_{M-1}[n], \tilde{X}_0[n], \cdots, \tilde{X}_{S-1}[n]\right)^T \quad (2.149)$$

Using (2.149) and recalling the structure of $\mathbf{v}_n^\Delta$ from (2.138), it can be seen that

$$\mathbf{v}_n^\Delta = \left(\tilde{X}_{M-P+\Delta}[n], \cdots, \tilde{X}_{M-1}[n], \tilde{X}_0[n], \cdots, \tilde{X}_{M-1}[n], \tilde{X}_0[n], \cdots, \tilde{X}_{S-1}[n], \cdots\right)^T \quad (2.150)$$

Notice that we assume $S \geq \Delta$ and therefore, as mentioned earlier, the last Δ entries of $\mathbf{v}_n$ or $\mathbf{v}_n^\Delta$ will not have any effect in the result of $\widetilde{\mathbf{R}}\widetilde{\mathbf{C}}_0\mathbf{v}_n$ and $\widetilde{\mathbf{R}}\widetilde{\mathbf{C}}_0\mathbf{v}_n^\Delta$, respectively. Now, similar to the identity in (2.148), we know that $\mathbf{F}\widetilde{\mathbf{R}}\widetilde{\mathbf{C}}_0\mathbf{v}_n = \widetilde{\mathbf{D}}\tilde{\mathbf{x}}_n$, where

$$\widetilde{\mathbf{D}} = \mathrm{diag}\left(\tilde{C}(e^{\jmath 0}), \tilde{C}(e^{\jmath\frac{2\pi}{M}}), \cdots, \tilde{C}(e^{\jmath\frac{2\pi}{M}(M-1)})\right) \quad (2.151)$$

where $\tilde{C}(e^{\jmath\omega})$ is the Fourier transform of $\tilde{c}[k]$. Now, while noticing from comparison of (2.149) and (2.150), that each entry of $\mathbf{v}_n^\Delta$ is a shifted version of the corresponding entry of $\mathbf{v}_n$ by the amount of Δ, recall that since $\tilde{X}_\imath[n]$ is the inverse discrete Fourier transform of $\tilde{x}_k[n]$, we have that $\tilde{X}_{\imath+\Delta}[n]$ is the inverse discrete Fourier transform of $\tilde{x}_k[n]e^{\jmath\frac{2\pi}{M}k\Delta}$. Thus, we have

$$\mathbf{F}\widetilde{\mathbf{R}}\widetilde{\mathbf{C}}_0\mathbf{v}_n^\Delta = \widetilde{\mathbf{D}}\tilde{\mathbf{x}}_n^\Delta \quad (2.152)$$

where $\tilde{\mathbf{x}}_n^\Delta$ is the $M \times 1$ vector where its kth entry is

$$\tilde{x}_k^\Delta[n] = \tilde{x}_k[n]e^{\jmath\frac{2\pi}{M}k\Delta} \quad (2.153)$$

Substituting (2.152) and (2.148) into (2.145), we get

$$\mathbf{y}_n = \mathbf{D}\mathbf{x}_n + \widetilde{\mathbf{D}}\tilde{\mathbf{x}}_n^\Delta + \mathbf{F}\widetilde{\mathbf{R}}\boldsymbol{\gamma}_n \quad (2.154)$$

Notice that $\mathbf{x}_n$ is the $M \times 1$ subchannel input vector of upstream transmission by Transceiver 4, and $\tilde{\mathbf{x}}_n$ is the $M \times 1$ subchannel input vector of downstream transmission by Transceiver 1 (the NEXT signal source in Figure 2.22), and $\tilde{\mathbf{x}}_n^\Delta$ is related to $\tilde{\mathbf{x}}_n$ as described by (2.153). From (2.154) it can be seen that since $\mathbf{D}$ and $\widetilde{\mathbf{D}}$

are diagonal matrices, if distinct subchannels are used for upstream and downstream transmissions, the downstream transmission (NEXT signal) will have no interference with the upstream signal. Thus, NEXT will be totally eliminated.

Notice that in a communication network, e.g., the DSL network, there are several transceivers which can be sources of NEXT for eachother. In order to eliminate NEXT, synchronization should be provided among all the transmitters at both ends (both at CO and CPE), and a cyclic suffix which is at least as long as the delay in the longest channel in the network has to be used.

The cyclic suffix technique described in this section is a useful approach for removing near-end crosstalk, but the requirement of a cyclic suffix in this scheme reduces the bandwidth efficiency. In addition, as mentioned earlier, this technique requires synchronization among all transceivers that can impose NEXT on each other. The messaging required to achieve such a synchronization increases the complexity of the system and can further reduce the bandwidth efficiency. Therefore, the schemes that mitigate NEXT via spectral containment and do not require a complicated synchronization, such as FMT and windowed DMT schemes, remain attractive, and hence, they remain as the main focus of this thesis.

Chapter 3

Efficient Design of FMT Systems

In this chapter an efficient channel-independent design method for the prototype filter in the FMT filter bank is proposed. This method allows efficient evaluation of the inherent trade-off between the subchannel spectral containment provided by the prototype filter and the intersymbol interference (ISI) that the filter generates. An appropriate operating point on this trade-off curve is then identified by computing the achievable bit rate for FMT systems with prototype filters which lie on the curve. The numerical results indicate that careful exploration of the filter design trade-off results in a considerable gain in the achievable bit rate. Furthermore, the insight gained from this design can be transferred to the choice of the optimal number of subchannels. Finally, since the presence of ISI in FMT subchannels renders the conventional water-filling power loading algorithm suboptimal. an efficient power loading algorithm for FMT that enables higher achievable bit rates is proposed.

3.1 Introduction

In Chapter 2, the FMT scheme was studied as a multi-carrier modulation scheme that offers improved spectral characteristics compared to DMT. This makes FMT a potential candidate for applications where a high level of subchannel spectral containment is required at the transmitter and a high level of subchannel frequency selectivity is needed at the receiver. An example of such application is DSL, in which it is required to mitigate narrowband noise and near-end crosstalk (NEXT), and satisfy the egress standards. Indeed, it has been shown that FMT-based DSL systems offer the potential for larger achievable bit rates than DMT-based DSL systems [26].

In Section 2.1.3, it was indicated that the FMT transceiver is implemented using a modulated filter bank structure. The prototype filter for this filter bank is a key design parameter, and some preliminary design methods have been proposed [26, 28, 89, 90].[1] In this chapter, we develop a more comprehensive approach to the design of prototype filter, in which we quantify an inherent trade-off between channel-independent measures of intersymbol interference (ISI) and intersubchannel interference (ICI), and we demonstrate the engineering insight that this method generates. Since our proposed prototype filter design method is a channel-independent approach, the subchannels are synthesized in a channel-indepentent manner. This allows a cost-efficient implementation of the proposed FMT filter bank. The proposed filter design approach begins with the derivation of design criteria which lead to increased subchannel signal to interference and noise ratios (SINRs) at the receiver. The design of the filter requires a compromise between these criteria and therefore there is a trade-off to be explored. In order to explore the trade-off we formally cast the design problem

[1]Some filter bank transceiver design schemes for time-varying frequency-selective fading wireless channels can be found in [91, 92], which are based on time-frequency localized pulse shaping and filtering design. In these schemes, the filter bank desig relies on the channel information, and thus, adaptive schemes for the synthesis of their filter banks are required, which imposes significant implementation complexity.

as an optimization problem. As we will show, the direct formulation of that optimization problem is non-convex in the design variables and hence the exploration of the trade-off is hindered by the intricacies of dealing with the potential for locally optimal solutions. However, we will show that the design problem can be precisely transformed into a convex optimization problem from which a globally optimal solution can be found. The convex formulation allows us to efficiently compute the inherent trade-off between the competing design criteria. Further numerical analysis then allows us to determine points on the trade-off curve that provide a large achievable bit rate. While the focus of our design examples will be on VDSL systems, FMT is also attracting attention as a candidate technology for certain wireless communication applications [39, 93]. The design methods developed herein remain valid for those applications.

To demonstrate the versatility of the proposed prototype filter design technique, we also use it to evaluate the trade-offs between ISI, ICI, and transceiver complexity that arise when choosing the number of subchannels in an FMT system. These evaluations provide important guidelines for the design of FMT systems.

As was explained in Section 2.1.3, one of the key differences between DMT and FMT systems is the high level of subchannel spectral containment provided by FMT. However, this spectral containment is achieved at the cost of ISI within each subchannel. (The trade-off between these criteria is a key component of our design approach.) The presence of ISI means that the conventional water-filling power loading algorithms developed for DMT systems yield suboptimal results unless a relatively high complexity decision feedback equalizer (DFE) is used in each subchannel of the receiver. For applications in which only simple DFEs are employed, we propose an efficient power loading algorithm that iteratively accounts for the residual ISI and hence enables higher achievable bit rates than conventional water-filling.

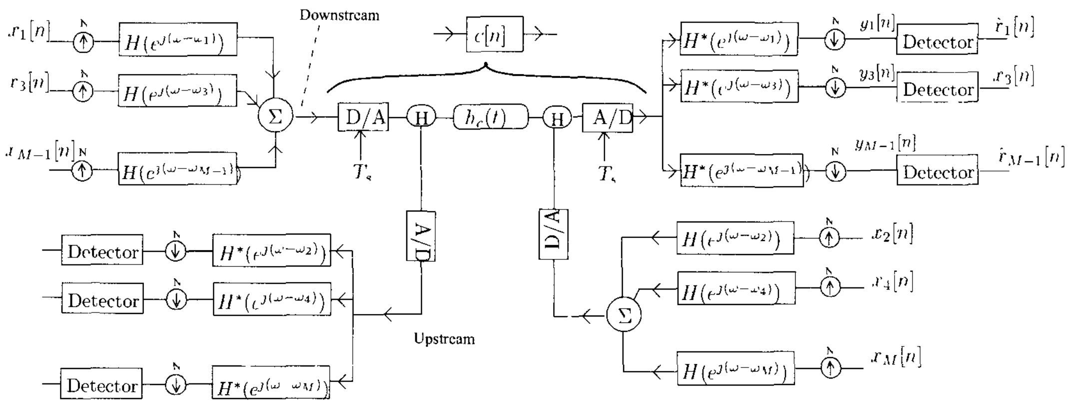

Figure 3.1: An M-channel filtered multitone (FMT) communication system. We will focus on systems in which the detector incorporates a decision feedback equalizer (DFE).

3.2 System description

The block diagram of an M-channel FMT system in which the upstream and downstream subchannels are interleaved is shown in Figure 3.1. The filter bank is constructed from a single real finite impulse response (FIR) prototype filter with impulse response $h[n]$ and frequency response $H(e^{j\omega})$. The transmission filter for each subchannel is a frequency-shifted version of the prototype filter and the first step performed by the receiver is matched filtering of each subchannel (the superscript * denotes complex conjugation). The separation between the centre frequencies of adjacent subchannels is equal to $2\pi/M$, where M is the number of subchannels. For ease of exposition, in Figure 3.1 we have considered an equal number of subchannels for upstream and downstream directions (symmetric communication) arranged in a "zipper-like" duplexing pattern [94]. However, the discussion in this thesis is applicable to other carrier arrangements as well (e.g., asymmetric communication).

We now provide a brief review of the operation of this system in the downstream direction (the upstream direction is analogous). Sequences of complex-valued symbols

$x_i[n]$ are chosen from not necessarily identical constellations at the symbol rate $1/T$. These symbols are then processed using an efficient FFT-based polyphase implementation [26, 35, 95] of the upsampling and filtering operations illustrated in Fig 3.1. The transmit signal is then formed by adding all the filtered sequences and applying digital to analog conversion (D/A) at a sampling rate of $1/T_s = N/T$. This signal is then transmitted over the channel (with impulse response $h_c(t)$) that forms the subscriber line. The received signal is sampled every T_s seconds and is passed through (an efficient implementation of) a bank of subchannel matched filters and then downsampled by a factor of N. Since the combined frequency response of the subchannel filters and the channel is not necessarily flat over the bandwidth of the subchannels, intersymbol interference (ISI) is present at the subchannel outputs. In order to mitigate the effects of this ISI without incurring large computational expense, FMT schemes typically incorporate a symbol-rate decision feedback equalizer (DFE) into the detector in each subchannel [26, 39, 97]. We focus our attention on such systems in this chapter. Although not shown in Figure 3.1, thermal noise is modelled as additive white Gaussian noise (AWGN) at the receiver input and colored interference from other sources is also considered at the receiver. The blocks marked by "H" in Figure 3.1 are line hybrids [15], which are used to provide isolation between the transmitter and the near-end receiver and thereby suppress self-echo. The equivalent discrete-time channel impulse response for the concatenation of the D/A, the analog channel, and the A/D is denoted by $c[n]$.

The fundamental idea behind FMT modulation is subchannel separation via filtering. This enables effective detection of the transmitted symbols using a per-subchannel detector rather than joint detection. In order to provide sufficient subchannel separation with filters of reasonable complexity, redundant filter banks are usually employed; i.e., $N > M$. This results in a digital analogue of conventional frequency division multiple access techniques with guard bands. In the following section, we derive design criteria for the prototype filter of the filter bank which measure the degree of subchannel separation and the ISI induced by subchannel filters.

3.3 System analysis and filter design

To simplify the analysis of the system of Figure 3.1 we assume that the input data sequences of different subchannels are uncorrelated and that the symbols for each input sequence are uncorrelated with each other; i.e.,

$$E\left\{x_i[n_1]x_\ell^*[n_2]\right\} = P_i\,\delta[i-\ell]\delta[n_1-n_2], \tag{3.1}$$

where $E\{\cdot\}$ denotes the statistical expectation operation, $\delta[\cdot]$ is the Kronecker delta, and P_i is the power of the ith input sequence $x_i[n]$. In the following analysis we will study the input-output equations for downstream communication. A similar analysis applies in the upstream case. For ease of exposition, the initial analysis in this section will be done in the absence of external noise/interference (including AWGN of the analog channel, echo, NEXT, and FEXT). Thus, the output signal for each subchannel will include only components due to the desired symbol, intersymbol interference (ISI), and intersubchannel interference (ICI). Later, we will comment on the effects of external interference.

Let $\mathcal{A}$ denote the set of carrier indices used for downstream communication. (In Figure 3.1, $\mathcal{A} = \{1, 3, \cdots, M-1\}$.) For the mth subchannel at the receiver, $m \in \mathcal{A}$, the signal at the input to the detector in Figure 3.1 depends on the downstream input sequences through the following equation

$$y_m[n] = \sum_{i\in\mathcal{A}} x_i[n] \star f_{mi}[n]\ . \tag{3.2}$$

where i denotes the index of the subchannel at the transmitter, the symbol $\star$ denotes convolution, and

$$f_{mi}[n] = g_{mi}[Nn] \ , \tag{3.3}$$

where

$$g_{mi}[n] = h_i[n] \star c[n] \star h^*_m[-n], \tag{3.4}$$

$h_i[n] = h[n]e^{j\omega_i n}$ is the inverse Fourier transform of $H(e^{j(\omega-\omega_i)})$, and for notational convenience we have allowed non-causal (matched) filtering at the receiver. For data symbols that satisfy (3.1), the power spectral density (PSD) of $y_m[n]$ can be written as

$$S_{y_m}(e^{j\omega}) = \sum_{i\in\mathcal{A}} P_i|F_{mi}(e^{j\omega})|^2 \tag{3.5}$$

$$= P_m|F_{mm}(e^{j\omega})|^2 + \sum_{\substack{i\in\mathcal{A}\\ i\neq m}} P_i|F_{mi}(e^{j\omega})|^2, \tag{3.6}$$

where $F_{mi}(e^{j\omega})$ is the Fourier transform of $f_{mi}[n]$. In (3.6), the first term on the right hand side is the PSD of the matched filtered signal from the mth transmitter, i.e., the component of $S_{y_m}(e^{j\omega})$ due to the desired symbol and the ISI. The second term is the PSD of the signals from other downstream subchannels at the mth subchannel output, i.e., the component of $S_{y_m}(e^{j\omega})$ due to ICI.

If we let $S_{\text{ICI}}(e^{j\omega})$ denote the PSD of ICI, the power of ICI can be written as

$$P_{\text{ICI}} = \frac{1}{2\pi}\int_0^{2\pi} S_{\text{ICI}}(e^{j\omega})\,d\omega = \frac{1}{2\pi}\int_0^{2\pi} \sum_{\substack{i\in\mathcal{A}\\ i\neq m}} P_i|F_{mi}(e^{j\omega})|^2\,d\omega. \tag{3.7}$$

In Appendix A, we show that P_{ICI} can be bounded by

$$P_{\text{ICI}} \leq P_I U_c^2(U_p^2 E_{sb} + U_{sb}^2 E_h + U_{sb}^2 E_{sb}), \tag{3.8}$$

where $P_I = \max_{i\in\mathcal{A}}\{P_i\}$, E_{sb} is the stopband energy of the prototype filter,

$$E_{sb} = \frac{1}{2\pi}\int_{\frac{\pi}{M}}^{2\pi-\frac{\pi}{M}} |H(e^{j\omega})|^2\,d\omega, \tag{3.9}$$

E_h is the energy of the prototype filter, $E_h = \frac{1}{2\pi}\int_0^{2\pi} |H(e^{j\omega})|^2\, d\omega$, and U_p and U_{sb} are the maximum values of $|H(e^{j\omega})|$ in the passband ($\omega \in (-\pi/M, \pi/M]$), and stopband ($\omega \in [\pi/M, 2\pi - \pi/M]$), respectively. In (3.8), U_c is an upper bound for $|C(e^{j\omega})|$, $\forall\omega$.

The value of (3.8) is that it provides an upper bound on the power of the ICI in terms of standard characteristics of the prototype filter. A similar analysis can be performed for NEXT and echo, since both of these effects can be modelled in a similar way but with a different channel model replacing $c[n]$. Thus, corresponding upper bounds hold for the power of NEXT and echo, but with different models for $c[n]$.

Another performance measure that we consider in filter design is ISI. From (3.2), we have that the power of the desired signal component at the input to the detector is $P_m|f_{mm}[d]|^2$, where the delay d is typically chosen to be $d = \arg\max_n |f_{mm}[n]|$. The power of the ISI component is

$$P_{\text{ISI}} = P_m \sum_{n\neq d} |f_{mm}[n]|^2. \tag{3.10}$$

In the FMT system of Figure 3.1, ISI is introduced both by the filter bank and the channel. To study the ISI which is introduced by the filter bank alone, we assume that the frequency response of the channel is ideal over the subchannel bandwidth. In that case, the appropriate delay is $d = 0$ and the signal to ISI power ratio is

$$\frac{\text{Signal power}}{\text{ISI power}} = \frac{E_h^2}{\sum_{n\neq 0}(\sum_k h[k]h[k-Nn])^2}, \tag{3.11}$$

where the denominator is obtained by substituting (3.3) and (3.4) into (3.10). Combining equations (3.8) and (3.11) we obtain the following design criteria for the prototype filter of the filter bank in Figure 3.1:

1. Small values of the stopband energy, E_{sb}, the maximum stopband level, U_{sb}, and the maximum passband level, U_p, of the prototype filter will guarantee that the power of the ICI, NEXT and echo at the input to the detector are small.

2. When the energy of the prototype filter (E_h) is normalized, small values of the ISI factor $\sum_{n,n\neq 0}\left(\sum_k h[k]h[k-Nn]\right)^2$, will guarantee that the power of ISI at the input to the detector is small.

Therefore, a natural design problem for the prototype filter would be to minimize the stopband energy of the filter, subject to upper bounds on the stopband level, the passband level, and the ISI power when the filter energy is normalized. That is,

$$\text{minimize} \quad \frac{1}{2\pi}\int_{\pi/M}^{2\pi-\pi/M} |H(e^{j\omega})|^2\, d\omega \tag{3.12a}$$

$$\text{subject to} \quad |H(e^{j\omega})| \leq t_{sb}, \quad \frac{\pi}{M} \leq \omega \leq \pi\,, \tag{3.12b}$$

$$|H(e^{j\omega})| \leq t_p \qquad \forall\omega\,, \tag{3.12c}$$

$$\sum_{n,n\neq 0}\left(\sum_k h[k]h[k-Nn]\right)^2 \leq t_d^2\,. \tag{3.12d}$$

$$\sum_k (h[k])^2 = E_h\,, \tag{3.12e}$$

where t_{sb}, t_p, and t_d^2 are positive real numbers that constrain the stopband level, passband level and ISI power, respectively. In (3.12e), E_h is a positive real number to which the energy of the prototype filter is normalized.

Unfortunately, the constraint in (3.12d) is not convex, and hence algorithms for solving (3.12) are complicated by the need to deal with the intricacies of potential local minima. However, by using the autocorrelation function of $h[n]$ as the design variable, the problem in (3.12) can be precisely transformed [96] into the following convex optimization problem which can be efficiently solved for a globally optimal solution. In order to state the convex problem explicitly, we let L denote the length of the prototype filter and $r_h[n]$ denote the autocorrelation function $r_h[n] = \sum_\ell h[\ell]h[-n+\ell]$. We also let $R_h(e^{j\omega})$ denote the Fourier transform of $r_h[n]$, and define $b[0] = 1 - 1/M$ and $b[n] = -2/(\pi n)\sin(\pi n/M)$, $n = 1, 2, \cdots, L-1$. The problem in (3.12) can then be precisely transformed into the following convex optimization problem

$$\begin{aligned}
\text{minimize} \quad & \sum_{n=0}^{L-1} r_h[n]b[n] && (3.13a)\\
\text{subject to} \quad & R_h(e^{j\omega}) \le t_{sb}^2 , \quad \frac{\pi}{M} \le \omega \le \pi , && (3.13b)\\
& R_h(e^{j\omega}) \le t_p^2 , \quad \forall \omega , && (3.13c)\\
& \sum_{n\ge 1} r_h^2[Nn] \le \frac{t_d^2}{2} , && (3.13d)\\
& r_h[0] = E_h , && (3.13e)\\
& R_h(e^{j\omega}) \ge 0 , \quad \forall \omega . && (3.13f)
\end{aligned}$$

While the problem in (3.13) is convex, equations (3.13b), (3.13c) and (3.13f) generate an infinite number of constraints (equations (3.12b) and (3.12c) also generate an infinite number of constraints). These constraints can be approximated by discretization or precisely enforced using linear matrix inequalities [98]. Once formulated in one of those forms, the problem in (3.13) can be efficiently solved for the optimal $r_h[n]$ using general purpose implementations of interior point methods, such as [99]. We can then extract a corresponding $h[n]$ using standard spectral factorization techniques [100, 101].[2] As we will demonstrate below, the convexity of the transformed optimization problem in (3.13) allows effective evaluation of the trade-off between subchannel separation and the ISI induced by the filter bank in an FMT system.

[2]While the application of the results in [96, 98, 101] has enabled us to transform the non-convex design formulation in (3.12) into the convex formulation in (3.13), the key contribution of the proposed prototype design lies in the derivation of the channel-independent design criteria for FMT prototype filter that appear in (3.12). In addition, (3.13) is only part of the prototype filter design procedure. In the numerical results section (Section 3.3.1) it is shown how the optimization problem (3.13) is used as part of the prototype filter design procedure in the FMT systems.

3.3.1 Numerical results for the filter design scheme

In this section we present numerical results for an FMT system with $M = 32$ subchannels, an up/down-sampling factor of $N = 36$ (for an excess bandwidth of 12.5%), and a prototype filter of length $L = 320$. For different values of the ISI factor, t_d, we found a prototype filter with minimum stopband energy by solving the convex optimization problem in (3.13). The resulting inherent trade-off is shown in Figure 3.2, where the normalized minimum stopband energy is plotted against the normalized ISI factor t_d/E_h. (In order to focus on the trade-off between the stopband energy and the ISI factor, the maximum stopband level, t_{sb}, and the maximum passband level, t_p, were chosen large enough so that these constraints were inactive.) Figure 3.2 represents the inherent trade-off in the sense that no point below this curve is achievable with a length 320 filter, and points on the curve are achieved by solving (3.13). From this figure, it can be seen that smaller values of the stopband energy can be achieved at the price of imposing larger ISI Smaller values of stopband energy are desirable because they result in improved subchannel isolation and hence smaller values for the power of NEXT, ICI, and echo at the receiver. On the other hand, smaller values of the ISI factor, t_d, result in less ISI. Now that we have an efficient method for computing this inherent trade-off, an important engineering design question is: At which point on this trade-off should the system operate? To provide an answer to this question, we will calculate the achievable bit rate for the system of Figure 3.1. An appropriate operating point on the trade-off curve would be the one that maximizes the achievable bit rate.

As described in Section 2.3, the number of bits per symbol interval that can be loaded on the ith subchannel is given by [15], [26]

$$\beta_i = \log_2\left(1 + \frac{\mathrm{SINR}_i\ \gamma_{\mathrm{code}}}{\Gamma\ \gamma_{\mathrm{margin}}}\right), \tag{3.14}$$

where SINR_i is the signal to noise plus interference ratio of the ith subchannel at the

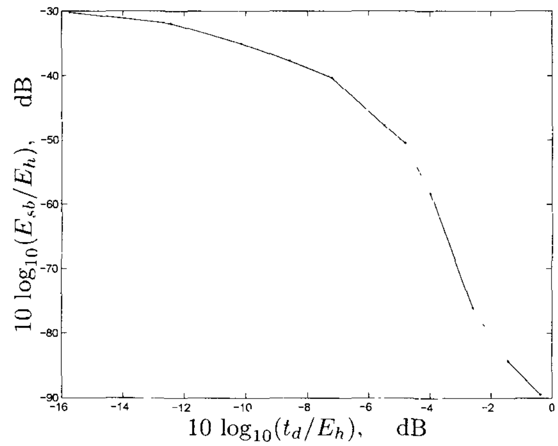

Figure 3.2: Trade-off curve for the normalized stopband energy against the normalized ISI factor of the prototype filter for an FMT system with $M = 32$ subchannels, up/down sampling factor $N = 36$, and a prototype filter of length 320.

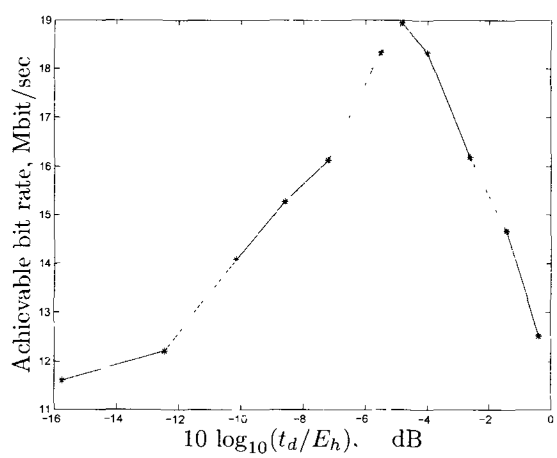

Figure 3.3: Achievable bit rate versus normalized ISI factor of the prototype filter for an FMT system with $M = 32$ subchannels, up/down sampling factor $N = 36$, a prototype filter of length 320, a sampling rate of 11 Msample/sec, and a cable length of 1 km.

input to the symbol detector embedded in the detector block[3] in Figure 3.1; Γ denotes the SNR gap, which for QAM modulation at a symbol error probability of 10^{-7} is about 9.8 dB [15]; γ_{code} is the coding gain; and γ_{margin} is the additional SNR margin which accounts for inaccuracies in the system model. For simplicity, we will assume that the coding gain is equal to the required additional margin in our example, i.e., $\gamma_{\text{code}}/\gamma_{\text{margin}} = 1$, but other values for this ratio can be easily incorporated. The achievable bit rate for assigned transmission is obtained by summing the values given by (3.14) over the assigned subchannels and then multiplying the result by the symbol rate $1/T$. For the downstream case we have

$$R = \frac{1}{T}\sum_{i\in\mathcal{A}}\beta_i. \tag{3.15}$$

We computed the achievable bit rates for the filters on the trade-off curve for a voice-grade unshielded twisted pair cable (UTP-3) model [26] for the DSL channel. Power spectral densities of NEXT and FEXT were computed based on the model for a 50-pair binder [15], [26], and the echo signal was deemed negligible compared to the other disturbances. The results were obtained for symmetric transmission with a sampling rate of 11 Msample/sec, a transmit signal power of 10 dBm, and an AWGN power spectral density equal to -140 dBm/Hz. The transmit power was uniformly distributed among all operating subchannels; i.e., no power was assigned to the subchannels that were not capable of carrying at least one bit per symbol interval.[4] In each subchannel, symbol-spaced minimum mean square error (MMSE) decision feedback equalization was applied, with 20 taps in the feedforward section and 15 taps in the feedback section. The equalizer was assumed to be free of error propagation. (The performance obtained under this assumption resembles that obtained with the corresponding Tomlinson-Harashima precoding [103, p. 365] at the

[3]As mentioned earlier, we will focus on symbol rate decision feedback detectors in this chapter.

[4]This is a simple power allocation scheme. While it is not optimal, in DMT systems its performance is close to that of the optimal scheme [102] at high SNRs. In Section 3.5 we will present a power allocation algorithm that is tailored to FMT.

transmitter; see, e.g. [26, 104].) Figure 3.3 contains a plot of the achievable bit rate against the normalized ISI factor of the prototype filter for a cable length of 1 km. It is observed that the achievable bit rate varies substantially as the designed filter traverses the trade-off in Figure 3.2. For a given filter length and DFE structure, reducing the normalized ISI factor t_d/E_h reduces the impact of ISI on the achievable bit rate. However, this reduction in ISI comes at the price of an increase in the stopband energy of the prototype filter, which reflects a reduction in the subchannel spectral containment and hence an increase in the impact of ICI and NEXT on the achievable bit rate. In contrast, allowing a larger normalized ISI factor enables the designer to achieve a smaller stopband energy and hence lower levels of ICI and NEXT, at the price of increased ISI. The position of maximum achievable bit rate on the trade-off curve is dependent on the DSL environment and the structure chosen for the DFE. However, that position can be found in a straightforward manner by traversing the trade-off curve that is efficiently generated by our design method.

To explore this trend in more scenarios, achievable bit rates for cable lengths of 600, 800, 1200, 1400, and 1600 meters were also computed (for different normalized ISI factors). They are plotted together with that of the 1 km cable in Figure 3.4. It can be seen that while the general trend is the same, there is a slight movement of the peak when the cable length changes. For the 600-meter cable, the peak has moved to smaller values of the ISI factor, t_d, and for the 1600-meter cable the peak has shifted marginally towards larger values of the ISI factor. The movement of the peak towards larger t_d values for longer cables is because the NEXT power at the receiver is independent of the cable length, whereas the signal itself suffers from a higher level of attenuation in longer cables. Thus, the signal to NEXT power ratio at the receiver is smaller for longer cables. Consequently, longer cables require greater spectral containment; i.e., smaller stopband energy for the prototype filter. From the inherent trade-off curve in Figure 3.2 it is clear that in order to provide smaller

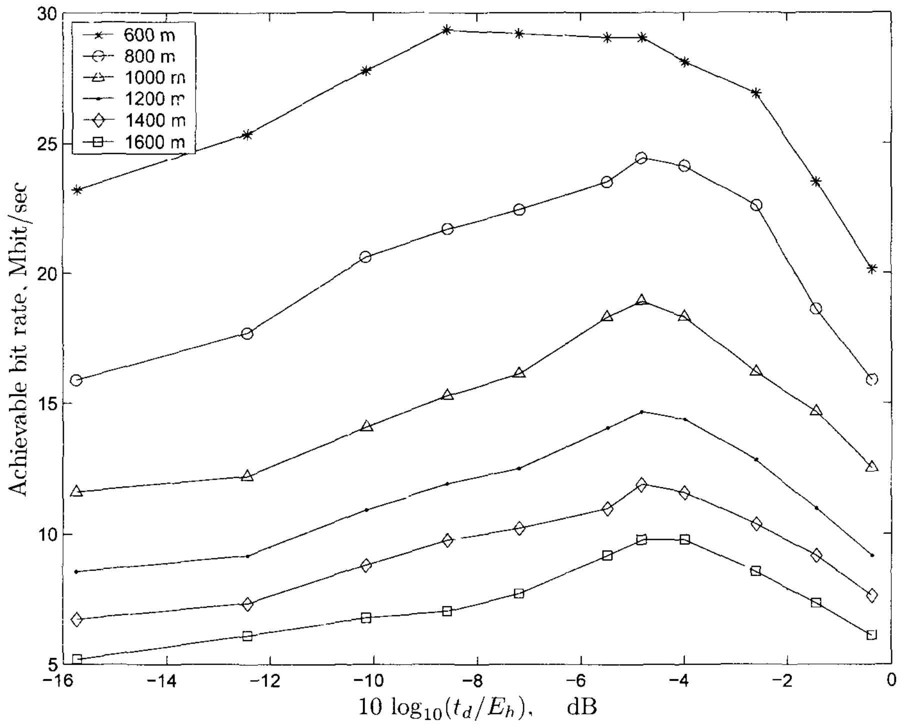

Figure 3.4: Achievable bit rate versus normalized ISI factor of the prototype filter for different cable lengths. The FMT system has the characteristics of $M = 32$ subchannels, up/down sampling factor $N = 36$, a prototype filter of length 320, and a sampling rate of 11 Msample/sec.

stopband energy, the prototype filter is forced to generate more ISI. Although the optimum level of spectral containment depends on the cable length, in our example it can be seen that choosing an average cable length (e.g., 1 km), and picking the optimum filter for that cable length, provides close to optimum performance for a variety of cable lengths.

As mentioned earlier, in the numerical example above a prototype filter length of ten times the number of subchannels was used, i.e., $L = 10M = 320$. While the design procedure is valid for other filter lengths as well, the length of $L = 10M$ was used as it provides one of the appropriate choices for the length of the prototype filter [26, 28].

Recall that in the FMT system, subchannel separation is obtained via subchannel spectral containment. For this to happen, the prototype filter length has to be much larger than the number of subchannels. If the prototype filter length is small, a larger amount of ISI must be imposed on the system in order to achieve sufficient subchannel separation, and therefore the achieveable bit rate of the system will be decreased. The longer the prototype filter the better the performance. However, longer prototype filters impose larger implementation complexities, and hence the choice of $L = 10M$ as a reasonable trade-off. As an extreme case, if the length of the prototype filter is allowed to grow without bound, the ideal prototype filter (Figure 2.3 of Chapter 2) is approached.

3.4 Number of subchannels

In Section 3.3.1 we observed that in the FMT system there is a trade-off between ISI and the combination of ICI and crosstalk. In particular, we observed that the optimal prototype filter for the system was the one that achieved the best balance between these competing characteristics. In a similar way, the trade-off between ISI and ICI also impacts the choice of the number of subchannels. If the number of subchannels is small, the wide-bandwidth subchannels will expose the system to a high level of ISI generated by the variation of the frequency response of the channel over each band. On the other hand, as the number of subchannels grows, the spectral containment required from the prototype filter in order to keep ICI and crosstalk to a manageable level increases. According to the trade-off curve obtained in Section 3.3.1, the system will therefore suffer from an increasing amount of ISI generated by the prototype filter. As one might expect, the optimal choice for the number of subchannels requires a balance between these two sources of ISI, and in the following example we demonstrate how the tools that were developed in Section 3.3 can be used to determine the appropriate number of subchannels.

We considered the FMT system in Figure 3.1 in which the prototype filter had a length $L = 320$, the channel model was that in Section 3.3.1 with a cable length of 1600 meters, and the MMSE DFE in each subchannel had 20 feedforward taps and 15 feedback taps. The redundancy of the filter bank is also fixed to 12.5%, i.e., $N/M = 1.125$. By applying the design method of Sections 3.3 and 3.3.1 we found the optimum prototype filters (and their corresponding achievable bit rates) for a few different values of M, the number of subchannels. In order to comply with efficient structures for implementing the FMT system we chose $M = 8, 16, 32, 64$, and 128. Table 3.4 provides the maximum achievable bit rates versus the number of subchannels. As expected, the highest bit rate is achieved by using a moderate number of subchannels. In particular, it can be seen that for a fixed length for the prototype filter, increasing the number of subchannels does not necessarily improve the performance of the system. As stated above, this is because the high spectral containment required for large values of M can only be achieved by a prototype filter which generates a substantial amount of ISI.

Table 3.4: Maximum achievable bit rate versus the number of subchannels for a cable length of 1600 meters.

M	N	Maximum achievable bit rate Mbit/sec
8	9	2.07
16	18	4.89
32	36	10.33
64	72	8.96
128	144	3.68

3.5 Power loading

To compute the achievable bit rates in Section 3.3.1, a simple loading algorithm was used: the total transmit power was uniformly distributed among the subchannels that were capable of reliably transmitting at least one bit per symbol interval. Although that algorithm performs reasonably well, in this section we will present a loading algorithm that is tailored to the FMT system. We will compare the performance of this algorithm with that of the algorithm used in Section 3.3.1 and that of the conventional water-filling approach. For DMT systems it is well known [15] that water-filling provides the optimal power loading. However, as we will see below, the existence of non-negligible ISI at the inputs to the detectors means that water-filling is not necessarily the optimal loading method in the FMT system.

The conventional power loading problem is to maximize the achievable bit rate subject to a fixed transmit power, i.e.,

$$\text{maximize} \quad \sum_{i\in\mathcal{A}} \beta_i \tag{3.16a}$$

$$\text{subject to} \quad \sum_{i\in\mathcal{A}} P_i = P_{\text{total}}\,, \tag{3.16b}$$

$$P_i \geq 0\,, i \in \mathcal{A}, \tag{3.16c}$$

where β_i is given by (3.14) and $\mathcal{A}$ is the set of carrier indices used for communication. Recall that SINR_i in (3.14) is the signal to interference plus noise ratio at the input to the symbol detector embedded in the decision feedback equalizer in the detector block for the ith subchannel. Our numerical computations show that for the well-designed prototype filters (e.g., the optimum filters found in Section 3.3.1) the ICI power is negligible compared to the other noise and interferences. We emphasize that while the ICI is negligible, the ISI can be quite large and cannot be ignored. With the assumption of negligible ICI, the SINR_i can be expressed as

$$\mathrm{SINR}_i = \frac{P_i|\tilde{f}_u[d_i]|^2}{P_i \sum_{k<d_i} |\tilde{f}_u[k]|^2 + P_{AWGN_i} + P_{NEXT_i} + P_{FEXT_i}} \tag{3.17}$$

where $\tilde{f}_u[n]$ is the sequence resulting from the convolution of $f_u[n]$ (which is described by (3.3) and (3.4)) with the impulse response of the feed-forward filter of the MMSE decision feedback equalizer for the ith subchannel, and d_i is the "cursor position" [103, p. 360] of the DFE. Note that we have assumed that there is no error propagation in the DFE, and hence, that the ISI from the previously detected symbols is eliminated. The terms P_{AWGN_i}, P_{NEXT_i}, and P_{FEXT_i} represent the power of the AWGN, NEXT, and FEXT components of the received signal at the output of the feed-forward filter of the DFE of the ith subchannel.

A key observation from (3.17) is that due to the non-negligible ISI term, both the numerator and denominator of SINR_i depend on P_i. Therefore, conventional water-filling [15] does not provide the optimum power loading. In the subsections below we will develop a power loading algorithm that explicitly incorporates the ISI. Our numerical results will show that the resulting algorithm can provide significantly higher achievable bit rates than those obtained by ignoring the ISI term and performing conventional water-filling.

3.5.1 Power loading algorithm

For the sake of notational simplicity, we re-write (3.17) as

$$\mathrm{SINR}_i = \frac{P_i a_i}{P_i b_i + c_i} \quad , \tag{3.18}$$

where

$$a_i = |\tilde{f}_{ii}[d_i]|^2 . \tag{3.19a}$$

$$b_i = \sum_{k<d_i} |\tilde{f}_{ii}[k]|^2 , \tag{3.19b}$$

$$c_i = P_{AWGN_i} + P_{NEXT_i} + P_{FEXT_i} . \tag{3.19c}$$

For a given set of feedforward filters in the DFEs, the terms a_i, b_i, and c_i are constant, and hence the numerator of SINR_i is linear in P_i and the denominator is affine. Since $\log(\cdot)$ is concave, it can be shown that the objective function in (3.16a) is a sum of concave functions and is thus concave. Furthermore, the constraints in (3.16b) and (3.16c) are linear. Therefore, for fixed a_i, b_i, and c_i the problem in (3.16) is convex in the allocated powers, P_is, and can be efficiently solved (using, e.g., interior point methods) to find the optimum subchannel power allocation. Once the subchannel powers are found and allocated to the FMT subchannels, the DFE coefficients have to be readjusted. When the DFE coefficients change, a_i, b_i, and c_i may change; c.f., (3.19). Thus, we propose the following iterative algorithm for power loading in an FMT system:

1. Starting point: Distribute the total transmit power uniformly among all the available subchannels.

2. Calculate the DFE coefficients for each subchannel.

3. Compute the power distribution by efficiently solving (3.16).

4. Assess progress via the two-norm of the update to the vector of power allocations and return to step 2 unless progress is negligible.

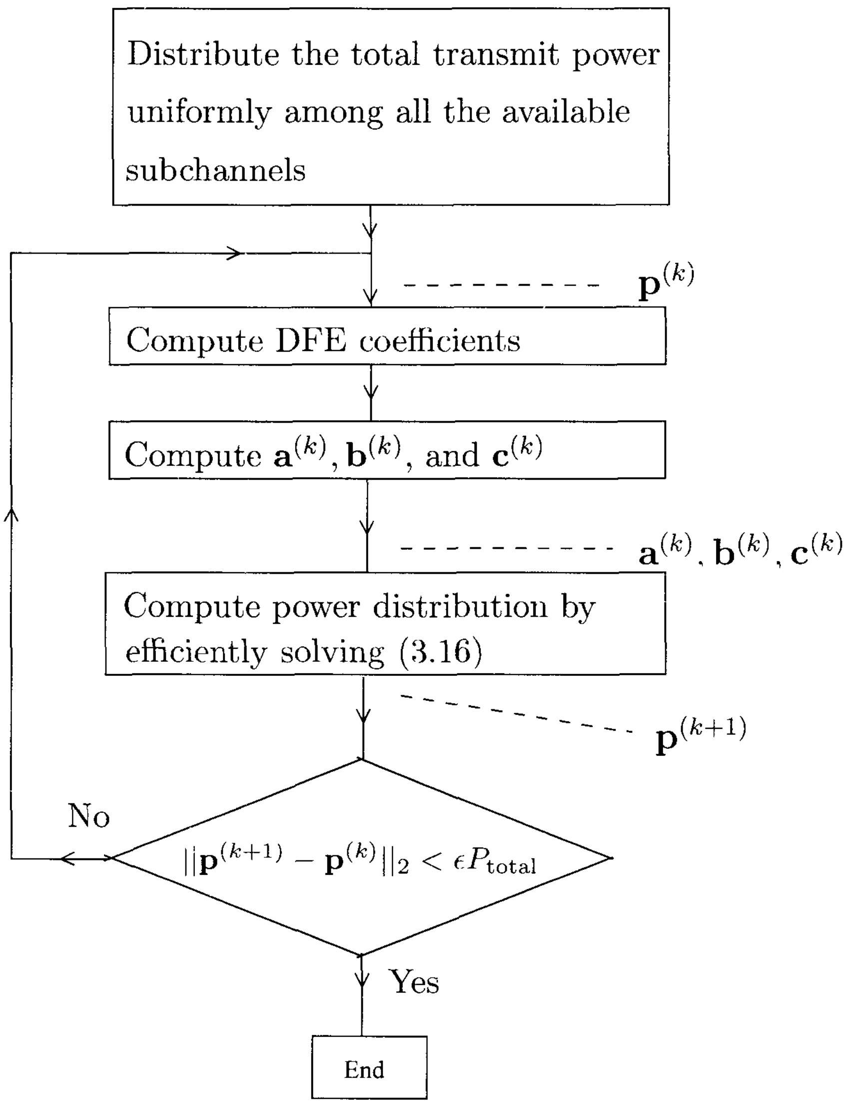

Figure 3.5: The proposed power loading algorithm for the FMT system.

A flow diagram for this algorithm is provided in Figure 3.5, where

$$\mathbf{a}^{(k)} = [a_1^{(k)}, a_3^{(k)}, \cdots, a_{M-1}^{(k)}], \tag{3.20a}$$

$$\mathbf{b}^{(k)} = [b_1^{(k)}, b_3^{(k)}, \cdots, b_{M-1}^{(k)}], \tag{3.20b}$$

$$\mathbf{c}^{(k)} = [c_1^{(k)}, c_3^{(k)}, \cdots, c_{M-1}^{(k)}], \tag{3.20c}$$

$$\mathbf{p}^{(k)} = [P_1^{(k)}, P_3^{(k)}, \cdots, P_{M-1}^{(k)}], \tag{3.20d}$$

represent the vectors of the coefficients a_i, b_i, c_i, and P_i at the kth iteration of the algorithm, $||.||_2$ denotes the two-norm, and ϵ denotes the stopping parameter. A typical value for ϵ is 0.001. An important property of this iterative algorithm is that it is guaranteed to converge.

Theorem 3.1 *The algorithm of Figure 3.5 converges.*

Proof. The proof is available in Appendix B.

3.5.2 Numerical results for the loading algorithm

In this section we compare the performance of the following three loading schemes by computing the achievable bit rate for the FMT system when each of these schemes is used as the power loading method in the system. The three schemes are

1. The power loading algorithm proposed in Figure 3.5;
2. Uniform distribution of the transmit power among the subchannels that are capable of carrying at least one bit information per symbol interval (this technique was used in Section 3.3.1);
3. Water-filling power loading in which the ISI component of the SINR is ignored.

Figure 3.6 shows the achievable bit rates for the FMT system with parameters as in Section 3.3.1, for different cable lengths using each of the three loading schemes.

For the proposed loading algorithm, the stopping criterion was chosen to be $\epsilon = 0.001$, and for different cable lengths of Figure 3.6, it was observed that the proposed loading algorithm converged in four or five iterations. For this system, the MMSE-DFE on each subchannel had 20 taps in the feedforward filter and 8 taps in the feedback filter. It can be seen from the figure that the new loading scheme offers larger achievable bit rates than the other two schemes. The key factor in this rate gain is the appropriate treatment of ISI. To demonstrate this fact, in Figure 3.7 we provide the numerical results for the achievable bit rates in the same environment as in Figure 3.6 but with a stronger MMSE-DFE in each subchannel. This stronger DFE had 15 feedback taps rather than the 8 taps in Figure 3.6. This stronger DFE provides much greater ISI suppression, and hence the difference between the achievable bit rates provided by the three loading schemes are much smaller. However, the proposed algorithm continues to provide the highest achievable bit rates. (Observe that the greater ISI suppression provided by the stronger DFE results in each loading method achieving a higher bit rate than in Figure 3.6.)

Figures 3.6 and 3.7 expose a trade-off between design and implementation complexity. If the designer chooses a lower complexity receiver (i.e., fewer taps in the DFEs), then considerable achievable rate gains can be obtained by using the power loading algorithm developed in this section. On the other hand, if the designer chooses a higher complexity receiver, as we did in the examples of Sections 3.3.1 and 3.4, then a simple power loading algorithm will suffice.

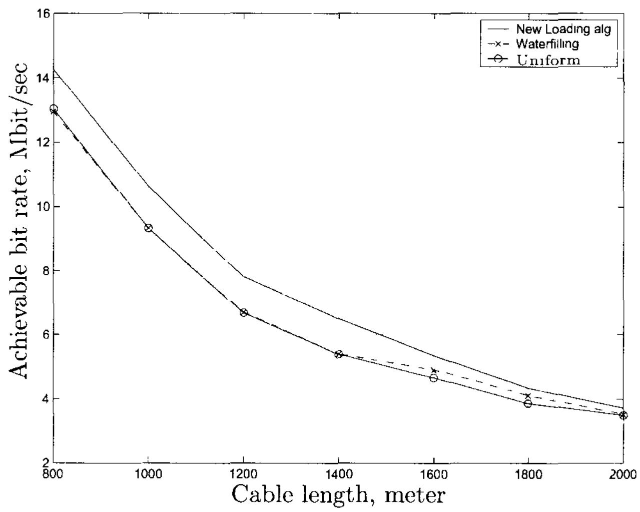

Figure 3.6: Achievable bit rate versus cable length for the three loading schemes. The FMT system had the following characteristics: $M = 32$, $N = 36$, prototype filter of length $L = 320$, and a sampling rate of 11 Msample/sec. DFE for the subchannels had 20 taps in the feedforward section and 8 taps in the feedback section.

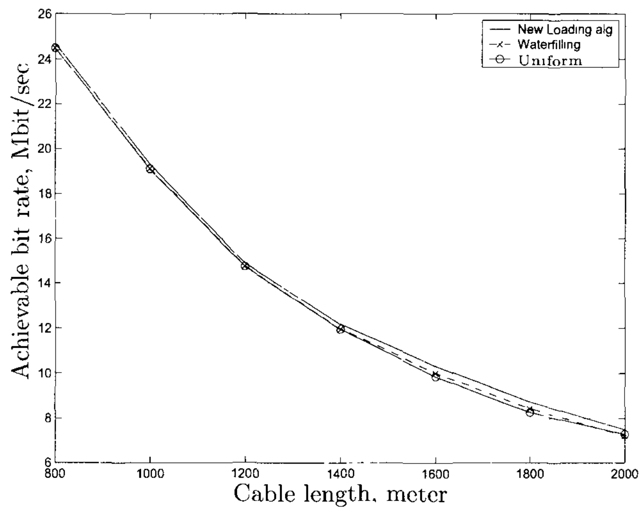

Figure 3.7: Achievable bit rate versus cable length for the three loading schemes. The FMT system had the following characteristics: $M = 32$, $N = 36$, prototype filter of length $L = 320$, and a sampling rate of 11 Msample/sec. DFE for the subchannels had 20 taps in the feedforward section and 15 taps in the feedback section.

Chapter 4

Bi-windowed discrete multitone transceiver design

In Chapter 2 it was explained that while DMT systems are the most widely used multi-carrier transceivers due to their desirable properties and, especially their comparatively low complexity, they suffer from poor spectral characteristics. It was also mentioned in Section 2.4 that windowing techniques can be considered as one of the most practical methods for improving the spectral characteristics of DMT system. In this chapter, a family of bi-windowed DMT transceivers is proposed which improves both the subchannel spectral containment at the transmitter and the spectral selectivity at the receiver. These systems have the attractive feature that they provide spectral shaping at both ends of the transceiver without requiring the cyclic prefix to be longer than the order of the channel impulse response. The windows are designed in a channel independent manner and are constrained to produce subchannel outputs that are free from (intrasubchannel) intersymbol interference (ISI). Furthermore, the design allows the intersubchannel interference (ICI) to be controlled in such a way that it can be mitigated using a relatively simple minimum mean square error (MMSE) successive interference cancellation scheme. Under a realistic model for a digital subscriber line (DSL) environment, the achievable bit rate of the proposed system is significantly higher than that of the conventional DMT system and some established windowed DMT systems with receiver-only windowing. This performance gain is a result of the capability of the proposed system to combat the near-end crosstalk (NEXT) at the transmitter and receiver and to mitigate the narrowband noise at the receiver, without the requirement of excess cyclic prefix.

4.1 Introduction

It was stated in Chapter 2 that among different classes of multi-carrier communication schemes, DMT and OFDM have attracted more attention, mainly due to their comparatively low complexity, and it was discussed that the (implicit) pulse shaping and receive filters in DMT and OFDM [1] systems are rectangular windows, and hence they suffer from rather poor spectral characteristics. The poor spectral containment at the transmitter can make it quite awkward to design schemes that are required to satisfy certain egress standards, such as those related to the amateur radio (HAM) bands in very high speed digital subscriber line (VDSL) transceivers [15, 16]. This poor spectral containment also makes the system susceptible to performance loss caused by near-end crosstalk (NEXT). The poor spectral selectivity at the receiver makes the system susceptible to NEXT and to narrowband noise, such as radio frequency interference (RFI) emerging from AM broadcast and HAM radio signals. Therefore, there is the potential for significant performance gains if one can improve both the subchannel spectral containment at the transmitter and the spectral selectivity at the receiver.

Various schemes have been proposed to improve the spectral characteristics of

[1]For simplicity, we will use the term DMT for the systems of interest, but the proposed designs apply equally well to OFDM.

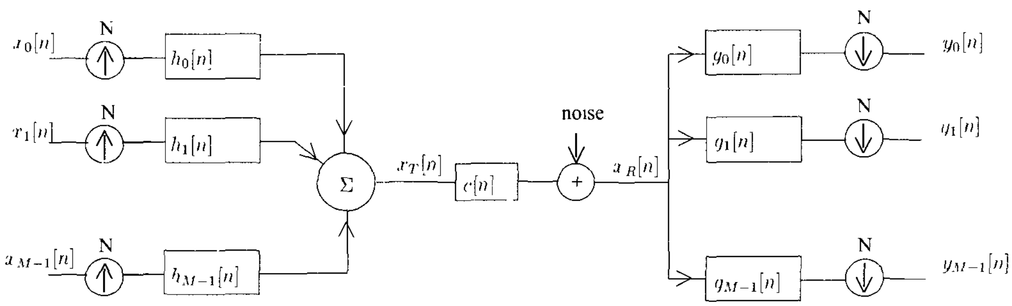

Figure 4.1: M-subchannel filter bank communication system.

DMT. These schemes involve different trade-offs between the redundancy of the transmitted symbol stream, the complexity of the transmitter and receiver, and the amount of information about the channel (and the noise) that is required to synthesize the subchannels. The approach that will be proposed herein will have the same transmission redundancy as DMT, essentially the same transmitter complexity, and the synthesis of the subchannels will be independent of the channel (as in DMT). Consequently, there will be a moderate increase in the complexity of the receiver, but we feel that the performance gains offered by the proposed design make this a compelling trade-off.

A convenient framework for comparing the proposed trade-off with those (implicitly) chosen in some other schemes is that of the filter bank transceiver in Figure 4.1, [27,28]. (Recall from Chapter 2 that DMT is a special case of this framework.) For this system, the interference components of the subchannel outputs can be classified as being either intersubchannel interference (ICI), which arises from symbols transmitted on other subchannels, or (intrasubchannel) intersymbol interference (ISI), which arises from other symbols transmitted on the same subchannel. In the following discussion we will focus on schemes in which the subchannels are synthesized in a channel-independent manner.

As was studied in Chapter 2, DMT operates on a block-by-block basis, in the sense that the blocks of transmitted symbols generated by subchannel inputs at consecutive instants do not overlap. One approach to achieving better spectral properties than DMT is to allow the transmitter filters to be longer than N, and hence allow the transmitted blocks to overlap; e.g., DWMT [27] and FMT [26]. Recall from Chapter 2 that in DWMT, the subchannels are synthesized using a "critically sampled" perfect reconstruction filter bank. This provides a considerable improvement in the spectral properties at both transmitter and receiver without requiring redundancy in the transmitted symbol stream; i.e., $N = M$. However, the lack of redundancy in DWMT makes it sensitive to channel distortion. Indeed, when the channel is frequency selective, the high levels of ISI and ICI require the use of complicated equalization and ICI cancellation schemes. In contrast to DWMT, recall from Chapter 2 that the FMT scheme retains the redundant DFT modulated filter bank structure of DMT. As was studied in Chapter 3, the prototype filter in the FMT filter bank can be designed in a channel-independent manner to provide excellent spectral properties and negligible ICI. However, recall from Chapters 2 and 3 that the FMT prototype filter is usually quite long—often of the order of ten times the number of subchannels—which increases the complexity of the transceiver. Furthermore, in order to achieve negligible ICI, some residual ISI is incurred, and hence significant per-subchannel equalization is required. Consequently, while FMT provides subchannels with desirable spectral properties and systems with large achievable rates, its implementation is significantly more complex than that of DMT. Therefore, multi-carrier communication systems with a complexity comparable to that of DMT, but with improved spectral characteristics are of significant interest. Recall from Chapter 2 that windowed DMT schemes represent category of such systems. Like FMT, these schemes can be viewed as redundant DFT modulated filter bank transceivers, but they typically have a shorter prototype filter. As was studied in Chapter 2, some of the windowed DMT schemes involve windowing at the transmitter to reduce the out of band energy of the transmitter subchannel signals [25, 77, 78, 80], while others involve windowing at the receiver to improve the robustness of the transmission scheme to narrowband interference [74–76]. As was discussed in Chapter 2, in most of these techniques, the design is contingent on the cyclic prefix being longer than the channel order, in order to avoid window-induced ISI and ICI. Unfortunately, this requirement reduces the spectral efficiency of the transmitted symbol stream. It was also discussed in Chapter 2 that there has been some progress in the design of transmitter or receiver windowed DMT schemes without the requirement of excess cyclic prefix [25, 80], but these schemes only operate at one end of the transceiver, and additional processing in the form of equalization and ICI cancellation is required at the receiver.

A shortcoming of the existing channel-independent windowing methods is that they require excess redundancy, in the form of a cyclic prefix that must be longer than the order of the channel, and/or they are designed to improve the subchannel spectrum only at one end of the transceiver. In this chapter, we propose a channel-independent windowing method that improves both the subchannel spectral containment at the transmitter and the subchannel spectral selectivity at the receiver, without the requirement of excess redundancy. Since improved subchannel spectra are obtained at both ends of the transceiver, the egress standards are easier to meet, NEXT is reduced, and mitigation of narrowband noise is improved. As we will show in our numerical results, the reduction of NEXT, the mitigation of narrowband noise, and the absence of a requirement for excess cyclic prefix can result in a significant gain in the achievable bit rate. The proposed bi-windowed DMT system preserves many of the desirable features of DMT. In particular, block-by-block transmission is maintained at the same level of redundancy, the subchannel outputs are free from ISI, no knowledge of the channel is required in the design of the windows, and a closed-form expression for the designed window can be obtained. In order to achieve the desired spectral characteristics while preserving these features, some ICI is allowed, but the ICI is controlled in such a way that it can be mitigated using a relatively simple minimum mean square error (MMSE) successive interference cancellation scheme. While this interference canceller does increase the receiver complexity to some degree, our numerical results suggest that in a realistic DSL environment, the proposed scheme provides a significant increase in the achievable bit rate over that of the standard DMT.

This chapter is organized as follows: In Section 4.2, the system is analyzed and the channel-independent ISI-free conditions are derived. The proposed window design is presented in Section 4.3, and Section 4.4 contains the description of the MMSE successive ICI canceller. In Section 4.5, we provide numerical results which illustrate the performance achieved by the proposed system in a realistic DSL environment.

4.2 System analysis

In order to facilitate comparisons to a broad range of multi-carrier systems, we will develop our windowed transceiver within the framework of the filter bank transceiver in Figure 4.1. Recall from Chapter 2 that DMT and OFDM are special cases of this framework in which $N = M + P$, where P is the length of the cyclic prefix, and the transmit and receive filters are obtained by DFT modulation (of fundamental frequency $2\pi/M$) of rectangular windows of lengths N and M, respectively. We will denote the impulse response of the equivalent discrete-time channel (including any time domain equalization) by $c[n]$, and it will be assumed that $c[n]$ can be non-zero only for $0 \leq n \leq L$. The additive noise in Figure 4.1 represents all external noise and interferences, including additive white Gaussian noise (AWGN), radio frequency interference (RFI), and crosstalk. Recall from (2.4)-(2.9) in Section 2.1.3 that the output of the mth subchannel of the receiver in Figure 4.1 can be written as

$$y_m[n] = \sum_{k=-\infty}^{\infty} g_m[k] \sum_{p=0}^{L} c[p] \sum_{i=0}^{M-1} \sum_{\ell=-\infty}^{\infty} x_i[\ell] h_i[N(n-\ell) - k - p] + v_m[n] \tag{4.1}$$

$$= \sum_{i=0}^{M-1} \sum_{k=-\infty}^{\infty} x_i[n-k] c_{mi}[Nk] + v_m[n], \tag{4.2}$$

where

$$c_{mi}[n] = h_i[n] \star c[n] \star g_m[n], \tag{4.3}$$

the symbol $\star$ denotes the convolution operator, and $v_m[n]$ represents the (zero-mean) additive noise of Figure 4.1 after being filtered by $g_m[n]$ and downsampled by a factor of N. If k_0 denotes the synchronization delay of the system, then as in Section 2.1.1, the term $\sum_{k \neq k_0} x_i[n-k] c_{mm}[Nk]$ in (4.2) is the ISI on subchannel m, and $\sum_{i \neq m} \sum_k x_i[n-k] c_{mi}[Nk]$ is the ICI.

The first goal of our design is to preserve the property of standard DMT systems that the subchannel outputs are free from ISI for any channel $c[n]$ of order L, as long as the order of channel is not longer than the cyclic prefix length, i.e., $L \leq P$. Assume the transmit and receive filters are FIR filters with the following support intervals

$$h_i[n] = 0, \quad n \notin [n_1, n_2] \tag{4.4}$$

and

$$g_m[k] = 0, \quad k \notin [k_1, k_2] \tag{4.5}$$

In Appendix C we show that with the parameters defined in (4.4) and (4.5), the transceiver of Figure 4.1 has zero ISI at its outputs for any given channel of order at most L if and only if one of the following conditions holds:

$$(k_2 - k_1) + (n_2 - n_1) < N - L, \qquad \text{if } k_1 + n_1 = jN, \tag{4.6a}$$

$$N - L \leq (k_2 - k_1) + (n_2 - n_1) + d < 2N - L, \qquad \text{if } k_1 + n_1 = jN + d. \tag{4.6b}$$

where j is an arbitrary integer value and $d \in [1, N-1]$. While both (4.6a) and (4.6b) impose upper bounds on the total length of the transmit and receive filters, it can be seen that (4.6b) allows longer transmit and receive filters. Since longer filter lengths allow for better spectral characteristics for the transmit and receive filters, from these two possible choices for the channel-independent zero ISI conditions, we will impose (4.6b) in our design. Without loss of generality, we choose $j = 0$. Moreover, in order to maximize the lengths of the filters while keeping the channel-independent zero ISI property of the system, we choose d in (4.6b) to be equal to one. That is, we will impose the following condition on our design

$$\begin{cases} n_1 + k_1 = 1, \\ N - L \leq (n_2 - n_1) + (k_2 - k_1) + 1 < 2N - L. \end{cases} \tag{4.7}$$

With this assumption, the expression in (4.1) reduces to

$$y_m[n] = \sum_{i=0}^{M-1} x_i[n-1] \sum_{k=k_1}^{k_2} g_m[k] \sum_{p=0}^{L} c[p] h_i[N-k-p] + v_m[n] \tag{4.8}$$

$$= \sum_{i=0}^{M-1} x_i[n-1] c_{mi}[N] + v_m[n], \tag{4.9}$$

As expected, from (4.9) it can be seen that if the transmitter and receiver filters satisfy (4.7), the subchannel outputs are ISI-free for any FIR channel of order at most L. Notice from (4.9) however, that although $y_m[n]$ is ISI-free, in general it is not free from ICI. Indeed, from (4.9) one can see that in general, the output of each subchannel at instant n is a weighted sum of all subchannel inputs at instant $n-1$, but it does not depend on the subchannel inputs at other instants.

The channel-independent zero-ISI property of the system at hand holds for a variety of choices for the support intervals of the transmitter and receiver filters, so long as (4.7) is satisfied. However, in order to involve all the coefficients of the transmitter filters in the spectral shaping of the transmitted subchannel signals, and, at the same time, ensure that all the coefficients of the receiver subchannel filters are used in the filtering of the received signal, we choose the limits of the support of $h_i[\cdot]$ to be $n_1 = N-k_2-L$, $n_2 = N-k_1$. Therefore, $(n_2-n_1)+(k_2-k_1)+1 = 2(k_2-k_1)+L+1$. In order to obtain the maximum number of degrees of design freedom, we choose $k_2 - k_1$ so that the length of the windows that satisfy (4.7) is maximized. That is, we choose $k_2 - k_1 = N - L - 1$. All that remains is to determine k_1. To that end, we note from (4.7) that we have $n_1 + k_1 = 1$, and that without loss of generality we can choose $n_1 = 0$. Therefore, the longest support intervals for transmitter and receiver windows that retain the channel-independent zero ISI property of DMT are

$$h_i[n] = 0,\ n \notin [0, N-1], \tag{4.10}$$

$$g_m[k] = 0,\ k \notin [1, N-L]. \tag{4.11}$$

These conditions are satisfied in the conventional DMT system and in the windowed DMT systems based on Nyquist windowing [74–76]. For the rest of this chapter we assume that (4.10) and (4.11) hold.

Recall from (4.9)-(4.11) that with the assumption made for the length of the transmit and receive filters a channel-independent zero ISI property is achieved, but, in general, the ICI is not zero. To simplify the analysis of the ICI of the system, we define

$$f_{mi}[n] = h_i[n] \star g_m[n]. \tag{4.12}$$

Substituting (4.12) into (4.3), the ICI coefficients in (4.9) can be written as

$$c_{mi}[N] = \sum_{k=0}^{L} c[k] f_{mi}[N-k]. \tag{4.13}$$

This expression makes it clear that if we wish to ensure that the ICI coefficients, $c_{mi}[N]$, $i \neq m$, are small for any channel of order at most L, we must ensure that $f_{mi}[n]$ coefficients are small for all $N - L \leq n \leq N$ and $i \neq m$. Moreover, the channel-independent zero ICI condition reduces to $f_{mi}[n] = 0$ for all $i \neq m$ and $N - L \leq n \leq N$.

4.3 Window design

Having established the conditions for an ISI-free filter bank transceiver, we now develop a channel-independent design method for the transmitter and receiver windows. The goal is to obtain both a high level of subchannel spectral containment at the transmitter and a high level of spectral selectivity at the receiver, while limiting the impact of ICI. The windowed DMT system is embedded in the filter bank model in Figure 4.1, and is exposed when the filter bank has the following DFT modulated structure:

$$h_i[n] = h[n]e^{j\frac{2\pi}{M}in}, \tag{4.14}$$

$$g_m[n] = g[n]e^{j\frac{2\pi}{M}mn}, \tag{4.15}$$

where $h[n]$ and $g[n]$ are the transmit and receive windows, respectively. In that case, the term $f_{mi}[n]$ in (4.12) can be written as

$$f_{mi}[n] = e^{j\frac{2\pi}{M}nm} \sum_{k=0}^{N-1} h[k]g[n-k]e^{j\frac{2\pi}{M}k(i-m)}. \tag{4.16}$$

In the case that $L = P$, (i.e., $N = M + L$), and $h[\cdot]$ and $g[\cdot]$ are rectangular windows supported on the intervals in (4.10) and (4.11), respectively, we have a standard DMT system.[2] In that case, it can be verified that $f_{mi}[n] = 0$ for all $N - L \leq n \leq N$ and all $i \neq m$. Hence, $c_{mi}[N] = 0$ for all $i \neq m$, and there is no ICI at the receiver. When the cyclic prefix is longer than is required for the given channel (i.e., when $P > L$), the excess redundancy in the transmitted signal can be exploited to design systems

[2] In systems in which the actual length of the channel is not known (e.g., wireless OFDM systems), the appropriate statement is $L_{\max} = P$, where $L_{\max}$ is the order of the longest channel that is postulated in the design.

with zero ICI and a spectral shaping window at the receiver (e.g., the receiver Nyquist windowing in [74–76]), or a spectral shaping window at the transmitter (e.g., [77,78]). The goal of the present chapter is to design systems with spectral shaping windows at both the transmitter and receiver, without requiring the cyclic prefix to be longer than the order of the channel.

Seeing as the goal for our window design is to improve the spectral properties of the system without requiring excess redundancy, we will set the length of the cyclic prefix to be equal to the order of the channel; i.e., $P = L$. We will ensure that the subchannel outputs are free from ISI by constraining $h[\cdot]$ and $g[\cdot]$ to comply with (4.10) and (4.11), respectively. Our design strategy is to seek a pragmatic channel-independent design procedure, and to show (in Section 4.5) that this procedure provides substantial performance improvement. We will adopt a sequential design procedure[3] in which we first design a receiver window, $g[\cdot]$, supported on the interval in (4.11) with desirable spectral characteristics; i.e., with small stopband energy and rapid spectral roll-off. This can be done using standard window design techniques, such as those in [36,105]. We will then design the transmitter window in a way that balances the objectives of transmit subchannel spectral containment and ICI suppression. The design procedure begins with the design of the receiver window because the receiver must mitigate both NEXT and narrowband noise.

In the design of the transmitter window, we will measure spectral containment using the energy in the stopband of the window, and we will measure ICI suppression using the sum of the squares of $f_{mi}[n]$ in (4.16) for $N - L \leq n \leq N$. Therefore, a

[3] Although a joint design procedure can be conceived, $f_{mi}[n]$ in (4.16) is a bilinear function of the windows, and hence the formulation of joint design problems is usually non-convex. As a result, joint design procedures may require careful management of locally optimal solutions in order to obtain a solution that is sufficiently close to a global optimum.

natural formulation of the design problem is

$$\text{minimize} \quad \frac{\lambda}{2\pi}\int_{\theta}^{2\pi-\theta} |H(e^{\jmath\omega})|^2\, d\omega + (1-\lambda)\sum_{p=1}^{M-1}\sum_{n=N-L}^{N}\left|\sum_{k=0}^{N-1} h[k]g[n-k]e^{\jmath\frac{2\pi}{M}kp}\right|^2 \tag{4.17a}$$

$$\text{subject to} \quad \sum_{n=0}^{N-1} h[n] = 1\,, \tag{4.17b}$$

where $H(e^{\jmath\omega})$ denotes the Fourier transform of $h[n]$, θ is a constant which defines the stopband for $H(e^{\jmath\omega})$ as $[\theta, 2\pi-\theta]$, and $\lambda \in [0, 1]$ weights the objectives of spectral containment and ICI suppression. The constraint in (4.17b) fixes the DC gain of the transmitter window, $H(e^{\jmath 0})$, to one. The optimization problem in (4.17) is a (strictly) convex quadratic program with a single linear equality constraint, and hence a closed form solution can be easily obtained using the classical Lagrange multiplier method [73]; the details are provided in Appendix D.[4]

It is clear from the formulation in (4.17) that the parameter λ allows the designer to adjust the relative importance of ICI suppression and spectral containment in the design of the window. Although λ provides some control over the level of ICI, our goal of improving the spectral containment at the transmitter over that of the conventional DMT scheme while retaining a cyclic prefix length that is equal to (not greater than) the order of the channel means that ICI is inevitable. In order to mitigate the effect of the residual ICI, we propose the use of minimum mean square error (MMSE) successive ICI cancellers.

[4]An alternative to (4.17b) is energy normalization, $\sum_n h[n]^2 = 1$. The closed-form solution of that problem is also well known (e.g., [106]), and is the eigenvector that corresponds to the minimum eigenvalue of the matrix $\boldsymbol{\Psi}$ given by (D.5) in Appendix D. In the design examples in Section 4.5, the spectrum of the optimal window for the DC constraint of (4.17b) and that of the optimal window for the energy constraint are indistinguishable.

4.4 ICI Cancellation

The behavior of the intersubchannel interference (ICI) of the proposed system is captured by the ICI coefficients $c_{mi}[N]$; c.f., (4.9). Since we have a DFT modulated filter bank (c.f., (4.14), (4.15)), the frequency domain counterpart to (4.3) can be written as

$$C_{mi}(e^{j\omega}) = H(e^{j(\omega-2\pi i/M)})C(e^{j\omega})G(e^{j(\omega-2\pi m/M)}), \tag{4.18}$$

where $X(e^{j\omega})$ denotes the Fourier Transform of $x[\cdot]$. Since $g[\cdot]$ is chosen so that $G(e^{j\omega})$ has a small stopband energy, and $h[\cdot]$ is designed using (4.17) which ensures a small stopband energy for $H(e^{j\omega})$, one can see from (4.18) that $C_{mi}(e^{j\omega})$ will have non-negligible values only if $|m-i|$ is close to zero or close to M. In order to suppress the non-negligible ICI terms at the subchannel outputs, we propose the use of MMSE successive ICI cancellers. Since the output of each subchannel at instant n depends on subchannel inputs at instant $n-1$, but not on subchannel inputs at other instants, we will simplify our notation by dropping the time arguments n and $n-1$ in (4.9) and rewriting it as

$$y_m = \sum_{i=0}^{M-1} x_i \tilde{c}(m,i) + v_m, \tag{4.19}$$

where

$$\tilde{c}(m,i) = c_{mi}[N]. \tag{4.20}$$

Since only a few of the $M-1$ ICI terms in (4.19) will have non-negligible values, we will only take those non-negligible values into account in the design of the ICI cancellers. In other words, we will assume that

$$y_m \approx \sum_{i=m\ominus\nu}^{m\oplus\nu} x_i \tilde{c}(m.i) + v_m, \tag{4.21}$$

where it has been assumed that 2ν ICI terms have non-negligible values, and $\oplus$ and $\ominus$ represent the modulo-M addition and subtraction operators, respectively.

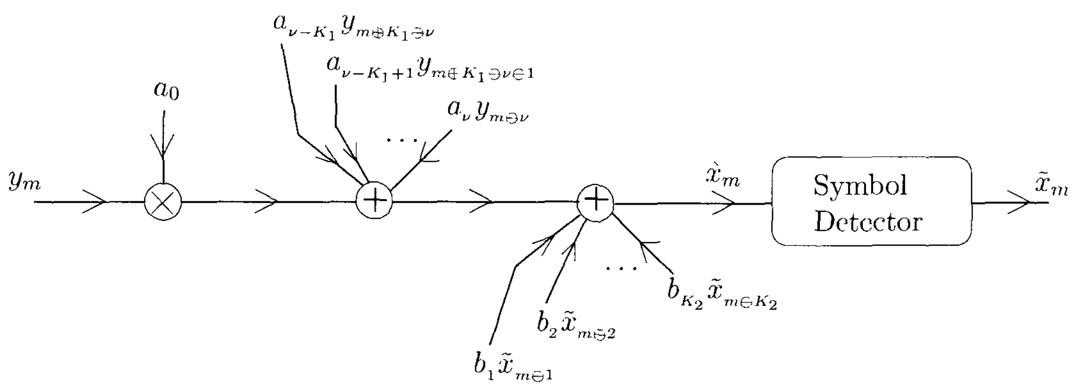

Figure 4.2: Successive ICI canceller with decision feedback.

To detect x_m from y_m we employ an MMSE successive ICI canceller with $K_1 + 1$ "feedforward" coefficients, and K_2 "feedback" coefficients. (These terms are borrowed from the terminology of decision feedback equalization.) A block diagram of such an ICI canceller is shown in Figure 4.2, where the input to the symbol detector is

$$\hat{x}_m = \sum_{k=-K_1+\nu}^{\nu} a_k y_{m\ominus k} + \sum_{k=1}^{K_2} b_k \tilde{x}_{m\ominus k}\,, \tag{4.22}$$

and $\tilde{x}_k$ denotes the decision made on the symbol in subchannel k. An interesting feature of this scheme is that it operates within each block of the received symbols, and independently of other blocks; c.f., (4.19). To compute the feedforward and feedback coefficients of the ICI canceller, we make the standard assumption that in the system of Figure 4.1 the input data sequences of different subchannels are uncorrelated, and we will denote the power of the ith input sequence $x_i[\cdot]$ by P_i. By applying the orthogonality principle [2] for MMSE estimation, it can be shown that the feedforward coefficients can be obtained from the following set of linear equations

$$\sum_{n=-K_1+\nu}^{\nu} a_n \psi_{jn} = P_m \hat{c}^*(m\ominus j, m), \quad j = -K_1+\nu, \cdots, \nu-1, \nu \tag{4.23}$$

where

$$\psi_{jn} = \sum_{r=-\nu}^{-j} \tilde{c}^*(m \ominus j, m - j - r)\tilde{c}(m \ominus n, m - j - r)P_{m\ominus j\ominus r}$$
$$+ R_v(m\ominus n, m\ominus j), \qquad j, n = -K_1 + \nu, \cdots, \nu - 1, \nu, \tag{4.24}$$

and $R_v(k, \ell) = E\{v_k v_\ell^*\}$ is the noise covariance at the subchannel outputs. The feedback coefficients are given by

$$b_\ell = -\sum_{j=-K_1+\nu}^{\nu} a_j \tilde{c}(m \ominus j, m \ominus \ell), \quad \ell = 1, 2, \cdots, K_2. \tag{4.25}$$

In Section 4.5, examples of the proposed bi-windowed DMT system are presented for a realistic digital subscriber line (DSL) environment, and we will see that for values of ν, K_1, and K_2 as small as 3, 6, and 6, respectively, significant performance gains can be achieved. Being able to obtain a high level of subchannel spectral containment at the transmitter and a high level of subchannel spectral selectivity at the receiver with such small values of ν, K_1, and K_2 is an attractive feature of the proposed system.

Recall from (4.22) that for the detection of the symbol transmitted on a given subchannel, the previously detected symbols on K_2 subchannels are used. Thus, for each block of the received signal, the process of detection and successive ICI cancellation requires a starting point. If we assume that this process starts from the jth subchannel, the symbols that are sent through subchannels $j \ominus 1$, $j \ominus 2$, $\cdots$, $j \ominus K_2$ have to be known symbols for the receiver. In other words, among the M subchannels of the system, the symbols transmitted on a contiguous set of K_2 of them are assumed to be known at the start of the detection and ICI cancellation procedure. Fortunately, most DMT systems use digital duplexing [16], in which the upstream and downstream frequency bands are specified by dividing the M subchannels into a number of groups, each representing an upstream or downstream band. A typical example of such subchannel grouping into downstream and upstream bands is given in Section 4.5; see Figure 4.6. In such scenarios, the detection for the subchannels of each downstream or upstream frequency band can be performed independently of the other bands. Moreover, in each frequency band, one can choose to start the detection procedure at the lower edge of the band. In this case, the K_2 subchannels that lie below the subcarrier on the lower edge of the band belong to a band that is assigned to the opposite direction of communication. Therefore, the corresponding symbol values in the current direction can be set to zero, and hence, it will not be necessary to restrict K_2 subchannels to carry known symbols.

4.5 Numerical Results

In this section we will provide examples of the subchannel spectra that can be achieved by the proposed system, and will provide a numerical comparison of the achievable rates of the proposed system and those of receiver-only Nyquist windowed DMT schemes [74, 75] in a realistic model for a digital subscriber line (DSL) environment. We consider windowed DMT systems with $M = 512$ conjugate symmetric subchannels and a cyclic prefix of length $P = 40$; i.e., $N = 552$. These values represent one set of valid values for M, P, and N adopted in the VDSL2 standard [16].

Recall from Section 4.3 that in the proposed method, the receiver window is designed using existing techniques or is chosen from the set of standard windows, and we design the transmitter window using the optimization problem in (4.17), for which the closed-form solution is provided in Appendix D. Among the standard windows [36,105,107], the Hann and Blackman windows have small stopband energies and a rapid spectral roll-off, and hence we chose the Hann and Blackman windows as the candidate receiver windows for the proposed system.

In the examples that we will present for the bi-windowed system, we assume that the shortest admissible cyclic prefix is used. Therefore, we assume that the channel (if not already short enough) is shortened using a time-domain equalizer (TEQ) [52,54,60] to length $L+1 = P+1 = 41$. Hence, the receiver window will be of length $N-L = 512$; c.f., (4.11). The receiver-only Nyquist windowing schemes [74,75] require extra redundancy, and for those schemes we will use a TEQ with a shorter target impulse response length.

In our first design, we chose the receiver window, $g[\cdot]$, to be a Hann window [36] of length 512, and we designed the transmitter window, $h_1[\cdot]$, of length $N = 552$ using the closed-form solution for the optimization problem in (4.17) with the parameters $\lambda = 0.5$ and $\theta = 4\pi/M$. The power spectrum of the designed transmitter window is shown in Figure 4.3, along with the power spectrum of a length-N rectangular window, which is the (implicit) transmitter window of the conventional DMT system. Similarly, we designed the transmitter window, $h_2[\cdot]$, of length 552 for the case in which the receiver window is the Blackman window [36] of length 512, using the same values of λ and θ. The power spectrum of that window is shown in Figure 4.4. Figure 4.5 shows the time-domain shapes of the designed transmitter windows.

In order to illustrate the performance improvement that can be achieved by the proposed transceiver, we will evaluate various system characteristics in a realistic model for a DSL environment. The voice-grade unshielded twisted pair cable (UTP-3) model [26] was used as the channel model, and an MMSE-TEQ [52,54,60] was used to shorten this physical channel to a given target length. Near-end cross-talk (NEXT) and far-end crosstalk (FEXT) were simulated using the model for a 50-pair binder [15]. Symmetric transmission with a sampling rate of $1/T_s = 2.208$ Msample/sec was implemented using digital duplexing [16] with the spectrum plan shown in Figure 4.6. The transmit signal power was 10 dBm, the additive white Gaussian noise (AWGN) power spectral density was -140 dBm/Hz, and it was assumed that echo was perfectly cancelled. Model 1 radio noise from [15,85] was used for the simulation of the RFI

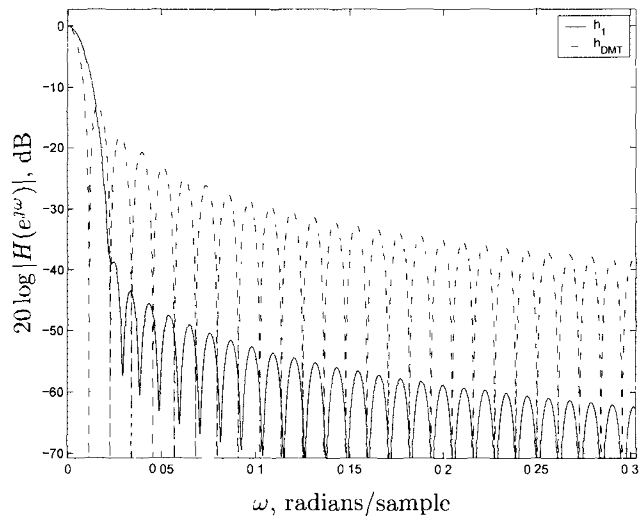

Figure 4.3: Frequency response of the designed transmitter window of length $N = 552$ (solid line) when the receiver window is a Hann window of length $M = 512$, $\lambda = 0.5$ and $\theta = 4\pi/M$. The dashed curve is the frequency response of the rectangular window of length $N = 552$.

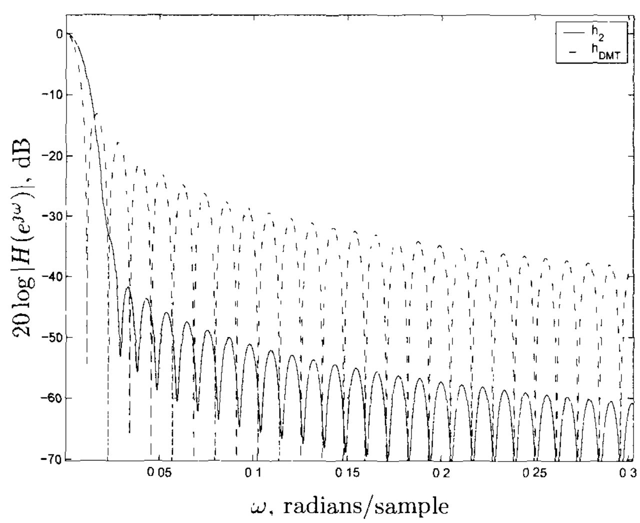

Figure 4.4: Frequency response of the transmitter window of length $N = 552$ (solid line) when the receiver window is a Blackman window of length The dashed curve is the frequency response of the rectangular window of length $N = 552$.

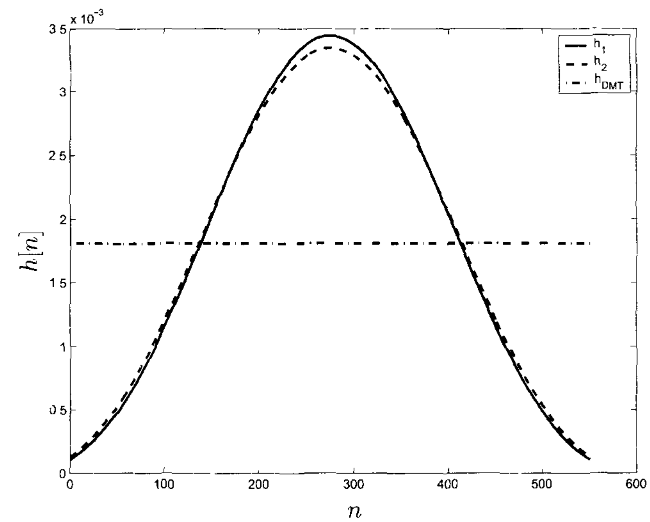

Figure 4.5: Time-domain shapes (interpolated) of the designed transmitter windows for the proposed system. For comparison, the rectangular transmitter window of the conventional DMT system is also plotted.

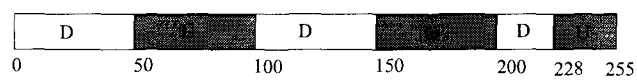

Figure 4.6: The spectrum plan used in the numerical examples. Subchannels 0–49, 100–149, and 200–227 are assigned for downstream communication (marked by "D"), and the remaining subchannels are used for upstream (U) transmission.

caused by the AM radio signals. Only the four of the ten AM signals of that model that lie below 1.104 MHz were used. Table 4.5 lists the frequency and power for these RFI signals.

Our first investigation concerns the ICI characteristics of the proposed system. In order to visualize the localized nature of the significant ICI components, in Figure 4.7 we have depicted the normalized magnitudes of the ICI coefficients, $\tilde{c}(m, i)$, for three representative subchannels, $m = 20, 60$ and 100. This figure is for the case of the first design (c.f., Figure 4.3), and the length of the cable is 2000 m. If we deem an ICI component to be negligible if its power is at least 60 dB below the power of the desired component, then it can be seen from Figure 4.7 that for each of the illustrated

Table 4.5: Model 1 radio noise of [85] for AM radio signals for frequencies below 1.104 MHz.

Frequency kHz	Differential mode power dBm
660	-60
710	-30
770	-70
1050	-55

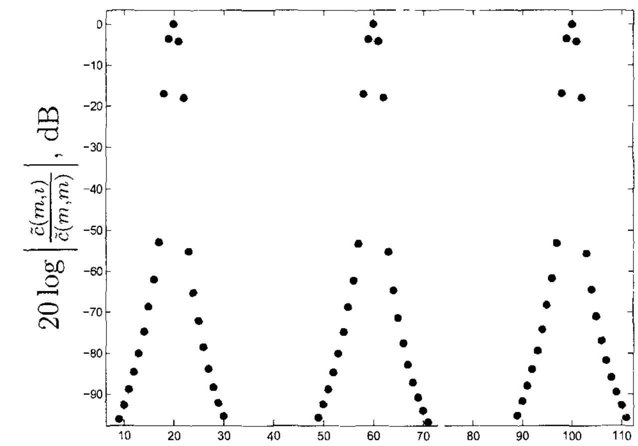

Figure 4.7: Normalized ICI factors corresponding to the subchannels $m = 20$, 60 and 100; see (4.19).

subcarriers, the number of non-negligible ICI terms is 6. In fact, this holds true for all subcarriers in both example designs of the proposed system. Therefore, in the implementation of the ICI cancellers, we chose $\nu = 3$ in (4.21), and hence the number of coefficients for the feedforward and feedback sections of the MMSE successive ICI cancellers at the subchannel outputs were chosen to be 7 and 6, respectively.

Our second performance evaluation is that of the achievable bit rate for the downstream communication. This was evaluated using the standard expression (c.f., Section 2.3)

$$R = \frac{1}{T}\sum_{i\in\mathcal{A}}\log_2\left(1+\frac{\mathrm{SINR}_i\gamma_{\mathrm{code}}}{\Gamma\gamma_{\mathrm{margin}}}\right), \tag{4.26}$$

where SINR_i is the signal-to-noise-plus-interference ratio of the ith subchannel at the input to the symbol detector in the ICI canceller, and Γ denotes the SINR gap. which for QAM modulation at a bit error probability of 10^{-7} is 9.8 dB, [15]. The parameter γ_{code} is the coding gain, which is assumed to be 3 dB, and γ_{margin} is the additional SINR margin, which, in the absence of error propagation, is chosen to be 3 dB. For the two examples of the proposed system, our simulation studies show that at a bit error probability of 10^{-7}, error propagation can result in a maximum SNR loss of 0.52 dB. Thus, for the two examples of the proposed system we will choose an SNR margin of $3 + 0.52 = 3.52$ dB. In (4.26), $\mathcal{A}$ denotes the set of downstream subchannel indices, and $1/T = 1/(NT_s) = 4$ kHz is the symbol rate. The SINR of each downstream subchannel of the proposed system was obtained in the above-mentioned DSL environment, and the achievable rate was computed using (4.26) with $\gamma_{\mathrm{margin}} = 3.52$ dB. The achievable rates of the two examples of the proposed system are plotted against the cable length in Figure 4.8. In order to indicate the improvement that can be obtained by the proposed system, we also provide in Figure 4.8 the achievable bit rates for the standard DMT system, and for the Nyquist receiver-only windowed DMT systems with a piecewise constant window [75], and a raised cosine window [74,75]. (Notice that for these schemes $\gamma_{\mathrm{margin}} = 3$ dB.) These Nyquist receiver-only windowing schemes require excess redundancy. We considered an excess redundancy of length $\mu = 10$ and we realized this excess redundancy by setting the target length for the TEQ-shortened channel to $P + 1 - \mu = 31$. (For the proposed bi-windowed system, the TEQ need only shorten the channel to a length of $L = 41$.)[5] From the comparisons in Figure 4.8 it can be seen that the proposed bi-windowed DMT system provides a considerably higher achievable rate than the receiver-only

[5]We used an MMSE-TEQ [51] with 15 taps for the target impulse response (TIR) of length 41 and an MMSE-TEQ with 20 taps for the TIR of length 31. This choice was made in order to obtain similar values for the residual mean square error. Moreover, the synchronization delay for each of the TEQs was optimized by numerical search.

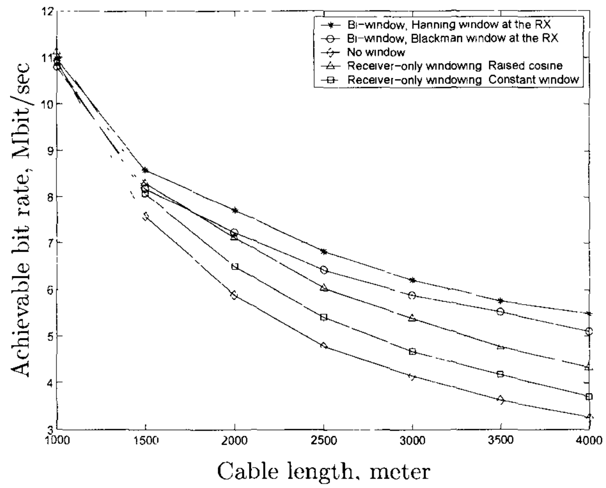

Figure 4.8: Achievable bit rate versus the cable length for the downstream communication.

windowing schemes for all the considered cable lengths, with the proposed system that employs the Hann window at the receiver providing a slightly higher rate than that based on the Blackman window. Figure 4.8 also suggests that the achievable rate gain obtained by the proposed system is more significant for longer cables.

The increased achievable rates obtained by the proposed system are a consequence of two mechanisms. First, in addition to the mitigation of the narrowband noise and the near-end cross-talk (NEXT) by the receiver window, NEXT is also mitigated by the transmitter due to the small stopband energy of the transmitter window. Secondly, in the proposed system the receiver window is not constrained to satisfy the time-domain Nyquist condition [74,75], and hence windows with smaller sidelobes and smaller stopband energy can be obtained. In order to illustrate the ability of the proposed system to suppress NEXT and narrowband noise, we have plotted in Figures 4.9 and 4.10, respectively, the NEXT-to-signal and RFI-to-signal power ratios at the receiver outputs of three systems for downstream transmission over a cable of length 2000 m. (Recall the downstream bands from the spectrum plan in Figure 4.6.)

The three systems are the proposed bi-windowed DMT system with Hann window at the receiver, a receiver-only windowed DMT system with a raised cosine window, and the standard DMT system with its rectangular windows. From Figure 4.9 it can be seen that the bi-windowed DMT system provides much stronger suppression of NEXT interference, due to the fact that it uses windowing at both the transmitter and the receiver. Figure 4.10 shows that the proposed system also provides stronger suppression of narrowband interference than the receiver-only windowing approach with a raised cosine window. As mentioned earlier, this is because in the proposed system, the receiver window is not constrained to satisfy the time-domain Nyquist condition [74, 75], and therefore receiver windows with smaller sidelobes and smaller stopband energy can be used.

From a complexity point of view, comparing the proposed bi-windowed DMT system with the conventional DMT system, it can be seen that due to the usage of the successive ICI cancellation in the bi-windowed DMT system, this scheme has a larger complexity than conventional DMT. However, as was expained in the previous sections and demonstrated in this section, the ICI is controlled by the proposed design method so that only a few non-negligible ICI terms exist at the input to the ICI canceller. In the example of Figure 4.7 it was seen that while the system had $M = 512$ subchannels, for each of the subchannels, the number of non-negligible ICI terms was equal to 6, and the number of coefficients for the feedforward and feedback sections of the MMSE successive ICI cancellers at the subchannel outputs were 7 and 6, respectively.

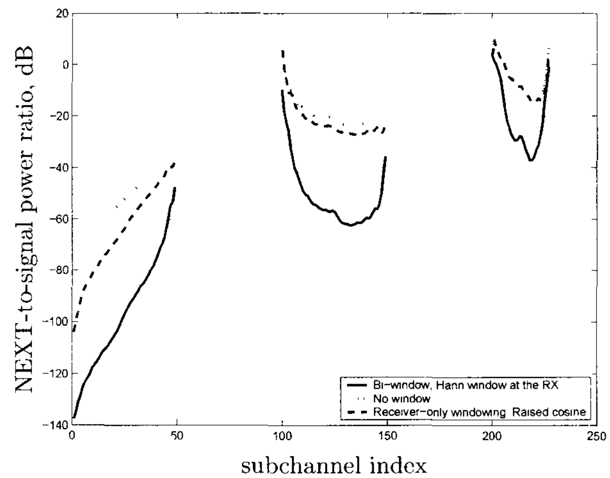

Figure 4.9: NEXT-to-signal power ratios at the subchannel outputs (interpolated) for the downstream transmission bands, with a cable length of 2000 m.

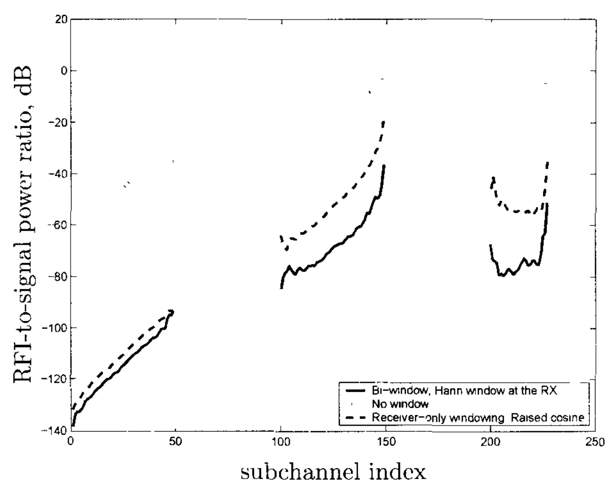

Figure 4.10: RFI-to-signal power ratios at the subchannel outputs (interpolated) for the downstream transmission bands, with a cable length of 2000 m.

Chapter 5

Concluding remarks and future work

In this chapter, some concluding remarks, and some suggestions for future work are presented.

5.1 Concluding remarks

In this thesis, multi-carrier communication systems were studied and several methods for improving the achievable bit rate in these systems were proposed.

In Chapter 1, the motivation for using multi-carrier communication schemes was studied, the history of multi-carrier communication systems was reviewed, and the major advantages of multi-carrier communications over single-carrier communications were discussed. In addition, in that chapter, the most popular multi-carrier communication schemes, i.e., DMT and OFDM, were briefly described and their applications and the standard bodies that have adopted these schemes as the modulation method were discussed. Finally, in Chapter 1, the major shortcomings of DMT and OFDM schemes were briefly described.

In Chapter 2, an overview of multi-carrier communication systems was presented. A unifying filter bank framework was used to facilitate comparisons between different multi-carrier schemes, including DMT. OFDM, FMT, and DWMT. The structure of each of these schemes was described in the context of the filter bank model, and the points of strength and shortcomings of each scheme were compared. Then, we reviewed different time domain equalizer (TEQ) methods that are used for impulse response shortening in multi-carrier communication systems. Among different TEQ methods, the minimum mean square error TEQ, which is the most widely used TEQ, was analyzed in detail. Loading methods for DMT transceivers were also studied in Chapter 2 and the water-filling algorithm, which is the optimal loading method in the absence of ISI and ICI, was presented. The established windowing techniques for DMT and OFDM systems were also studied in Chapter 2. Windowing techniques can be considered as some of the most efficient methods for improving the performance of DMT and OFDM transceivers, and several transmitter and receiver windowing methods were described. Since our numerical examples in Chapters 3 and 4 were developed under a model for the DSL environment, the fundamentals of digital subscriber lines were studied in order to provide the required background.

In Chapter 3, we proposed several signal processing schemes for improvement of the achievable bit rates in filtered multitone communication systems. A key contribution was the development of an efficient technique for the design of the prototype filter. The design criteria were derived based on channel-independent measures of the intersubchannel interference (ICI) and intersymbol interference (ISI) generated by the filter bank. It was argued that these criteria compete with each other and hence an effective design technique ought to enable efficient qualification of the inherent trade-off between these criteria. We were able to achieve this goal by transforming the direct formulation of the design problem into a convex optimization problem that can be efficiently solved. The resulting trade-off curves quantify the basic intuition that obtaining the optimal performance from an FMT system requires a compromise between ICI and ISI. Furthermore, this trade-off curve was shown to enable the designer to efficiently determine the appropriate compromise for a given scenario. As we demonstrated in our examples, the choice of an appropriate compromise between ICI and ISI offers a significant increase in the achievable bit rate. Furthermore, it was shown how the availability of an efficient method for obtaining an optimal prototype filter enables quantification of other design trade-offs, such as the appropriate number of subchannels in an FMT scheme.

One of the outcomes of our prototype filter design technique in Chapter 3 was that the most effective prototype filters generate a non-negligible amount of ISI at the subchannel outputs. As a result, the conventional water-filling algorithm for the allocation of the transmission power to the subchannels is suboptimal. The final contribution in that chapter was the development of a convergent iterative algorithm for power loading in the FMT system. This algorithm provides higher achievable bit rates than both conventional water-filling and a simpler loading algorithm that allocates power uniformly to those subchannels that can reliably support at least one bit per subchannel use. The improvement in the achievable bit rates was shown to be significant in scenarios in which implementation constraints significantly restrict the complexity of the decision feedback equalizer in each subchannel.

In Chapter 4, we proposed a family of bi-windowed DMT systems that provides improved subchannel spectral characteristics at both ends of the transceiver without the requirement of excess cyclic prefix. The development of this family of systems involved the derivation of the channel-independent necessary and sufficient conditions for the filter bank transceiver of Figure 4.1 to be free from ISI. Compared to the standard DMT system and to windowed DMT systems with receiver-only (Nyquist) windowing, the proposed system provides a considerable gain in the achievable bit rate in the presence of narrowband noise and crosstalk. The proposed design does not require the knowledge of the channel, other than the assumption that the order of the shortened equivalent discrete-time channel is not larger than the cyclic prefix length. In the proposed transceiver, the received signal in each subchannel is free from ISI and has only a small number of non-negligible ICI components. Successive ICI cancellers were proposed to suppress the non-negligible ICI terms that exist at the subchannel outputs. Numerical results demonstrated the capability of the proposed system to provide a significant increase in the achievable bit rate in a realistic DSL environment.

5.2 Future work

In Chapter 2, we explained the mechanism by which the DMT scheme achieves subchannel outputs that are both ISI-free and ICI-free when the length of the cyclic prefix is at least as large as the order of the channel, i.e., when $P \geq L$. Recall that TEQs are typically used in DMT transceivers to ensure this condition holds. However, if the condition of $P \geq L$ doesn't hold, both ISI and ICI will be present in the subchannel outputs of the DMT system. In contrast, the FMT scheme is robust to this problem. Indeed, the FMT scheme does not require the order of the channel to be constrained to a maximum value. As a future research work, it is suggested to investigate signal processing techniques that would make the DMT system more robust for applications in which the order of the channel exceeds the cyclic prefix length. This would include investigating signal processing techniques that can prevent (or reduce) ISI and ICI that appear at the subchannel outputs at the receiver, as well as techniques that will mitigate ISI and ICI.

Another suggestion for a future work is to implement each of the proposed systems of Chapters 3 and 4 on hardware, e.g., on field programmable gate arrays (FPGA), and verify the performance of these systems in practice. While theses systems were analyzed in this thesis, efficient methods for their hardware implementation need to be further investigated.

One other potential future work will be to combine channel coding schemes with the bi-windowed DMT system of Chapter 4 and evaluate the performance of the whole system. A challenge will be to look for appropriate coding schemes and especially for appropriate approaches for concatenating the coding scheme and the bi-windowed DMT system.

While the proposed systems of Chapters 3 and 4 were derived for general application, the numerical examples considered in this thesis were mainly for DSL environment. A suggested future work is to evaluate the performance of these systems in wireless environments.[1] A major challenge in wireless environment is the Doppler spread encountered in mobile applications. The presence of Doppler spread in mobile applications produces ICI. In Chapter 4, it was observed that, compared to the conventional DMT system, the proposed bi-windowed DMT system has improved subchannel spectral containment at the transmitter and improved subchannel spectral selectivity at the receiver. Because of these improvements in the spectral characteristics, it is likely that, in the presence of Doppler spread, the bi-windowed DMT system would offer more robustness compared to conventional DMT system. In addition, the application of successive ICI cancellation in the bi-windowed DMT system is expected to increase its robustness against Doppler spread.

In Chapters 1 and 2, the established multi-carrier communication systems including DMT, OFDM, FMT, and DWMT were studied. In all of these systems, the frequency bandwidth assigned to all the subchannels is of the same width. A more general multi-carrier system would be one in which different subchannels can use different bandwidths. It is likely that such a system could result in an improvement of the achievable bit rate in specific applications. This needs to be investigated and

[1]Some results on the performance of FMT in wireless channels are available in [108].

verified. A major challenge will be to find an efficient implementation method for that system.

It was studied in Chapters 2 and 3 that in the FMT system, while ICI is negligible at the receiver, ISI is present and needs to be mitigated using per subchannel equalization. In Chapter 3, per subchannel decision feedback equalization was used for this purpose. As an alternative method for per subchannel ISI mitigation, it is suggested to use DMT. In this system, each subchannel of the FMT system will be considered as an independent channel[2], and for transmission over that channel, DMT scheme is exploited. The overall system will be a combination (cascade) of FMT and DMT systems[3], and the only equalization used would be one-tap per subchannel equalizers used in DMT receiver (c.f. Section 2.1.2). Therefore, the advantage of this system over FMT system will be that it will not need per subchannel decision feed back equalization. The advantage of this system over DMT system will be that it will not require time-domain equalization. A challenge will be to find appropriate values for system parameters such as the number of subchannels in the FMT and each of the DMT subsystems. In addition, deriving the appropriate design method for the overall system, and efficient implementation of it will be some of the major challenges in that research work.

[2]This is a reasonable assumption when ICI is negligible.
[3]Some results on such a system can be found in [109].

Appendix A

Derivation of the upper bound for the ICI power

In this appendix, it is shown that the power of ICI can be bounded as in (3.8). Using (3.3), the Fourier transform of $f_{mi}[n]$ can be written as

$$F_{mi}(e^{j\omega}) = \frac{1}{N}\sum_{k=0}^{N-1} G_{mi}(e^{j(\frac{\omega-2k\pi}{N})}), \tag{A.1}$$

where $G_{mi}(e^{j\omega})$ is the Fourier transform of $g_{mi}[n]$. Using (3.4) we have that

$$G_{mi}(e^{j\omega}) = H(e^{j(\omega-\omega_i)})H^*(e^{j(\omega-\omega_m)})C(e^{j\omega}). \tag{A.2}$$

Applying the triangle inequality to the magnitude of (A.1) we have that

$$|F_{mi}(e^{j\omega})| \leq \frac{1}{N}\sum_{k=0}^{N-1} |G_{mi}(e^{j(\frac{\omega-2k\pi}{N})})| \tag{A.3}$$

and using the inequality $|\sum_{i=1}^{n} a_i|^2 \leq n\sum_{i=1}^{n}|a_i|^2$ in (A.3) we have that

$$|F_{mi}(e^{j\omega})|^2 \leq \frac{1}{N}\sum_{k=0}^{N-1} |G_{mi}(e^{j(\frac{\omega-2k\pi}{N})})|^2. \tag{A.4}$$

If we let U_c denote an upper bound on the magnitude of the channel spectrum, i.e., $|C(e^{\jmath\omega})| \leq U_c$, then from (A.2) and (A.4) we conclude that

$$|F_{mi}(e^{\jmath\omega})|^2 \leq \frac{U_c^2}{N} \sum_{k=0}^{N-1} |H(e^{\jmath(\frac{\omega-2k\pi}{N}-\omega_i)})H^*(e^{\jmath(\frac{\omega-2k\pi}{N}-\omega_m)})|^2. \tag{A.5}$$

To calculate the bound for $\int_0^{2\pi} |F_{mi}(e^{\jmath\omega})|^2\, d\omega$, we define the new variable $\Omega = \frac{\omega-2k\pi}{N}$, which in combination with (A.5) allows us to write

$$\int_0^{2\pi} |F_{mi}(e^{\jmath\omega})|^2\, d\omega \leq U_c^2 \sum_{k=0}^{N-1} \int_{\frac{-2k\pi}{N}}^{\frac{2\pi-2k\pi}{N}} |H(e^{\jmath(\Omega-\omega_i)})|^2 |H(e^{\jmath(\Omega-\omega_m)})|^2\, d\Omega. \tag{A.6}$$

Combining the summation and the integral in (A.6) we obtain the bound

$$\int_0^{2\pi} |F_{mi}(e^{\jmath\omega})|^2\, d\omega \leq U_c^2 \int_0^{2\pi} |H(e^{\jmath(\Omega-\omega_i)})|^2 |H(e^{\jmath(\Omega-\omega_m)})|^2\, d\Omega. \tag{A.7}$$

If we define P_I to be $P_I = \max_{i\in\mathcal{A}}\{P_i\}$, then using (3.7) and (A.7) we have that

$$\begin{aligned} P_{\text{ICI}} &\leq \frac{U_c^2 P_I}{2\pi} \sum_{\substack{i\in\mathcal{A}\\ i\neq m}} \int_0^{2\pi} |H(e^{\jmath(\Omega-\omega_i)})|^2 |H(e^{\jmath(\Omega-\omega_m)})|^2\, d\Omega \\ &\leq \frac{U_c^2 P_I}{2\pi} \sum_{\substack{i=1\\ i\neq m}}^{M} \int_0^{2\pi} |H(e^{\jmath(\Omega-\omega_i)})|^2 |H(e^{\jmath(\Omega-\omega_m)})|^2\, d\Omega. \end{aligned} \tag{A.8}$$

Recall that $\omega_i = (i-1)2\pi/M$ Therefore, (A.8) can be simplified to

$$P_{\text{ICI}} \leq \frac{U_c^2 P_I}{2\pi} \sum_{\ell=1}^{M-1} \int_0^{2\pi} |H(e^{\jmath\omega})|^2 |H(e^{\jmath(\omega-\ell\frac{2\pi}{M})})|^2\, d\omega. \tag{A.9}$$

In order to simplify the remaining analysis, the spectral mask of the prototype filter is depicted in Figure A.1. The integral in (A.9) can be calculated as the integral over the passband of $H(e^{\jmath\omega})$ plus the integral over the stopband of $H(e^{\jmath\omega})$, i.e.,

$$\sum_{\ell=1}^{M-1} \int_0^{2\pi} |H(e^{\jmath\omega})|^2 |H(e^{\jmath(\omega-\ell\frac{2\pi}{M})})|^2\, d\omega = I_1 + I_2\,, \tag{A.10}$$

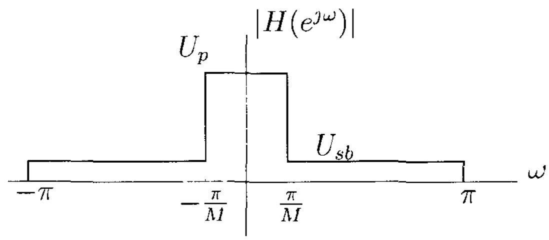

Figure A.1: Prototype filter spectrum mask.

where

$$I_1 = \sum_{\ell=1}^{M-1} \int_{-\frac{\pi}{M}}^{\frac{\pi}{M}} |H(e^{\jmath\omega})|^2 |H(e^{\jmath(\omega-\ell\frac{2\pi}{M})})|^2 \, d\omega, \tag{A.11}$$

and

$$I_2 = \sum_{\ell=1}^{M-1} \int_{\frac{\pi}{M}}^{2\pi-\frac{\pi}{M}} |H(e^{\jmath\omega})|^2 |H(e^{\jmath(\omega-\ell\frac{2\pi}{M})})|^2 \, d\omega. \tag{A.12}$$

In the passband of the prototype filter, the spectrum is bounded by U_p. Therefore,

$$\begin{aligned} I_1 &\leq U_p^2 \sum_{\ell=1}^{M-1} \int_{-\frac{\pi}{M}}^{\frac{\pi}{M}} |H(e^{\jmath(\omega-\ell\frac{2\pi}{M})})|^2 \, d\omega \\ &= U_p^2 \sum_{\ell=1}^{M-1} \int_{\frac{-\pi-2\pi\ell}{M}}^{\frac{\pi-2\pi\ell}{M}} |H(e^{\jmath\omega})|^2 \, d\omega \\ &= U_p^2 \int_{-2\pi+\frac{\pi}{M}}^{-\frac{\pi}{M}} |H(e^{\jmath\omega})|^2 \, d\omega \\ &= 2\pi \, U_p^2 \, E_{sb}, \end{aligned} \tag{A.13}$$

where E_{sb} is the stopband energy of the prototype filter and is given by (3.9). On the other hand, the stopband magnitude of the prototype filter is bounded by U_{sb}. Thus, from (A.12) we have that

$$\begin{aligned}
I_2 &\le U_{sb}^2 \sum_{\ell=1}^{M-1} \int_{\frac{\pi}{M}}^{2\pi-\frac{\pi}{M}} |H(e^{\jmath(\omega-\ell\frac{2\pi}{M})})|^2\, d\omega \\
&= U_{sb}^2 \sum_{\ell=1}^{M-1} \int_{\frac{\pi-2\pi\ell}{M}}^{2\pi-\frac{\pi+2\pi\ell}{M}} |H(e^{\jmath\omega})|^2\, d\omega \\
&= U_{sb}^2 \int_{-2\pi+\frac{3\pi}{M}}^{2\pi-\frac{3\pi}{M}} |H(e^{\jmath\omega})|^2\, d\omega \\
&\le 2\pi\, U_{sb}^2\, (E_h + E_{sb}),
\end{aligned} \tag{A.14}$$

where E_h is the energy of the prototype filter, $E_h = \frac{1}{2\pi}\int_0^{2\pi} |H(e^{\jmath\omega})|^2\, d\omega$. The last inequality in bounding I_2 (in (A.14)) can be simply verified using Figure A.1.

Finally, using (A.9), (A.10), (A.13), and (A.14) we conclude that

$$P_{\text{ICI}} \le P_I U_c^2 (U_p^2 E_{sb} + U_{sb}^2 E_h + U_{sb}^2 E_{sb}). \tag{A.15}$$

Appendix B

Proof of Theorem 1

Refer to the flow diagram of the power loading algorithm given in Fig. 3.5. When the kth iteration of the algorithm begins, the subchannel powers are given by the vector $\mathbf{p}^{(k)}$. Once the MMSE-DFE coefficients are adjusted for the given $\mathbf{p}^{(k)}$, the achievable bit rate of the system can be calculated as a function of $\mathbf{a}^{(k)}, \mathbf{b}^{(k)}, \mathbf{c}^{(k)}$ and $\mathbf{p}^{(k)}$ using (3.15). We denote this rate as $R(\mathbf{a}^{(k)}, \mathbf{b}^{(k)}, \mathbf{c}^{(k)}, \mathbf{p}^{(k)})$. In the next stage of the algorithm, for the given $\mathbf{a}^{(k)}, \mathbf{b}^{(k)}, \mathbf{c}^{(k)}$ the optimization problem (3.16) is solved which results in $\mathbf{p}^{(k+1)}$. Obviously,

$$R(\mathbf{a}^{(k)}, \mathbf{b}^{(k)}, \mathbf{c}^{(k)}, \mathbf{p}^{(k+1)}) \geq R(\mathbf{a}^{(k)}, \mathbf{b}^{(k)}, \mathbf{c}^{(k)}, \mathbf{p}^{(k)}). \tag{B.1}$$

In the next iteration, the MMSE-DFE coefficients are calculated for the new power allocation vector $\mathbf{p}^{(k+1)}$, resulting in $\mathbf{a}^{(k+1)}, \mathbf{b}^{(k+1)}, \mathbf{c}^{(k+1)}$. Since the adjustment of the MMSE-DFE coefficients for the new power vector $\mathbf{p}^{(k+1)}$ results in an improvement in the SINR of the subchannels, we obtain an increase in the achievable bit rate. More precisely,

$$R(\mathbf{a}^{(k+1)}, \mathbf{b}^{(k+1)}, \mathbf{c}^{(k+1)}, \mathbf{p}^{(k+1)}) \geq R(\mathbf{a}^{(k)}, \mathbf{b}^{(k)}, \mathbf{c}^{(k)}, \mathbf{p}^{(k+1)}). \tag{B.2}$$

Equations (B.1) and (B.2) show that the achievable bit rate of the system increases monotonically. On the other hand, we know that the achievable bit rate of the system is bounded above, say by the capacity of the system. Thus, the algorithm converges.

Appendix C

Derivation of the channel-independent zero ISI conditions

In this appendix it is shown that the filter bank transceiver of Fig. 4.1 has zero ISI at its subchannel outputs for every channel of order at most L (i.e., with the condition $c[n] = 0$, $n \notin [0, L]$) if and only if either (4.6a) or (4.6b) is satisfied.

Recall that for the transceiver of Fig. 4.1 the output of the mth subchannel is given by (4.1). Substituting (4.5) into (4.1) we have that

$$y_m[n] = \sum_{i=0}^{M-1} \sum_{\ell=-\infty}^{\infty} x_i[\ell] \sum_{k=k_1}^{k_2} g_m[k] \sum_{p=0}^{L} c[p] h_i[N(n-\ell) - k - p] + v_m[n]. \tag{C.1}$$

In order for the subchannel outputs to be free from ISI, $y_m[n]$ should depend on $x_i[\ell]$ for only one instant ℓ. To determine conditions for that to hold, we recall that $h_i[n]$ is supported on $[n_1, n_2]$, and hence $y_m[n]$ depends on $x_i[\ell]$ only if there exists a $k \in [k_1, k_2]$ and a $p \in [0, L]$ such that

$$k + p + n_1 \leq N(n - \ell) \leq k + p + n_2. \tag{C.2}$$

For the system to be ISI-free for any channel of order at most L, for each value of n and for all $k \in [k_1, k_2]$ and $p \in [0, L]$ there must be only one value of ℓ that satisfies (C.2). Therefore, considering the support intervals of $g_m[k]$ and $c[p]$, the system is free from ISI for any channel of order at most L if and only if there is one, and only one, integer $\tilde{\ell}$ that satisfies

$$k_1 + n_1 \leq N\tilde{\ell} \leq k_2 + n_2 + L. \tag{C.3}$$

To find conditions on k_1, k_2, n_1 and n_2 such that this relation holds, we will consider two cases. In the first case, $k_1 + n_1$ is an integer multiple of N, and in the second case, $k_1 + n_1$ is not an integer multiple of N.

C.1 First case: $k_1 + n_1 = jN$

In this case, there exists an integer j such that

$$k_1 + n_1 = jN. \tag{C.4}$$

In this case, one can simply verify that $\tilde{\ell} = j$ satisfies (C.3). Now, the channel-independent zero ISI condition is achieved so long as no other value for $\tilde{\ell}$ satisfies (C.3). If $\tilde{\ell} < j$, obviously $N\tilde{\ell} < Nj$ and therefore $\tilde{\ell}$ will not satisfy (C.3). In order to prevent any $\tilde{\ell} \geq j + 1$ from satisfying (C.3), the following must hold

$$k_2 + n_2 + L < (j + 1)N. \tag{C.5}$$

Using (C.4), the condition in (C.5) can be equivalently written as

$$(k_2 - k_1) + (n_2 - n_1) < N - L. \tag{C.6}$$

C.2 Second case: $k_1 + n_1 = jN + d$

In this case, $k_1 + n_1$ is not an integer multiple of N. Therefore, there is an integer j and an integer $d \in [1, N-1]$ such that

$$k_1 + n_1 = Nj + d. \tag{C.7}$$

Considering (C.7), for $\tilde{\ell}$ to satisfy the lower bound in (C.3), it must satisfy $\tilde{\ell} \geq j+1$. In order to obtain the channel-independent zero ISI condition, among these values for $\tilde{\ell}$, one and only one of them should satisfy the upper bound for $N\tilde{\ell}$ in (C.3). Thus, we must have $N(j+1) \leq k_2 + n_2 + L$ and $N(j+2) > k_2 + n_2 + L$. Using (C.7), these two conditions can be simplified to

$$N - L \leq (k_2 - k_1) + (n_2 - n_1) + d < 2N - L. \tag{C.8}$$

Appendix D

Closed form solution for the optimization problem (4.17)

A closed form solution to (4.17) can be obtained using the classical Lagrange multiplier method [73]. Let $\mathbf{h}$ denote the $N \times 1$ vector $\mathbf{h} = (h[0], h[1], \cdots, h[N-1])^T$, and let $\mathbf{d}$ denote the $N \times 1$ vector $\mathbf{d} = (1, 1, \cdots, 1)^T$. The constraint (4.17b) can then be written as $\mathbf{d}^T \mathbf{h} = 1$. Using the fact that $H(e^{\jmath\omega}) = \sum_{k=0}^{N-1} h[k] e^{-\jmath\omega k}$, we can write

$$\frac{1}{2\pi} \int_{\theta}^{2\pi-\theta} |H(e^{\jmath\omega})|^2 \, d\omega = \mathbf{h}^T \mathbf{U} \mathbf{h}, \tag{D.1}$$

where $\mathbf{U}$ is an $N \times N$ matrix with entries

$$[\mathbf{U}]_{\ell,k} = \begin{cases} 1 - \frac{\theta}{\pi}, & \ell = k \\ -\frac{\sin(k-\ell)\theta}{(k-\ell)\pi}, & \ell \neq k. \end{cases} \tag{D.2}$$

We can also write

$$\sum_{p=1}^{M-1} \sum_{n=N-L}^{N} \left| \sum_{k=0}^{N-1} h[k] g[n-k] e^{\jmath \frac{2\pi}{M} kp} \right|^2 = \mathbf{h}^T \mathbf{V} \mathbf{h}, \tag{D.3}$$

where $\mathbf{V}$ is the $N \times N$ matrix with entries

$$[\mathbf{V}]_{\ell,k} = \sum_{p=1}^{M-1} \sum_{n=N-L}^{N} g[n-\ell] g[n-k] \cos\Big(\frac{2\pi}{M}(k-\ell)p\Big). \tag{D.4}$$

Using (D.3) and (D.1), the objective function in (4.17a) can be written as $\mathbf{h}^T\mathbf{\Psi}\mathbf{h}$, where

$$\mathbf{\Psi} = \lambda\mathbf{U} + (1-\lambda)\mathbf{V}. \tag{D.5}$$

Hence, the optimization problem in (4.17) can be written as

$$\text{minimize} \quad \mathbf{h}^T\mathbf{\Psi}\mathbf{h} \tag{D.6a}$$

$$\text{subject to} \quad \mathbf{d}^T\mathbf{h} = 1. \tag{D.6b}$$

Using the classical Lagrange multiplier optimality method [73], it can be shown that the optimization problem (D.6) has a closed form solution given by

$$\begin{pmatrix} \mathbf{h}_{\text{opt}} \\ \gamma \end{pmatrix} = \mathbf{A}^{-1}\mathbf{q}, \tag{D.7}$$

where γ is a real scalar, $\mathbf{q}$ is the $(N+1)$th column of the identity matrix of size $(N+1)$, and

$$\mathbf{A} = \begin{pmatrix} 2\mathbf{\Psi} & \mathbf{d} \\ \mathbf{d}^T & 0 \end{pmatrix}. \tag{D.8}$$

From (D.1) it can be seen that $\mathbf{U}$ is symmetric positive definite, and from (D.3) it can be seen that $\mathbf{V}$ is symmetric positive definite. Since $\lambda \in [0,1]$, $\mathbf{\Psi}$ is symmetric positive definite, and therefore, it is full-rank. Using this fact and the structure of $\mathbf{A}$ given by (D.8) it can be shown that $\mathbf{A}$ is also full-rank and thus invertible.

Bibliography

[1] A. B. Carlson, *Communication Systems*, McGraw-Hill, 3rd ed., 1986.

[2] J. G. Proakis, *Digital Communications*, McGraw-Hill, 4th ed., 2001.

[3] S. U. H. Qureshi, "Adaptive equalizers," *Proc. IEEE*, vol. 37, pp. 1340-1387, Sept. 1985.

[4] M. L. Doelz, E. T. Heald, and D. L. Martin, "Binary data transmission techniques for linear systems," *Proc. IRE*, vol. 45, pp. 656-661, May 1957.

[5] B. R. Saltzberg, "Performance of an efficient parallel data transmission system," *IEEE Trans. Commun. Technol.*, vol. COM-15, pp. 805-811, Dec. 1967.

[6] S. Darlington, "On digital single-sideband modulators," *IEEE Trans. Circuit Theory*, vol. CT-17, pp. 409-414, Aug. 1970.

[7] R. Maruta, and A. Tomozawa, "An improved method for digital SSB-FDM modulation and demodulation," *IEEE Trans. Commun.*, vol. COM-26, pp. 720-725, May 1978.

[8] B. Hirosaki, "An orthogonally multiplexed QAM system using the discrete Fourier transform," *IEEE Trans. Commun.*, vol. COM-29, pp. 982-989, July 1981.

[9] I. Kalet, "The multitone channel," *IEEE Trans. Commun.*, vol. 37, pp. 119-124, Feb. 1989.

[10] B. Hirosaki, S. Hasegawa, and A. Sabato, "Advanced groupband data modem using orthogonally multiplexed QAM techniques," *IEEE Trans. Commun.*, vol. COM-34, pp.587-592, June 1986.

[11] J. A. C. Bingham, "Multicarrier modulation for data transmission: An idea whose time has come," *IEEE Commun. Mag.*, vol. 28, pp. 5-14, May 1990.

[12] M. Ghosh. "Analysis of the effect of impulse noise on multicarrier and singlecarrier QAM systems," *IEEE Trans. Commun.*, vol. 44, pp. 145-147, Feb. 1996.

[13] J. S. Chow, J. C. Tu. and J. M. Cioffi, "A discrete multitone transceiver system for HDSL applications," *IEEE J. Sel. Areas Commun.*, vol. 9, Aug. 1991.

[14] K. Sistanizadeh, P. Chow, and J. Cioffi."Multi-tone transmission for asymmetric digital subscriber lines (ADSL)," *in Proc. IEEE Int. Conf. Commun.*, vol. 2, pp. 756-760, May 1993.

[15] T. Starr. J. M. Cioffi, and P. J. Silverman, *Understanding Digital Subscriber Line Technology*, Prentice-Hall, 1999.

[16] T. Starr. M. Sorbara, J. M. Cioffi, and P. J. Silverman, *DSL Advances*, Prentice-Hall, 2003.

[17] DSL Forum website: http://www.dslforum.org

[18] N. Pavlidou, A. J. Han Vinck, J. Yazdani, and B. Honary, "Power line communications: State of the art and future trends," *IEEE Commun. Mag.*, vol. 41, pp. 34-40, Apr. 2003.

[19] A. Majumder. and J. Caffery, Jr., "Power line communications." *IEEE Potentials*, vol. 23, pp. 4-8, Oct.-Nov. 2004.

[20] ETSI, "Digital Video Broadcasting (DVB): Framing, channel coding, and modulation for digital terrestrial television," ETSI EN30 744 V1.3.1, Aug. 2000.

[21] IEEE Standard 802.11e, "IEEE Standard for Information technology - Telecommunications and information exchange between systems - Local and metropolitan area networks - Specific requirements Part 11: Wireless LAN Medium Access Control (MAC) and Physical Layer (PHY) specifications Amendment 8: Medium Access Control (MAC) Quality of Service Enhancements," pp. 1-189, 2005.

[22] IEEE Standard 802.16e, "IEEE Standard for Local and metropolitan area networks Part 16: Air Interface for Fixed and Mobile Broadband Wireless Access Systems Amendment 2: Physical and Medium Access Control Layers for Combined Fixed and Mobile Operation in Licensed Bands and Corrigendum 1," pp. 1-822, 2006.

[23] S. Chatterjee, W. A. C. Fernando, and M. K. Wasantha, "Adaptive modulation based MC-CDMA systems for 4G wireless consumer applications," *IEEE Trans. Consumer Electronics*, vol. 49, pp. 995-1003, Nov. 2003.

[24] S. Hara, and R. Prasad, "Overview of multicarrier CDMA," *IEEE Commun. Mag.*, vol. 35, pp. 126-133, Dec. 1997.

[25] G. Cuypers, K. Vanbleu, G. Ysebaert, and M. Moonen, "Egress reduction by intra-symbol windowing in DMT-based transmitters," *in Proc. IEEE Int. Conf. Acoust., Speech, Signal Processing*, vol. 4, pp. 532-535, Apr. 2003.

[26] G. Cherubini, E. Eleftheriou, and S. Ölçer, "Filtered Multitone Modulation for Very High-Speed Digital Subscriber Lines," *IEEE J. Sel. Areas Commun.*, vol. 20, pp. 1016-1028, June 2002.

[27] S. D. Sandberg, and M. A. Tzannes, "Overlapped discrete multitone modulation for high speed copper wire communications," *IEEE J. Sel. Areas Commun.*, vol. 13, pp. 1571–1585, Dec. 1995.

[28] G. Cherubini, E. Eleftheriou, S. Ölçer, and J. Cioffi, "Filter Bank Modulation Techniques for Very High-Speed Digital Subscriber Lines," *IEEE Commun. Mag.*, vol. 38, pp. 98-104, May 2000.

[29] Z. Wang, and G. B. Giannakis, "Wireless multicarrier communications," *IEEE Signal Processing Mag.*, vol. 17, pp. 29-48, May 2000.

[30] R. P. Ramachandran, and P. Kabal, "Bandwidth efficient transmultiplexers. I. Synthesis," *IEEE Trans. Signal Processing*, vol. 40, pp. 70-84, Jan. 1992.

[31] R. P. Ramachandran, and P. Kabal, "Bandwidth efficient transmultiplexers. II. Subband complements and performance aspects," *IEEE Trans. Signal Processing*. vol. 40. pp. 1108-1121, May 1992.

[32] Xiang-Gen Xia, "New precoding for intersymbol interference cancellation using nonmaximally decimated multirate filterbanks with ideal FIR equalizers," *IEEE Trans. Signal Processing*, vol. 45, pp. 2431-2441, Oct. 1997.

[33] A. Scaglione, G. B. Giannakis, and Barbarossa, "Redundant filterbank precoders and equalizers. I. Unification and optimal designs," *IEEE Trans. Signal Processing*, vol. 47, pp. 1988-2006, July 1999.

[34] A. Scaglione, Barbarossa, and G. B. Giannakis "Filterbank transceivers optimizing information rate in block transmissions over dispersive channels," *IEEE Trans. Inform. Theory*, vol. 45, pp. 1019-1032, Apr. 1999.

[35] P. P. Vaidyanathan, *Multirate Systems and Filter Banks*, Prentice-Hall, 1993.

[36] A. V. Oppenheim, and R. W. Schafer, *Discrete-Time Signal Processing*, Prentice Hall, 1989.

[37] B. Borna, and T. N. Davidson, "Efficient filter bank design for filtered multitone modulation," *in Proc. IEEE Int. Conf. Commun.*, vol. 1, pp. 38-42, June 2004.

[38] B. Borna, and T. N. Davidson, "Efficient design of FMT systems," *IEEE Trans. Commun.*, vol. 54, pp. 794-797, May 2006.

[39] N. Benvenuto, S. Tomasin, and L. Tomba, "Equalization methods in OFDM and FMT systems for broadband wireless communications," *IEEE Trans. Commun.*, vol. 50, pp. 1413-1418, Sept. 2002.

[40] T. Hunziker, and D. Dahlhaus, "Iterative detection for multicarrier transmission employing time-frequency concentrated pulses," *IEEE Trans. Commun.*, vol. 51, pp. 641-651, Apr. 2003.

[41] A. Tonello, "Asynchronous multicarrier multiple access: optimal and sub-optimal detection and decoding," *Bell Labs Technical Journal Fall 2002*, vol. 7, Feb. 2003.

[42] P. P. Vaidyanathan, "Multirate digital filters, filter banks, polyphase networks, and applications: a tutorial," *Proc. IEEE*, vol. 78, pp. 56-93, Jan. 1990.

[43] M. G. Bellanger, G. Bonnerot, and M. Coudreuse, "Digital filtering by polyphase network: application to sample-rate alteration,and filter banks," *in Proc. IEEE Int. Conf. Acoust., Speech, Signal Processing*, vol. ASSP-24, Apr. 1976.

[44] A. N. Akansu, P. Duhamel, X. Lin, and M. de Courville, "Orthogonal transmultiplexers in communication: A review," *IEEE Trans. Signal Processing*, vol. 46, pp. 979-995, April 1998.

[45] B. Farhang-Borojeny, "Multicarrier modulation with blind detection capability using cosine modulated filter banks," *IEEE Trans. Commun.*, vol. 51, pp. 2057-2070, Dec. 2003.

[46] K. M. Wong, J. Wu, T. N. Davidson, and Q. Jin, "Wavelet packet division multiplexing and wavelet packet design under timing error effects," *IEEE Trans. Signal Processing*, vol. 45, pp. 2877-2890, Dec. 1997.

[47] A. R. Lindsey, "Wavelet packet modulation for orthogonally multiplexed communication," *IEEE Trans. Signal Processing*, vol. 45, pp. 1336-1339, May 1997.

[48] M. Vetterli, and J. Kovacevic, *Wavelets and Subband Coding*, Prentice Hall, 1995.

[49] M. Vetterli, "Perfect transmultiplexers," *in Proc. IEEE Int. Conf. Acoust., Speech, Signal Processing*, vol. 11, pp. 2567-2570, Apr. 1986.

[50] B. Farhang-Boroujeny, and W. H. Chin, "Time domain equalizer design for DWMT multicarrier transceivers," *IEE Electronic Lett.*, vol. 36, pp. 1590-1592, Aug. 2000.

[51] J. S. Chow. J. M. Cioffi, and J. A. C. Bingham, "Equalizer training algorithms for multicarrier modulation systems," *in Proc. IEEE Int. Conf. Commun.*, vol. 2, pp. 761-765, May 1993.

[52] P. J. W. Melsa, R. C. Younce, and C. E. Rohrs, "Impulse response shortening for discrete multitone transceivers," *IEEE Trans. Commun.*, vol. 44, pp. 1662–1672, Dec. 1996.

[53] N. Al-Dhahir. and J. M. Cioffi, "Optimum finite-length equalization for multicarrier transceivers," *IEEE Trans. Commun.*, vol. 44, pp. 56-64, Jan. 1996.

[54] B. Farhang-Boroujeny and M. Ding, "Design methods for time-domain equalizers in DMT transceivers," *IEEE Trans. Commun.*, vol. 49, pp. 554–562, Mar. 2001.

[55] N. Al-Dhahir, and J. M. Cioffi, "A bandwidth-optimized reduced-complexity equalized multicarrier transceiver," *IEEE Trans. Commun.*, vol. 45, pp. 948-956, Aug. 1997.

[56] D. Daly, C. Heneghan, and A. D. Fagan, "Minimum mean-squared error impulse response shortening for discrete multitone transceivers," *IEEE Trans. Signal Processing*, vol. 52, pp. 301-306, Jan. 2004.

[57] G. Arsalan, B. Evans, and S. Kiaei, "Equalization for discrete multitone transceivers to maximize bit rate," *IEEE Trans. Signal Processing*, vol. 49, pp. 3123-3135, Dec. 2001.

[58] Y. P. Lin, L. H. Liang, P. J. Chung, and S. M. Phoong, "A frequency-domain SIR maximizing time-domain equalizer for VDSL systems," *in Proc. IEEE Int. Symp. Circuits Systems*, vol. 4, pp. 3163-3166, May 2005.

[59] K. Vanbleu, G. Ysebaert, G. Cuypers, M. Moonen, and K. V. Acker, "Bitrate-maximizing time-domain equalizer design for DMT-based systems," *IEEE Trans. Commun.*, vol. 52, pp. 871-876, June 2004.

[60] R. K. Martin, K. Vanbleu, M. Ding, G. Ysebaert, M. Milosevic, B. L. Evans, M. Moonen, and C. R. Johnson, Jr., "Unification and evaluation of equalization structures and design algorithms for discrete multitone modulation systems," *IEEE Trans. Signal Processing*, vol. 53, pp. 3880–3894, Oct. 2005.

[61] N. Al-Dhahir, and J. M. Cioffi, "Efficiently computed reduced-parameter input-aided MSE equalizers for ML detection: A unified approach," *IEEE Trans. Inform. Theory*, vol. 42, pp. 903-915, May 1996.

[62] A. Papoulis, *Probability, Random Variables, and Stochastic Processes*, McGraw-Hill, 3rd ed., 1991.

[63] B. Farhang-Boroujeni, *Adaptive Filters: Theory and Applications*, John Wiley and Sons, 1998.

[64] S. Haykin, *Adaptive Filter Theory*, 2nd ed., Prentice-Hall, 1991.

[65] C. E. Shannon, "A Mathematical Theory of Communications," *Bell Syst. Tech. J.*, vol. 27, pp. 379-423 and 623-656, 1948.

[66] P. S. Chow, J. M. Cioffi, and J. A. C. Bingham, "A practical discrete multitone transceiver loading algorithm for data transmission over spectrally shaped channels," *IEEE Trans. Commun.*, vol. 43, pp. 773-775, Feb.-Mar.-Apr. 1995.

[67] B. Borna, and S. H. Jamali, "Efficient design of trellis-coded CPM on Rician and Rayleigh fading channels," *IEE Proc.-Commun.*, vol. 147, pp. 226-230, Aug. 2000.

[68] J. P. Lauer, and J. M. Cioffi, "Turbo coding for discrete multitone transmission systems," *in Proc. IEEE Global Telecommun. Conf.*, vol. 6, pp. 3256-3260, Nov. 1998.

[69] E. Eleftheriou, and S. Olcer, "Low-density parity-check codes for digital subscriber lines," *in Proc. IEEE Int. Conf. Commun.*, vol. 3, pp. 1752-1757, April 2002.

[70] M. Ardakani, T. Esmailian, and F. R. Kschischang, "Near-capacity coding in multicarrier modulation systems," *IEEE Trans. Commun.*, vol. 52, pp. 1880-1889, Nov. 2000.

[71] J. Campello, "Optimal discrete bit loading for multicarrier modulation systems," *in Proc. IEEE Int. Symp. Inform. Theory*, pp. 193, Aug. 1998.

[72] J. Lee, S. T. Chung, and J. M. Cioffi, "Optimal Discrete Bit Loading for DMT-Based DSL Systems With Equal-Length Loops,"vol. 54, pp. 1760-1764, Oct. 2006.

[73] S. Boyd, and L. Vandenberghe, *Convex Optimization*, Cambridge University Press, 2004.

[74] C. Muschallik, "Improving an OFDM reception using an adaptive Nyquist windowing," *IEEE Trans. Consumer Electron.*, vol. 42, pp. 259-269, 1996.

[75] S. H. Muller-Weinfurtner, "Optimum Nyquist windowing in OFDM receivers," *IEEE Trans. Commun.*, vol. 49, pp. 417-420, March 2001.

[76] A. J. Redfern, "Receiver window design for multicarrier communications systems," *IEEE J. Sel. Areas Commun.*, vol. 20, pp. 1029-1036, June 2002.

[77] A. Vahlin, and N. Holte, "Optimal finite duration pulses for OFDM," *IEEE Trans. Commun.*, vol. 44, pp. 10-14, Jan. 1996.

[78] M. Pauli, and P. Kuchenbecker, "On the reduction of the out-of-band radiation of OFDM-signals," in *in Proc. IEEE Int. Conf. Commun.*, vol. 3, pp. 1304-1308, June 1998.

[79] Y. P. Lin, Y. Y. Jian, C. C. Su, and S. M. Phoong, "Windowed multicarrier systems with minimum spectral leakage," *in Proc. IEEE Int. Conf. Acoust., Speech, Signal Processing*, vol. 4, pp. 749-752, May 2004.

[80] Y. P. Lin, and S. M. Phoong, "Window designs for DFT-based multicarrier systems," *IEEE Trans. Signal Processing*, vol. 53, pp. 1015-1024, March 2005.

[81] B. Borna, and T. N. Davidson, "Biwindowed discrete multitone transceiver design," *IEEE Trans. Signal Processing*, vol. 55, pp. 4217-4226, Aug. 2007.

[82] G. H. Golub, and C. F. Van Loan, *Matrix Computations*, John Hopkins University Press, 1996.

[83] K. B. Song, S. T. Chung, G. Ginis, and J. M. Cioffi, "Dynamic spectrum management for next-generation DSL systems," *IEEE Commun. Mag.*, vol. 40, pp. 101-109, Oct. 2002.

[84] C. Zeng, C. Aldana, A. A. Salvekar, and J. M. Cioffi, "Crosstalk identification in xDSL systems," *IEEE J. Sel. Areas Commun.*, vol. 19, pp. 1488-1496, Aug. 2001.

[85] J. M. Cioffi, "VDSL system requirements document," *ANSI Contribution T1E1.4/98-043R3*, June 1998.

[86] D. Toumpakaris, J. M. Cioffi, and D. Gardan, "Reduced-delay protection of DSL systems against nonstationary disturbances," *IEEE Trans. Commun.*, vol. 52, pp. 1927-1938, Nov. 2004.

[87] M. Ho, J. M. Cioffi, and J. A. C. Bingham, "Discrete multitone echo cancelation," *IEEE Trans. Commun.*, vol. 44, pp. 817-825, July 1996.

[88] F. Sjöberg, Mikael Isaksson, R. Nilsson, P. Ödling, S. K. Wilson, and P. O. Börjesson, "Zipper: A duplex method for VDSL based on DMT," *IEEE Trans. Commun.*, vol. 47, pp. 1245-1252, Aug. 1999.

[89] S. Mirabbasi, and K. Martin, "Oversampled Complex-Modulated Transmultiplexer Filters with Simplified Design and Superior Stopbands," *IEEE Trans. Circuits Syst. II*, vol. 50, pp. 456-469, Aug. 2003.

[90] S. M. Phoong, Y. Chang, and C. Y. Chen, "SIR-optimized DFT-bank transceivers for multipath fading channels," *in Proc. IEEE Int. Conf. Acoust., Speech, Signal Processing*, vol. 4, pp. 729-732, May 2004.

[91] W. Kozek, and A. F. Molisch, "Nonorthogonal pulseshapes for multicarrier communications in doubly dispersive channels," *IEEE J. Sel. Areas Commun.*, vol. 15, pp. 1579-1589, Oct., 1998.

[92] T. Strohmer, and S. Beaver, "Optimal OFDM design for time-frequency dispersive channels," *IEEE Trans. Commun.*, vol. 51, pp. 1111-1122, July 2003.

[93] G. Cherubini, "Hybrid TDMA/CDMA based on filtered multitone modulation for uplink transmission in HFC networks," *IEEE Commun. Mag.*, vol. 41, pp. 108-115, Oct. 2003.

[94] D. Mestdagh, M. Isaksson, and P. Ödling, "Zipper VDSL: A Solution for Robust Duplex Communication over Telephone Lines," *IEEE Commun. Mag.*, vol. 38, pp. 90-96, May 2000.

[95] A. Tonello, "Time domain and frequency domain implementations of FMT modulation architectures," *in Proc. IEEE Int. Conf. Acoust., Speech, Signal Processing*, vol. 4, pp. 625-628, March 2006.

[96] M. R. Wilbur, T. N. Davidson, and J. P. Reilly, "Efficient design of oversampled NPR GDFT filter banks," *IEEE Trans. Signal Processing*, vol. 52, pp. 1947-1963, July 2004.

[97] L. Vandendorpe, L. Cuvelier, F. Deryck, J. Louveaux, and O. van de Wiel, "Fractionally spaced linear and decision-feedback detectors for transmultiplexers," *IEEE Trans. Signal Processing*, vol. 46, pp. 996-1011, Apr. 1998.

[98] T. N. Davidson, Z. Q. Luo, J. F. Sturm, "Linear matrix inequality formulation of spectral mask constraints with applications to FIR filter design," *IEEE Trans. Signal Processing*, vol. 50, pp. 2702-2715, Nov. 2002.

[99] J. F. Sturm, "Using SeDuMi 1.02, a MATLAB toolbox for optimization over symmetric cones", *Optimiz. Methods Softw.*, vol. 11-12, pp. 625-653, 1999.

[100] T. N. T. Goodman, C. A Micchelli, G. Rodriguez, and S. Seatzu, "Spectral factorization of Laurent polynomials," *Adv. Comput. Math.*, vol. 7, pp. 429-454, 1997.

[101] S. P. Wu, S. Boyd, and L. Vandenberghe, "FIR filter design via spectral factorization and convex optimization," in *Applied and Computational Control, Signals, and Circuits*, vol. 1, B. Datta, Ed., Birkhauser, 1997.

[102] W. Yu, and J. M. Cioffi, "Constant-power waterfilling: performance bound and low-complexity implementation," *IEEE Trans. Commun.*, vol. 54, pp. 23-28, Jan. 2006.

[103] J. R. Barry, E. A. Lee, and D. G. Messerschmitt, *Digital Communication*, 3rd ed., Kluwer, 2004.

[104] N. Benvenuto, and S. Tomasin, "Efficient pre-coding schemes for FMT broadband wireless systems," in *Proc. IEEE Int. Symp. Personal, Indoor, Mobile Radio Commun.*, vol. 4, pp. 1493-1497, Lisbon, Sept. 2002.

[105] F. J. Harris," On the use of windows for harmonic analysis with the discrete Fourier transform," *Proc. IEEE*, vol. 66, pp. 51-83, Jan. 1978.

[106] A. Tkacenko, P. P. Vaidyanathan, and T. Q. Nguyen, "On the eigenfilter design method and its applications: A tutorial," *IEEE Trans. Circuits Systems II*, vol. 50, pp. 497–517, Sept. 2003.

[107] S. K. Mitra, *Digital Signal Processing*, McGraw-Hill, 1998.

[108] A. Tonello, "Performance limits for filtered multitone modulation in fading channels," *IEEE Trans. Wireless Commun.*, vol. 4, pp. 2121-2135, Sept. 2005.

[109] A. Tonello, "A concatenated multitone multiple-antenna air-interface for the asynchronous multiple-access channel," *IEEE J. Sel. Areas Commun.*, vol. 24, pp. 457-469, Mar. 2006.